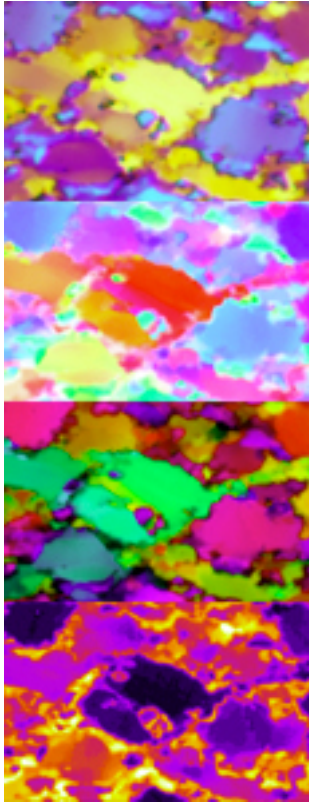




OPTICAL ORIENTATION IMAGING



[Contents](#)

[About OPTICAL ORIENTATION IMAGING](#)

[Acknowledgements](#)

Renée Heilbronner
Department of Earth Sciences
Basel University

renee.heilbronner@unibas.ch

Heilbronner, R. 2000. Optical Orientation Imaging. In: Stress, Strain and Structure, A volume in honour of W D Means. Eds: M.W. Jessell and J.L.Urai. Volume 2, Journal of the Virtual Explorer. ISSN 1441-8126 (Print). ISSN 1441-8134 (CD-ROM). ISSN 1441-8126 (On-line at www.virtual-explorer.com.au/VEjournal/Volume2).

CONTENTS

[top /](#) [section 1](#) -- [section 2](#) -- [section 3](#) -- [section 4](#) -- [section 5](#) --
[contents /](#) [section 6](#)
[appendix 1](#) -- [appendix 2](#)

sections

1 WHAT IS ORIENTATION IMAGING ?

2 CALCULATING THE PRIMARY IMAGES

3 VISUALIZING ORIENTATIONS

4 ORIENTATION IMAGES OF EXPERIMENTALLY DEFORMED ROCKS

5 ORIENTATION IMAGES OF NATURALLY DEFORMED ROCKS

6 WHERE CAN WE GO FROM HERE ?

appendices

A1 LIBRARY OF ORIENTATION AND MISORIENTATION IMAGES

A2 SOFTWARE, LOOK-UP TABLES AND REFERENCES

ABOUT ORIENTATION IMAGING

[top](#) / [contents](#) / [section 1](#) -- [section 2](#) -- [section 3](#) -- [section 4](#) --
[section 5](#) -- [section 6](#) -- [appendix 1](#) -- [appendix 2](#)

How to use this contribution

"OPTICAL ORIENTATION IMAGING" is written in HTML and consists of a number of web pages which can be viewed with any regular browser. Still the design of the contribution is basically a running text which takes the reader through a sequence of six sections that follow each other. These sections are not meant to convey scientific content, rather they are meant to be demonstrations of what can be done with optical orientation imaging, of how this technique can be used in the earth materials research. It is hoped that they stimulate the reader to try using this tool. It is also possible to access the folders directly and to work with the images directly.

File Structure

The text and image files of "OPTICAL ORIENTATION IMAGING" are stored in a folder "OrientationImaging". This folder contains four folders: "CLUTs", "figures", "images", and "text" (A list of all microstructure images in original TIFF format can be found [here](#)). The "text" and "figures" folders are subdivided into sections, the subfolders of the "images" folder refer to topics or specific samples. The starting page is in the folder "text":
<file:///OrientationImaging/text/0000.html>.

Dragging the folders into the open window of Netscape will display this file structure.



You can browse through the folders and copy whichever file seems interesting.

Organization of sections

Each section is colour-coded, the pages are numbered and displayed at the top of each page. The reader can page through each section or go to the index of the section by clicking on the appropriate page number. [top](#) and [contents](#) are links to the title page and the table of contents respectively. From each page, one can get to the top of the section and the table of contents but not to the individual pages of the other sections; the [about page](#) (the one you are reading right now) can only be

reached via the title page.

Organisation of appendices

The appendices are guides to the images, to software and to references.

section 1 - WHAT IS ORIENTATION IMAGING ?

- [1.1](#) Imaging, look-up tables and conoscopic images
- [1.2](#) Orientation imaging through the light microscope
- [1.3](#) ... using crossed polarizers
- [1.4](#) ... using crossed polarizers and lambda plate
- [1.5](#) ... using crossed polarizers, lambda plate and narrowband infrared filter
- [1.6](#) ... using circular polarization: crossed polarizers and two quarterwave plates

- [1.7](#) Optical orientation imaging

section 2 - CALCULATING THE PRIMARY IMAGES

- [2.1](#) Setting up the microscope, the scanner and the computer
- [2.2](#) Recording the input images
- [2.3](#) Checking the input
- [2.4](#) Calculation of azimuth, inclination, and error images
- [2.5](#) The azimuth image
- [2.6](#) The inclination image (amplitude)
- [2.7](#) The inclination image (circular polarization)
- [2.8](#) The error image
- [2.9](#) The misorientation images
- [2.10](#) The orientation gradient images
- [2.11](#) The c-axis polefigure

section 3 - VISUALIZING ORIENTATIONS

- [3.1](#) Colour-coding the azimuth image
- [3.2](#) Colour-coding the inclination image
- [3.3](#) Checking the inclination image (cirpol)
- [3.4](#) The c-axis orientation image (COI)
- [3.5](#) Various colour look-up tables (CLUTs) for the c-axis orientation image
- [3.6](#) Making masks from the error and background images
- [3.7](#) Principal misorientation images
- [3.8](#) Misorientation with respect to reference direction
- [3.9](#) Analysis of orientation gradient images

section 4 - ORIENTATION IMAGES OF EXPERIMENTALLY DEFORMED ROCKS

- [4.1](#) Starting material: Black Hills quartzite and Heavitree quartzite
- [4.2](#) Regime 1, 2 and 3 of dynamic recrystallization
- [4.3](#) Partial textures of regime 1, 2 and 3 of dynamic recrystallization
- [4.4](#) Annealed microstructures of regime 1, 2 and 3 of dynamic recrystallization
- [4.5](#) More detail on regime 3 of dynamic recrystallization
- [4.6](#) Making use of sample heterogeneity
- [4.7](#) Dynamic recrystallization of quartzite along deformation gradient

section 5 - ORIENTATION IMAGES OF NATURALLY DEFORMED ROCKS

- [5.1](#) Quartz mylonite from the Simplon fault zone
- [5.2](#) Quartz mylonite from the Corvatsch (Christian Pauli)
- [5.3](#) Quartz veins from the Glarus thrust (Mirjam VanDaalen)
- [5.4](#) Quartz veins from the Tonale fault (Michael Stipp)
- [5.5](#) ...more on the quartz veins from the Tonale fault
- [5.6](#) Carrara Marble (Nils Oesterling)

section 6 - WHERE CAN WE GO FROM HERE ?

- [6.1](#) Grain boundary detection based on misorientations
- [6.2](#) Grain size sensitive texture analysis
- [6.3](#) Grain size analysis
- [6.4](#) Comparing CIP and EBSD
- [6.5](#) Shape - texture relations
- [6.6](#) Misorientation analysis of grains undergoing dynamic recrystallization
- [6.7](#) Misorientation analysis of host grain - recrystallised grain relation
- [6.8](#) Misorientations at grain boundaries of "flat" orientation images

appendix 1 - LIBRARY OF ORIENTATION AND MISORIENTATION IMAGES

- [A1.1](#) Micrographs, circular polarization
- [A1.2](#) Orientation images
- [A1.3](#) Input images
- [A1.4](#) List of image sets
- [A1.5](#) List of topics

appendix 2 - SOFTWARE, LOOK-UP TABLES AND REFERENCES

- [A2.1](#) Lazy stack
- [A2.2](#) Lazy LUT
- [A2.3](#) Lazy grain boundaries
- [A2.4](#) StripStar
- [A2.5](#) Colour look-up tables
- [A2.6](#) References

Acknowledgements

[top](#) / [contents](#) / [section 1](#) -- [section 2](#) -- [section 3](#) -- [section 4](#) --
[section 5](#) -- [section 6](#) -- [appendix 1](#) -- [appendix 2](#)

People who have contributed....

First, I would like to thank Christian Pauli, Mirjam van Daalen, Michael Stipp and Nils Oesterling, four Ph.D. students who have worked with me - two are still with me, I hope. They have not only risked their mental health by venturing in the world of orientation imaging by a method called computer-integrated polarization microscopy (or CIP); they have actually written parts of the program or contributed subroutines, they have used and expanded the method and applied it to quartz and calcite during their Ph.D. research. By doing so they have continuously challenged the program, the method and the entire approach. At the same time they have pushed the limit of what can be done and made me push it with them. They have taught me immensely.

Of equal importance was the positive feed-back I got during a stay at Brown University in 1998 in the context of a research project that Jan Tullis, Greg Hirth, Holger Stunitz and myself had designed to compare and correlate natural and experimental microstructures of quartz, feldspar and olivine. Bringing my microscope and computer with me I had five months to look at the quartz deformation experiments that Jan and Greg had performed. This was some sort of heaven for me: to be able to look at this incredible wealth of material stacked away in those little thin section boxes. The samples may be small - but they provide one hundred percent outcrop!

A year later I returned to the scene of the crime, this time, without microscope and without computer. I need to thank Peter Gromet for admitting me to his lab and letting me use his brand new G3. I am still not sure he knew what he consented to when he said I could use it. The major part of this contribution was written on that computer. I also need to thank Fritz Roesel of the Basel University Computer Center and Ingeno Data Basel who somehow conspired towards putting a fast Mac on my Basler desk...

But most of all I am indebted to the person in whose honour we produce this CD. Win, I have tried to copy you and make this paper simple, convincing, easy to read, useful, exciting, imaginative, just like you taught us. In as much as achieved this, I owe it to you, in as much as I failed, I blame it on myself... and the billion bug.

October, 10th, 1999, Renée Heilbronner, Department of Earth Sciences, Basel University

Funding by:

- Swiss National Science Foundation: NF21-36008.92, NF20-42134.94, NF2000-049562.96 and NF2000-055420.98.
- US National Science Foundation: EAR9725623
- Swiss National Science foundation: R'Equip 2160-051625.97

1 WHAT IS ORIENTATION IMAGING ?

[top](#) / [contents](#) / [section 1](#) / pages [1.1](#) -- [1.2](#) -- [1.3](#) -- [1.4](#) -- [1.5](#) -- [1.6](#) -- [1.7](#)

[1.1](#) Imaging, look-up tables and conoscopic images

[1.2](#) Orientation imaging through the light microscope

[1.3](#) ... using crossed polarizers

[1.4](#) ... using crossed polarizers and lambda plate

[1.5](#) ... using crossed polarizers, lambda plate and narrowband infrared filter

[1.6](#) ... using circular polarization: crossed polarizers and two quarterwave plates

[1.7](#) Optical orientation imaging

1.1 WHAT IS ORIENTATION IMAGING ?

[top](#) / [contents](#) / [section 1](#) / [pages 1.1](#) -- [1.2](#) -- [1.3](#) -- [1.4](#) -- [1.5](#) -- [1.6](#) -- [1.7](#)

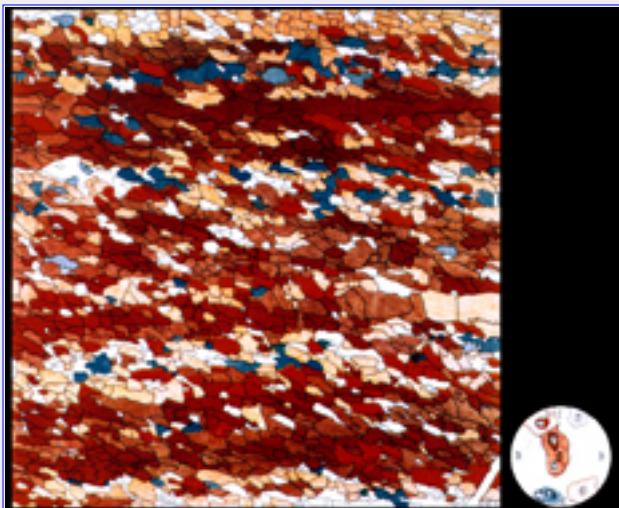
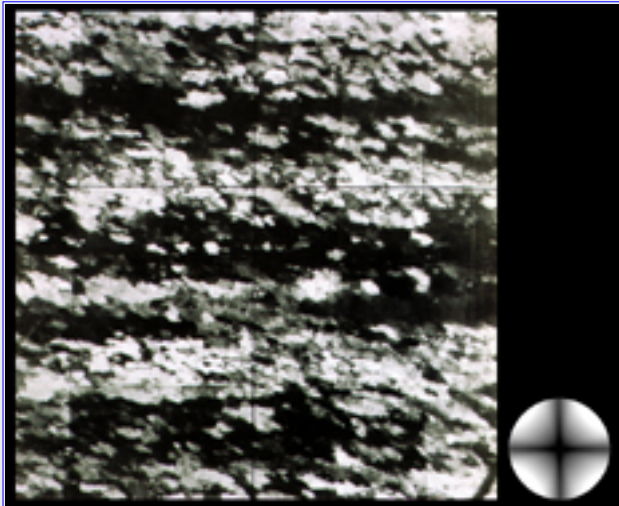
Introduction

Imaging

The process of imaging refers to colour-coding physical information on a two-dimensional image plane. For example, if the physical information is the brightness variation on an illuminated object the image is a regular black and white photograph. If the physical information is the concentration of an element or the surface temperature the resulting image would be a chemical map or a thermograph. Many other examples could be given. Here we are interested in obtaining orientation images, i.e., maps of crystallographic directions, more specifically colour-coded maps of the optical axis orientations of uniaxial minerals (quartz, calcite, ice, norcamphor, etc.).

The first orientation images were produced by Bruno Sander and his collaborators in the early forties. In order to perform what they called an "Achsen-Verteilungs-Analyse" (AVA), they placed a given microstructure in the optical microscope, drew a grain boundary map, measured the c-axis orientation of each of the grains with the Universal stage, and assigned colours to certain regions in the pole figure. Using this colour-code the grainboundary map was filled.

Nowadays we can produce such orientation images by means of digital image processing. Not only is this a much faster way of doing it, it is also a more precise and rigorous way. First of all, the orientation is determined at each point of the image and not only once per grain, secondly, we may also derive misorientation and deformation gradient images, thirdly we may select texture domains interactively which means that we can perform strain- shape- and grain size analysis as a function of crystallographic orientation.



Micrograph (crossed polarizers) and Achsenverteilungs-Analysen (AVA) of quartzite

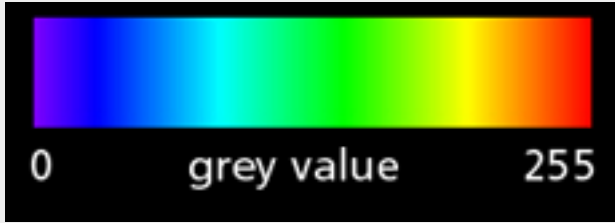
Look-up tables and conoscopic images

The concept of look-up tables (LUTs) is going to be of prime importance.

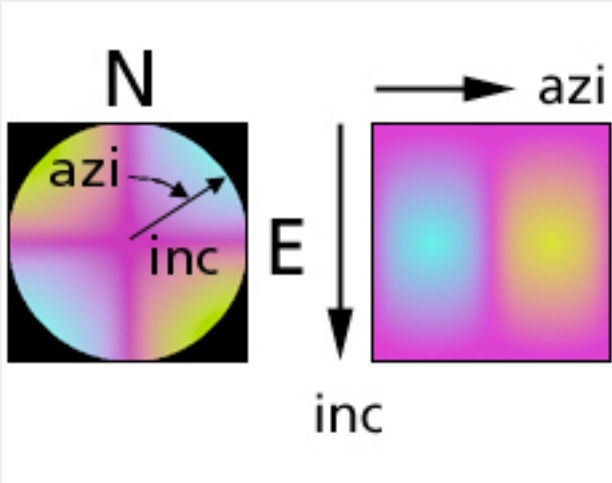
The typical LUT is one-dimensional assignment of colours or grey values to input values. Here we will use two-dimensional LUTs to assign colours to pairs of azimuth and inclination values.

We will consider the conoscopic image as a look-up table (more precisely, as the stereographic projection of a look-up table) from which we derive the orientation of the optical axis of any pixel in the image.

We will adopt the following conventions: Orientations of the c-axes are given in terms of azimuth and inclination, the principal directions being N (North), E (East), and H (Heaven) with respect to the plane of the thin section, i.e., the image plane. North-South is vertical, East-West is horizontal, Heaven-Hell is normal to the image plane. The azimuth is measured from N = 0° clockwise to South = 180°, the inclination from Heaven = 0° downwards to Hell = 180°. An axis oriented East-West parallel to the plane of the thin section would be denoted 90/90, one striking NW/SE, dipping 30° below the plane of the thin section would be denoted 135/120.



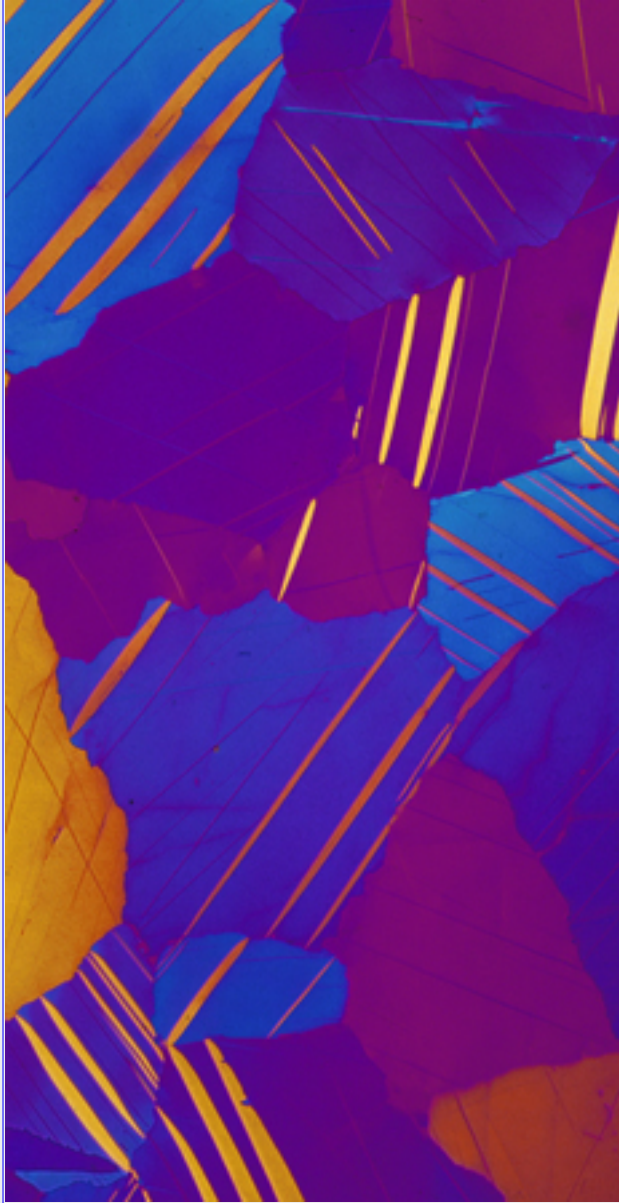
1-D look-up table



conoscopic image and 2-D look-up table of quartz

1.2 WHAT IS ORIENTATION IMAGING ?

[top](#) / [contents](#) / [section 1](#) / pages [1.1](#) -- [1.2](#) -- [1.3](#) -- [1.4](#) -- [1.5](#) -- [1.6](#) -- [1.7](#)



Ultrathin section of Carrara marble
crossed polarizers, lambda plate

Orientation imaging through the light microscope

Without knowing - or without calling it so - we are all quite familiar with orientation imaging. Everytime we use a polarizing microscope to observe a thin section, we look at an orientation image.

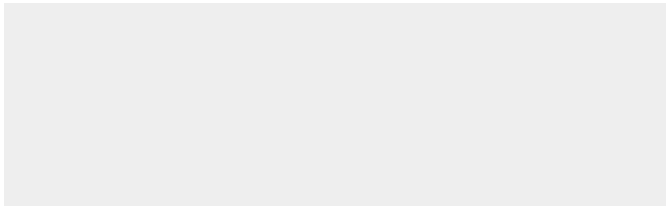
Depending on

- the birefringence of the mineral,
- the orientation of the optical axis with respect to the polarizers,
- the thickness of the thin section,
- the number of polarizers and their relative orientation,
- the spectral transmission of the filters and
- the number and types of compensators

placed in the optical path, the resulting interference colours are different and have to be interpreted differently. If we keep everything but the orientation of the crystal lattice constant (as is the case in a monophasic material, and constant thin section thickness), the interference colours vary solely as a function of the orientation of the optical axis of the mineral.

Unfortunately, however, this dependence of interference colour on c-axis orientation is not unique: there are always a number of orientations that produce the same interference colour. If we think of ordinary polarization microscopy in terms of "analogue orientation imaging", we would say that it is a type of orientation imaging where the "choice of look-up tables" is "somewhat unfortunate" or limited. True orientation imaging always seeks to find a unique representation of crystallographic orientation, assigning each possible orientation exactly one colour and vice versa.

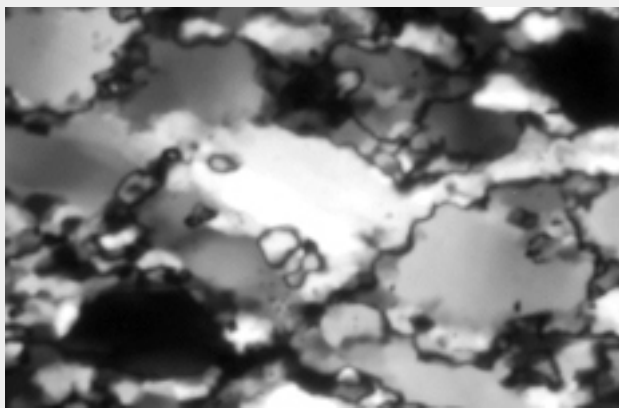
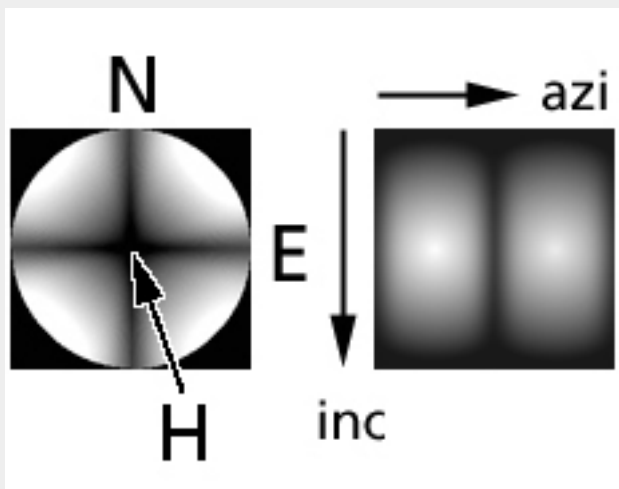
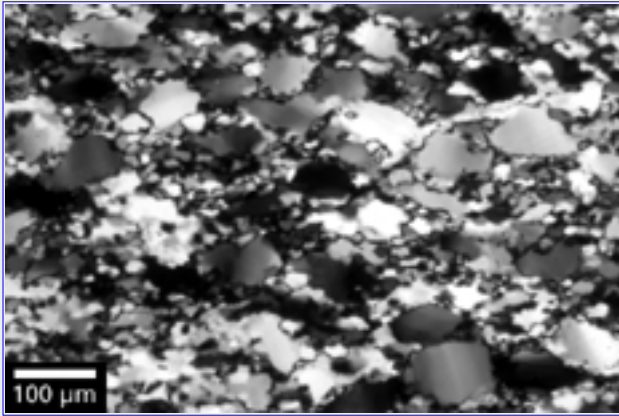
In this section, we will look at differently polarized and filtered images of an



experimentally deformed quartzite with the aim of extracting whatever orientation information we can from the observable interference colours.

1.3 WHAT IS ORIENTATION IMAGING ?

[top](#) / [contents](#) / [section 1](#) / [pages 1.1](#) -- [1.2](#) -- [1.3](#) -- [1.4](#) -- [1.5](#) -- [1.6](#) -- [1.7](#)



... using crossed polarizers

The quartzite is shown under crossed polarizer conditions. Grains or pixels that appear black can have any c-axis orientation parallel to the East-West or the North-South plane, i.e., they can have any inclination provided the azimuth is 0° or 90° . Grains that appear grey to white can have any other orientation, striking approximately NE-SW or NW-SE.

The brightness-orientation relation is contained in the conoscopic image. The latter can be interpreted as the stereographic projection of the look-up table. The orthogonal representation of the look-up table is shown on the right.

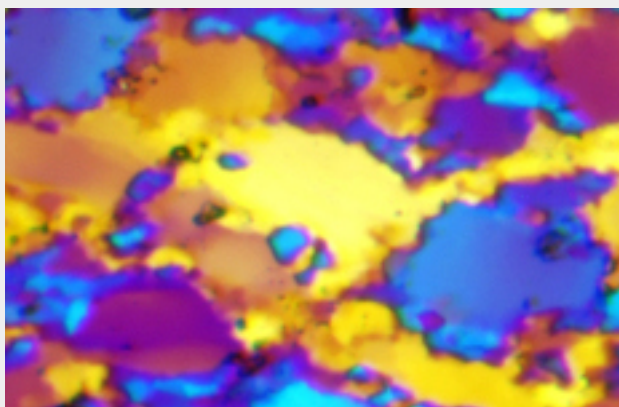
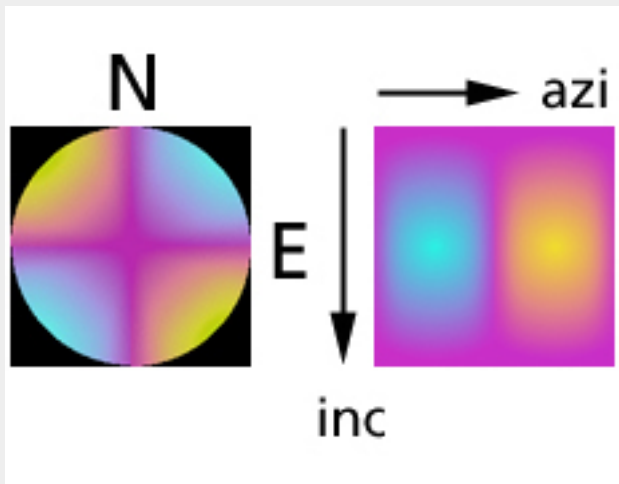
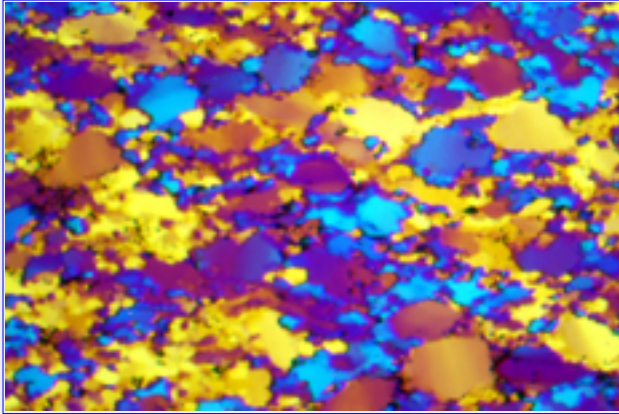
Because of the symmetry of the conoscopic image, i.e., of the look-up table, there are always a number of possible c-axis orientations that can be found for any given grey value.

Left, from top to bottom:

- Experimentally deformed Black Hills quartzite under crossed polarizer conditions
- conoscopic image and look-up table for crossed polarizer conditions
- detail of micrograph... meet the chipmunk.

1.4 WHAT IS ORIENTATION IMAGING ?

[top](#) / [contents](#) / [section 1](#) / pages [1.1](#) -- [1.2](#) -- [1.3](#) -- [1.4](#) -- [1.5](#) -- [1.6](#) -- [1.7](#)



... using crossed polarizers and lambda plate

The quartzite is shown under crossed polarizer conditions with the lambda plate inserted. Grains or pixels that appear magenta coloured (first order red) can have any c-axis orientation parallel to the East-West or the North-South plane, i.e., they can have any inclination provided the azimuth is 0° or 90° . Grains that appear blue have c-axes that strike NE-SW (...BURP...blue upper right positive), those which appear yellow have axes striking NW-SE.

The colour-orientation relation is represented by the conoscopic image. The orthogonal representation of the look-up table is shown on the right.

The number of possible c-axis orientations for any given interference colour is reduced with respect to the previous representation (crossed polarizers only), but still there is no unique representation.

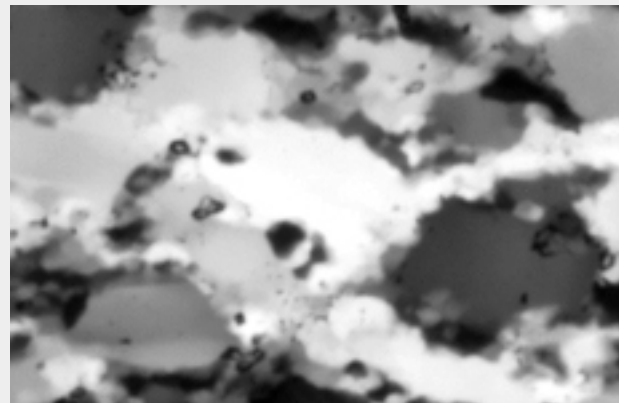
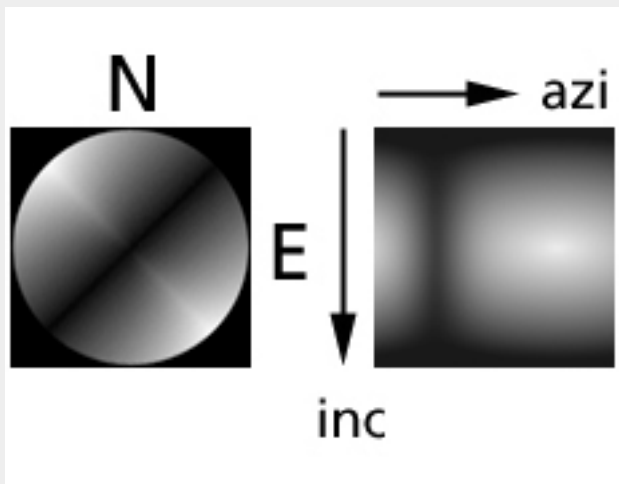
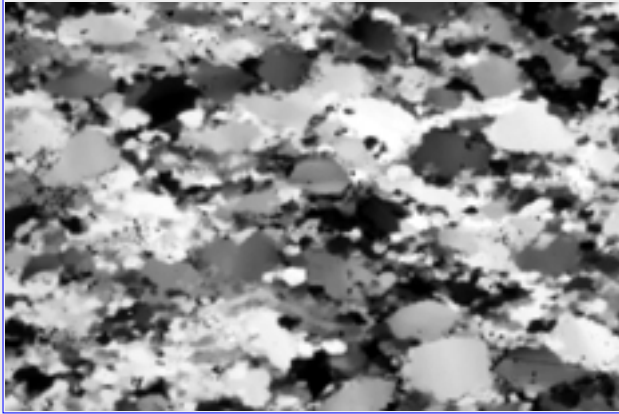
In the previous micrograph, the little chipmunk appeared nearly white, implying that its c-axis strikes either NW-SE or NE-SW at an inclination very close to the plane of the section. Now, the chipmunk appears yellow, that means that the c-axis of the chipmunk strikes NW-SE. The yellow colour is very bright, indicating again that the axis must have an inclination closer to 90° than $0^\circ / 180^\circ$.

Left, from top to bottom:

- Experimentally deformed Black Hills quartzite under crossed polarizer conditions and lambda plate
- conoscopic image and look-up table for crossed polarizer conditions and lambda plate
- the chipmunk has blue eyes!

1.5 WHAT IS ORIENTATION IMAGING ?

[top](#) / [contents](#) / [section 1](#) / [pages 1.1](#) -- [1.2](#) -- [1.3](#) -- [1.4](#) -- [1.5](#) -- [1.6](#) -- [1.7](#)



... using crossed polarizers, lambda plate and narrowband infrared filter

The quartzite is shown under crossed polarizer conditions with the lambda plate and a narrow band filter (transmission: 700 ± 9 nm, near infrared) inserted. This filter renders first order yellow as white, first order red as grey and first order blue as black.

Again, the brightness-orientation relation is represented by the conoscopic image. The orthogonal representation of the look-up table is shown on the right.

By inserting the filter, the interference colours (3 channels) are mapped uniquely into a grey value image (1 channel). As in the previous case the number of possible c-axis orientations for any given grey value is reduced with respect to the crossed polarizers conditions, but still there is no unique representation.

The little chipmunk appears nearly white, indicating that its c-axis strikes NW-SE at an inclination very close to the plane of the section. From the point of view of colour-coding (or grey-coding) the c-axis orientations, there is no advantage over the previous case except that the storage space for a monochrome image is less than that of a colour image.

Left, from top to bottom:

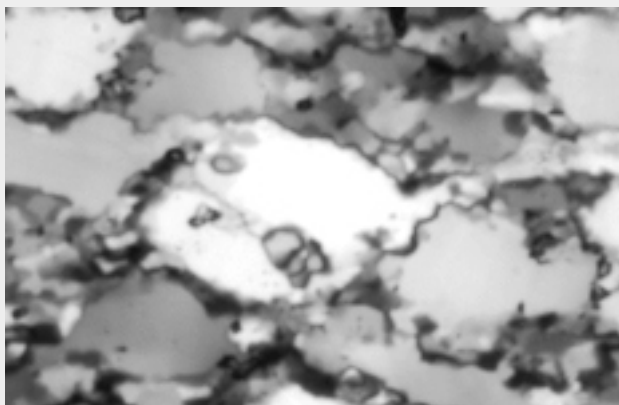
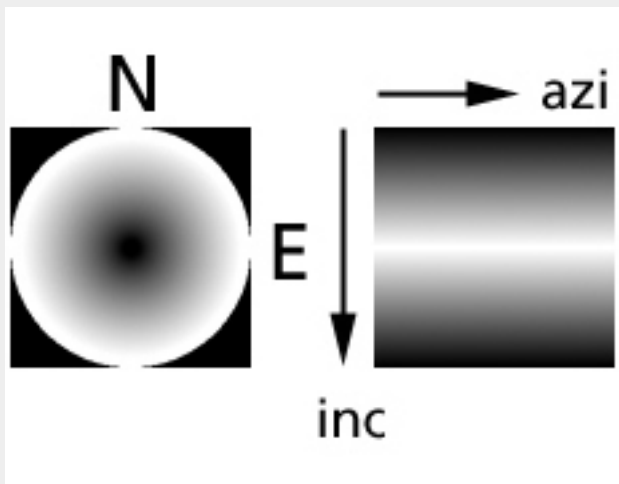
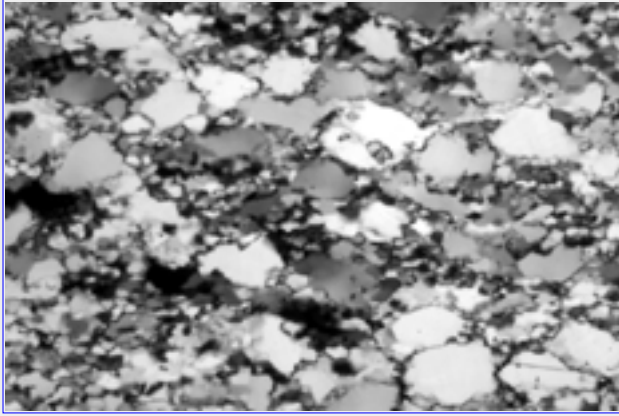
- Black Hills quartzite under crossed polarizer conditions, lambda plate and narrow band interference filter (660 nm).

- conoscopic image and look-up table for crossed polarizer conditions, lambda plate and 660nm interference filter.

- the "infra-red" chipmunk.

1.6 WHAT IS ORIENTATION IMAGING ?

[top](#) / [contents](#) / [section 1](#) / pages [1.1](#) -- [1.2](#) -- [1.3](#) -- [1.4](#) -- [1.5](#) -- [1.6](#) -- [1.7](#)



... using circular polarization: crossed polarizers and two quarterwave plates

The quartzite is shown under so-called circular polarization conditions with crossed polarizers and two quarter wave length plate ($1/4$ lambda plates) inserted. Circular polarization yields an inclination image, where the grains appear dark if the c-axes are normal to the plane of the section, and white if the c-axes are parallel to it. Circular polarization is not sensitive to the azimuth of the c-axis (no use turning the microscope table...)

Again, the brightness-orientation relation is represented by the conoscopic image. The orthogonal representation of the look-up table is shown on the right.

The little chipmunk appears nearly white, indicating that its c-axis lies very close to the plane of the section. In as much as some of the grain boundaries (probably the wider ones) are optically isotropic, they appear black

Left, from top to bottom:

- Experimentally deformed Black Hills quartzite under circular polarization (crossed polarizers and two $1/4$ lambda plates).
- conoscopic image and look-up table for circular polarization.
- the circularly polarized chipmunk.. does not seem to

mind it

1.7 WHAT IS ORIENTATION IMAGING ?

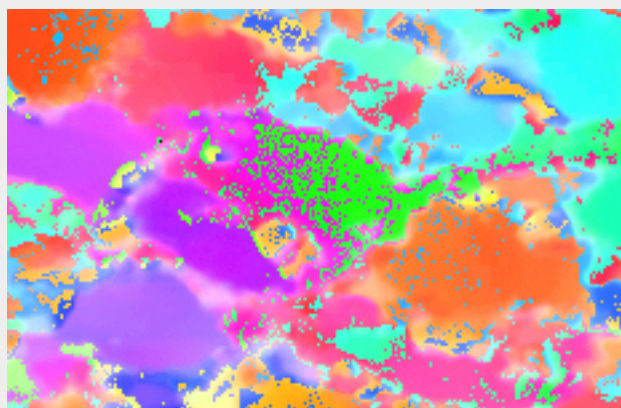
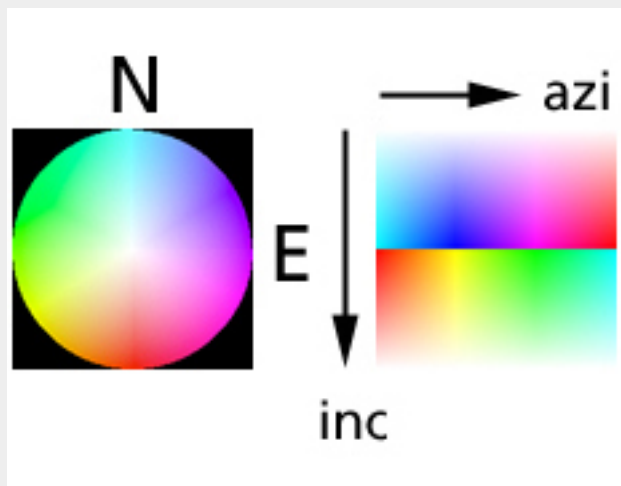
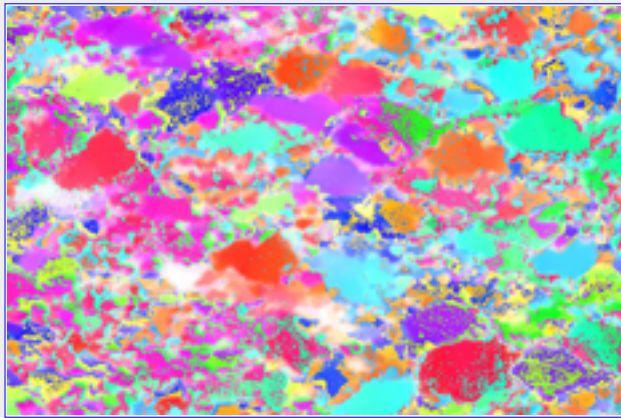
[top](#) / [contents](#) / [section 1](#) / [pages 1.1](#) -- [1.2](#) -- [1.3](#) -- [1.4](#) -- [1.5](#) -- [1.6](#) -- [1.7](#)

Optical orientation imaging

Using CIP (computer-integrated polarization microscopy), a mode of colour-coding can be obtained that is unique with respect to c-axis orientation, i.e., the orientation halfspace. To map the two-dimensional orientation space, i.e., to uniquely colour-code c-axis orientations, azimuth and inclination images are calculated and treated as two channels of a colour image.

Two-dimensional colour look-up tables (CLUTs) are used to assign unique colours to any given pixel depending on the azimuth and inclination values of the c-axis at that point.

The chipmunk is purple with green spots on its back. Both colours confirm a NW-SE strike (compare "analogue orientation imaging"). Obviously, the orientation of its c-axis varies gradually from dipping above the plane of the section to dipping below it. Due to the way in which the CLUT is set up (see left), this results in a strong (and somewhat misleading) colour contrast between $inc=90^\circ$ and $inc=91^\circ$ (dipping above and below the plane of the section respectively).



Left, from top to bottom:

- CIP calculated orientation image of Black Hills quartzite
- stereographic projection and orthogonal representation of standard colour look-up table (CIP-Standard CLUT)
- the purple chipmunk who rolled in peas.

2 CALCULATING THE PRIMARY IMAGES

[top](#) / [contents](#) / [section 2](#) / [2.1](#) -- [2.2](#) -- [2.3](#) -- [2.4](#) -- [2.5](#) -- [2.6](#) -- [2.7](#) -- [2.8](#) -- [2.9](#) -- [2.10](#) -- [2.11](#)

[2.1](#) Setting up the microscope, the scanner and the computer

[2.2](#) Recording the input images

[2.3](#) Checking the input

[2.4](#) Calculation of azimuth, inclination, and error images

[2.5](#) The azimuth image

[2.6](#) The inclination image (amplitude)

[2.7](#) The inclination image (circular polarization)

[2.8](#) The error image

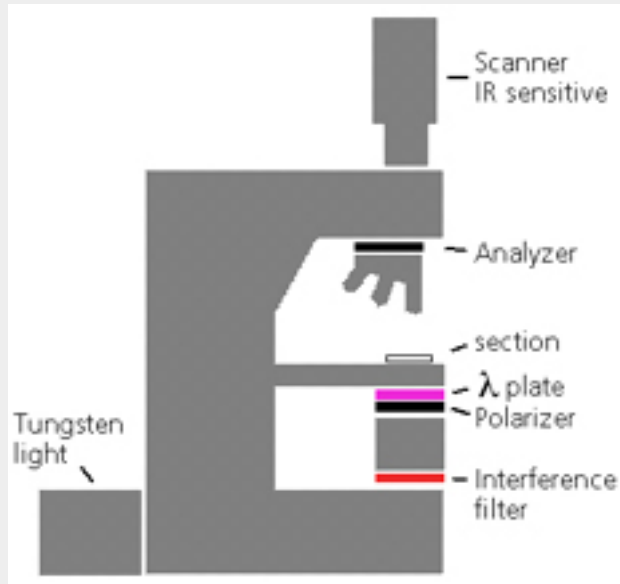
[2.9](#) The misorientation images

[2.10](#) The orientation gradient images

[2.11](#) The c-axis polefigure

2.1 CALCULATING THE PRIMARY IMAGES

[top](#) / [contents](#) / [section 2](#) / [2.1](#) -- [2.2](#) -- [2.3](#) -- [2.4](#) -- [2.5](#) -- [2.6](#) -- [2.7](#) -- [2.8](#) -- [2.9](#) -- [2.10](#) -- [2.11](#)



Setting up the microscope, the scanner and the computer

In this section, the steps necessary to obtain orientation images by computer-integrated polarization microscopy (CIP) are described.

Technical requirements for CIP:

- 1 polarization microscope equipped with linear analyzer and polarizer, lambda plate, and two 1/4- lambda plates (for circular polarization). Linear analyzer, polarizer and lambda plate must be fully rotatable (360°)
- 1 tilt stage (optional, but makes life much easier), manufactured by the Geo-Workshop, Dept. Earth Sciences, University Basel.
- 1 digital scanner camera, monochromatic, infrared sensitive
- 1 powerful graphic workstation with sufficient memory

Software requirements for CIP:

need to have:

- CIP package: for calculation of orientation images and pole figures
- [NIH Image](#), [Scion Image](#) or [Adobe Photoshop](#) and Plug In: for image capture
- Lazy LUT (macro for NIH Image): to manipulate input and output images

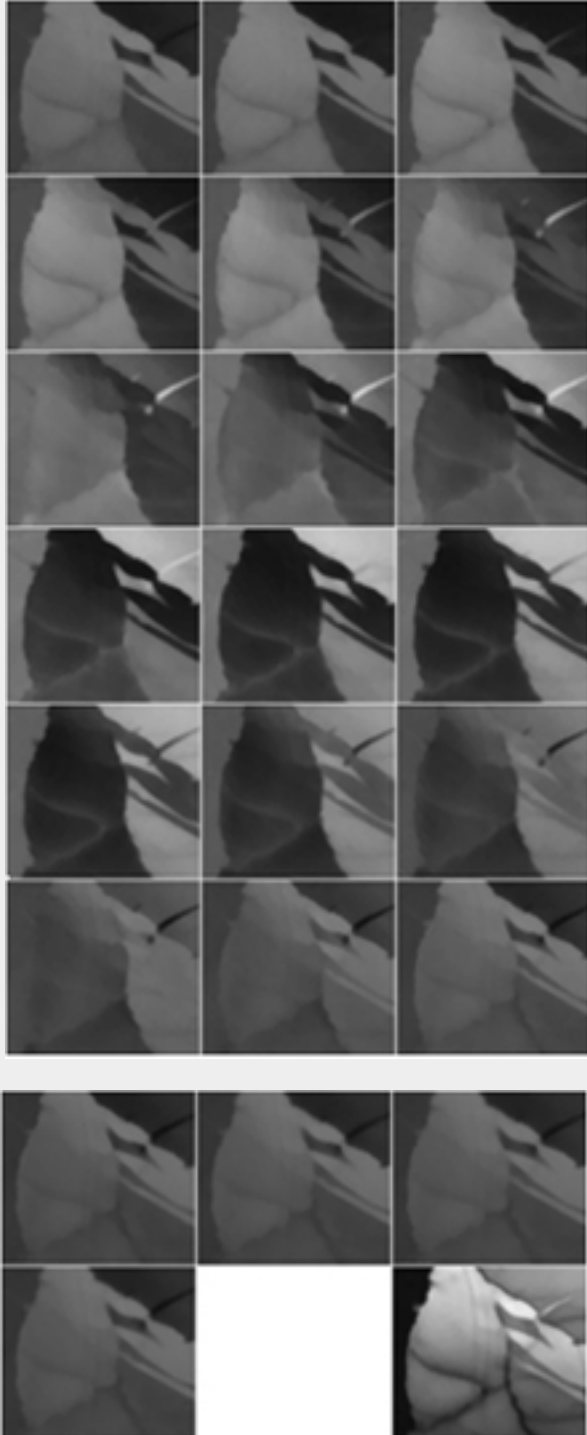
nice to have:

- Lazy stack: NIH Image macro for re-matching of input images

Adobe Photoshop: for postprocessing and editing of orientation images

2.2 CALCULATING THE PRIMARY IMAGES

[top](#) / [contents](#) / [section 2](#) / [2.1](#) -- [2.2](#) -- [2.3](#) -- [2.4](#) -- [2.5](#) -- [2.6](#) -- [2.7](#) -- [2.8](#) -- [2.9](#) -- [2.10](#) -- [2.11](#)



Recording the input images

The standard input for CIP calculations consists of 18 rotation images, 2 or 4 tilt images and a circular polarization image: the rotation images are a series of images with incremental relative rotation of the thin section with respect to the polarizers and the lambda plate (typically using a fixed interval of 10°), the tilt images are captured with the thin section tilted about the N-S and E-W axes. For the circular polarization image, crossed polarizers and two quarter-lambda plates (above and below the thin section) are used. 18 rotation images at 10° intervals and 2 tilt images are the absolute minimum; routinely, one circular polarization image is included.

Placing the input images in a stack (a multi-image sequence within NIH Image) and using the "Lazy stack" macro (appendix A2), the images are registered. We can think of them as a multichannel image in which, for each pixel, the following information is stored: (a) the grey level, $G(0), G(10) \dots G(170)$, for 18 different orientations, (b) 2 or 4 greylevels which - when compared to the greylevel $G(0)$, yield an information concerning whether the c-axis points above or below the thin section, and (c) a grey level indicative of the c-axis inclination w/r to the plane of the thin section.

Additional images may be taken with parallel polarizers to obtain an image of dust and scratches for masking purposes (see later), or one without the thin section in place in order to be able to correct uneven lighting.

Left, from top to bottom:
- 18 rotation images



- 4 tilt images

- 1 circular polarization image

2.3 CALCULATING THE PRIMARY IMAGES

[top](#) / [contents](#) / [section 2](#) / [2.1](#) -- [2.2](#) -- [2.3](#) -- [2.4](#) -- [2.5](#) -- [2.6](#) -- [2.7](#) -- [2.8](#) -- [2.9](#) -- [2.10](#) -- [2.11](#)

Checking the input

To check the orientation of the input stack, the first rotation image, (where rotation = 0°) is colour-coded, using the "Positive LUT" from the NIH Image Macro "Lazy LUT". Dark grains are assigned first order blue, light grains first order yellow. Postprocessing is nice but not necessary. Comparing this image to what can be observed through the microscope one immediately sees if everything is alright or not. - By choosing a negative instead of the positive LUT, quartzite is easily converted into a marble...(see below).

Left, from top to bottom:

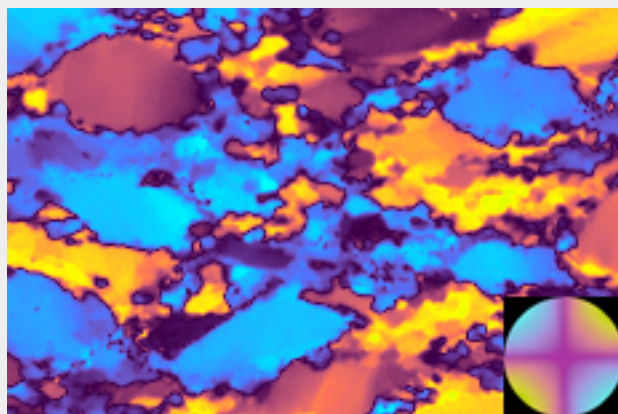
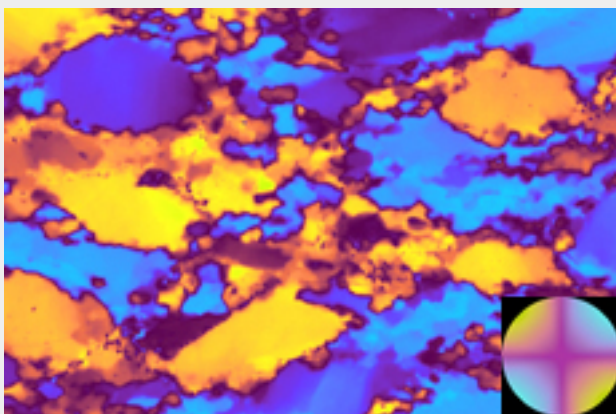
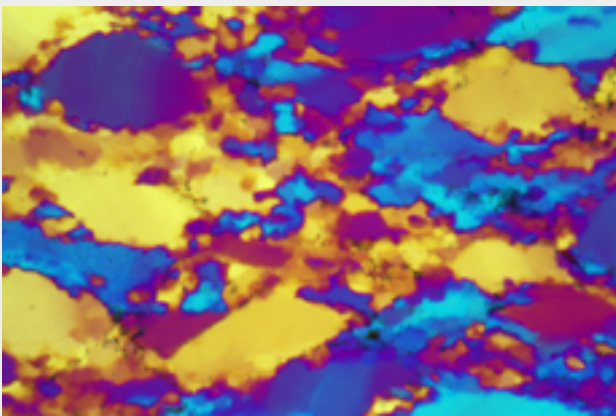
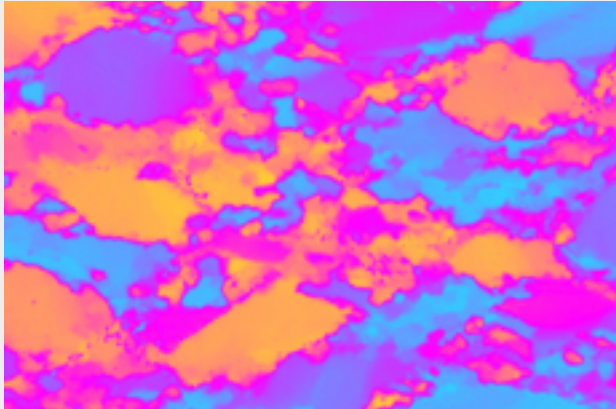
- Colour-coding of the first rotation image, using the positive LUT (see inset) from the "Lazy LUT" macro

- RGB image, as taken through the microscope

- Colour-coded rotation image (same as top) with some additional postprocessing

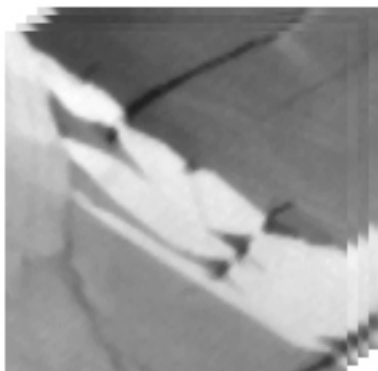
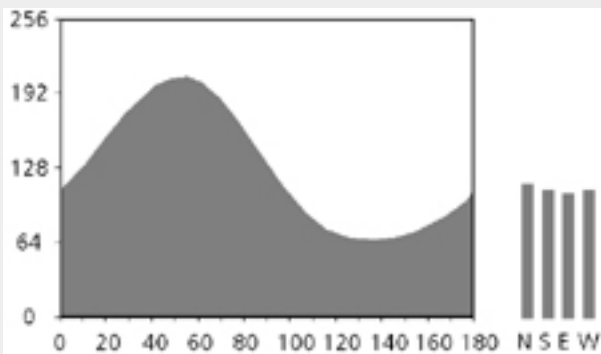
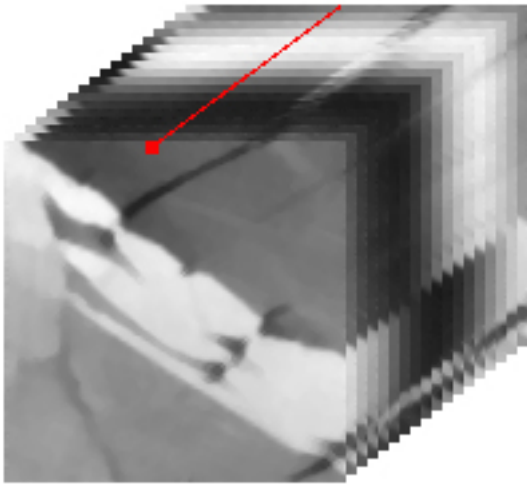
Below:

"Optical phase transformation" using the negative LUT (see inset)



2.4 CALCULATING THE PRIMARY IMAGES

[top](#) / [contents](#) / [section 2](#) / [2.1](#) -- [2.2](#) -- [2.3](#) -- [2.4](#) -- [2.5](#) -- [2.6](#) -- [2.7](#) -- [2.8](#) -- [2.9](#) -- [2.10](#) -- [2.11](#)



Calculation of azimuth, inclination, and error images

For each pixel, the grey levels in channel 1 to 18, determine a discrete optical density function (= inverse of brightness function). By fitting a curve to it (parabolic fit to the five largest and smallest values), the exact maximum and minimum of the curve and the phase angle are calculated. The error is given by the sum of all differences of the actual values to the ideal fit.

Subtracting the minimum of the curve from the maximum yields the amplitude. From the phase angle, the azimuth is calculated, and from the amplitude, a primary inclination between 0° and 90° is derived.

By comparing the grey values of the tilt images with the grey values in the zero rotation image, the tilt-correction is effected. This correction determines if a c-axis points above or below the plane of the thin section, and the primary inclination image is corrected accordingly. The final azimuth and inclination images are derived and saved.

The filename extension "azi" denotes the azimuth image, "inca" denotes that the inclination has been derived from the amplitude of the brightness curve, "incp" denotes that the inclination has been derived from the circular polarization image, "err" denotes the error image (= the inverse of it is the quality image).

Left, from top to bottom:

- Stack of 18 rotation images
- Schematic representation of optical density function from rotation images, i.e, density of a given pixel (red) as function of rotation, and four discrete density values from

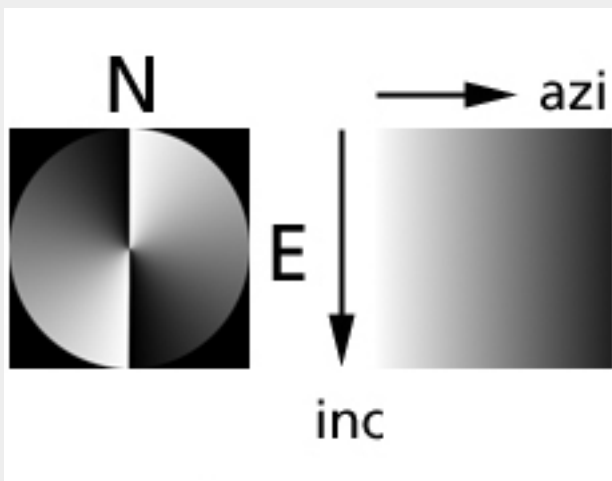
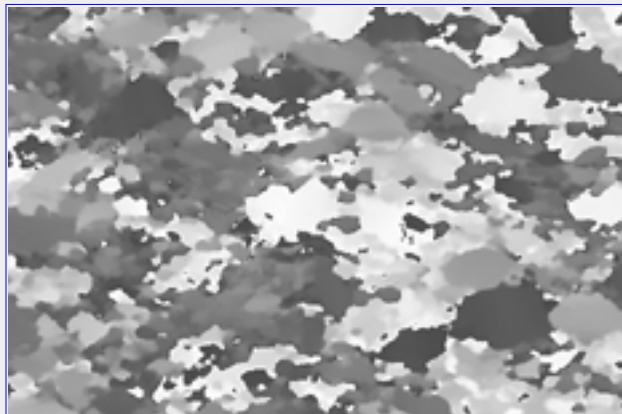


tilt images

- Stack of 4 tilt images

2.5 CALCULATING THE PRIMARY IMAGES

[top](#) / [contents](#) / [section 2](#) / [2.1](#) -- [2.2](#) -- [2.3](#) -- [2.4](#) -- [2.5](#) -- [2.6](#) -- [2.7](#) -- [2.8](#) -- [2.9](#) -- [2.10](#) -- [2.11](#)



The azimuth image

The azimuth of the c-axes refers to the image plane and runs clockwise from the vertical: up (North) is 0° , to the right (East) is 90° , down (South) is 180° . The azimuth file is monochrome (grey).

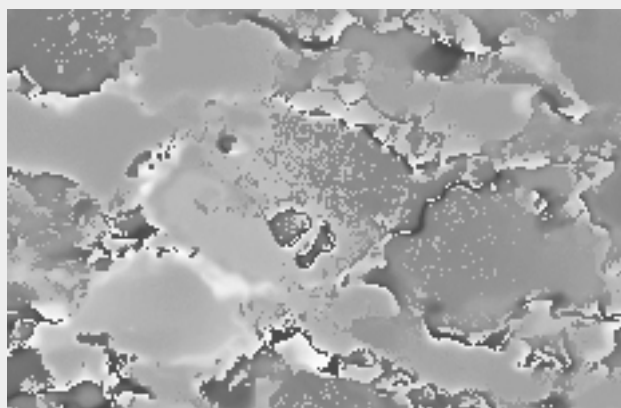
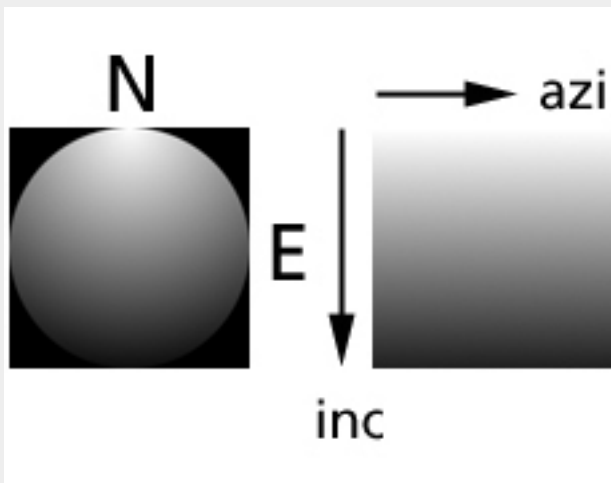
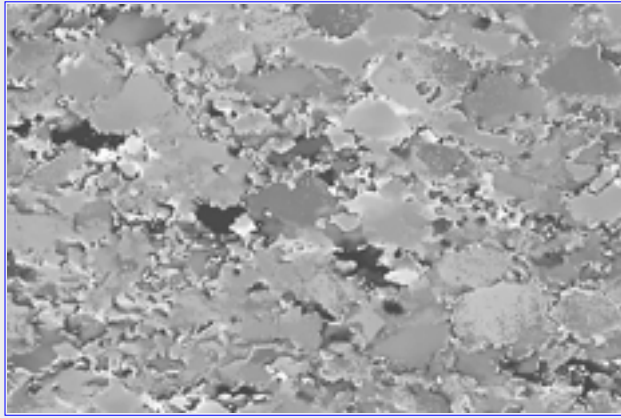
The chipmunk is a little darker than average grey, indicating c-axes striking more than 90° , i.e., NW-SE. Of course, the blue eye ([remember ?](#)) has an azimuth of less than 90° .

Left, from top to bottom:

- Azimuth image of Black Hills quartzite
- stereographic projection and orthogonal representation of look-up table for azimuth image
- the elephantine chipmunk...

2.6 CALCULATING THE PRIMARY IMAGES

[top](#) / [contents](#) / [section 2](#) / [2.1](#) -- [2.2](#) -- [2.3](#) -- [2.4](#) -- [2.5](#) -- [2.6](#) -- [2.7](#) -- [2.8](#) -- [2.9](#) -- [2.10](#) -- [2.11](#)



The inclination image (amplitude)

This inclination image has been derived from the amplitudes of the grey value functions $G(\text{rotation})$ of each pixel ([remember that?](#)).

The inclination of the c-axes refers to the image plane and runs from above the image plane to below: above (Heaven) is 0° , the horizontal is 90° , below (Hell) is 180° . The inclination file is monochrome (grey).

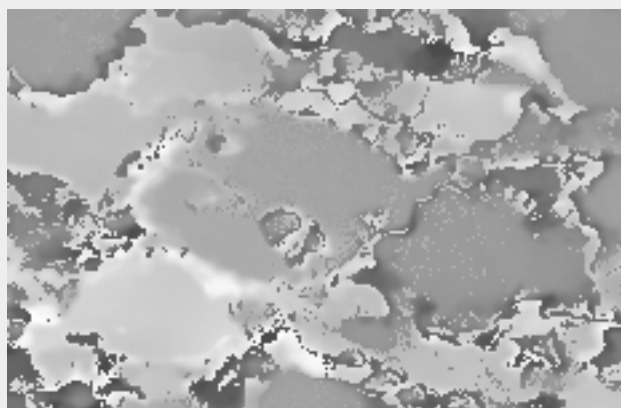
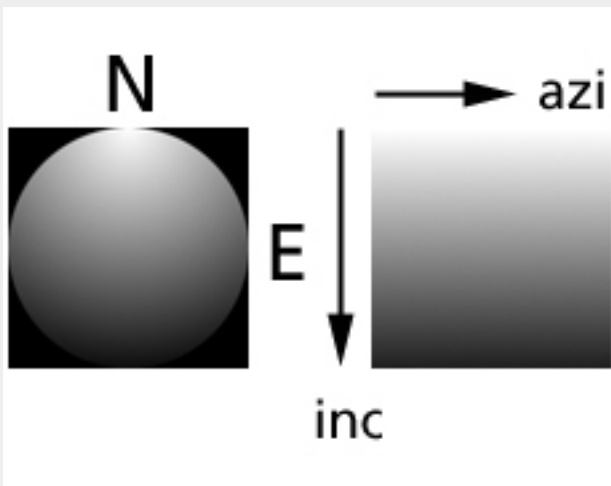
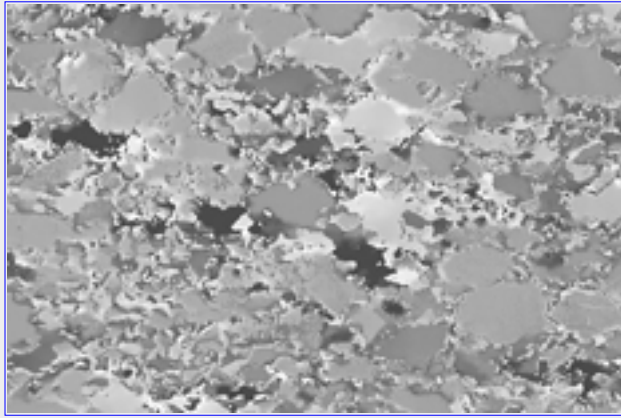
The chipmunk is a little spotty, grading from c-axes pointing above the image plane (lighter) to those pointing below it (darker). The fact that the transition is spotty rather than smooth is an artefact which is brought about by the tilt corrections for c-axes. There are many reasons why these artefacts occur: they can usually be traced to a critical c-axis orientation (azimuth around 0° , 90° or 180°), or to dust, inclusions or bubbles on the thin section...

Left, from top to bottom:

- inclination image (inca) of Black Hills quartzite
- stereographic projection (note orientation !) and orthogonal representation of look-up table for inclination image
- the spotty chipmunk...

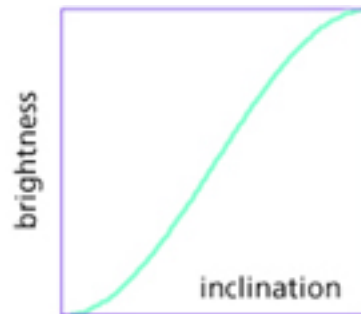
2.7 CALCULATING THE PRIMARY IMAGES

[top](#) / [contents](#) / [section 2](#) / [2.1](#) -- [2.2](#) -- [2.3](#) -- [2.4](#) -- [2.5](#) -- [2.6](#) -- [2.7](#) -- [2.8](#) -- [2.9](#) -- [2.10](#) -- [2.11](#)



The inclination image (circular polarization)

This inclination image is derived from the circular polarization image. The function relating the brightness of the image to the inclination of the c-axis is the sine-square (as shown below). Through this dependence (and the scanner calibration) one can derive the inclination directly from the grey values in the polarization image.



As before, the inclination of the c-axes refers to the image plane and runs from above the image plane to below: above (Heaven) is 0° , horizontal is 90° , below (Hell) is 180° . The inclination file is monochrome (grey).

If the circular polarization image and the rotation images are perfectly calibrated, the inclination images inca (from amplitude) and incp (from circular polarization) should be exactly the same.

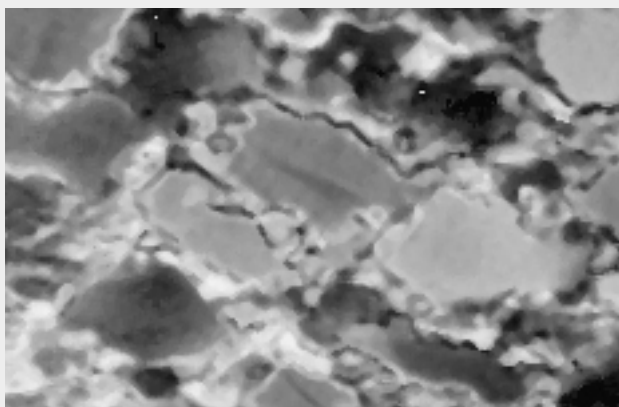
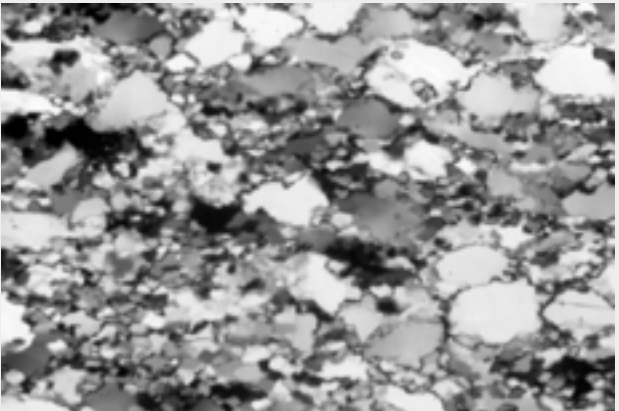
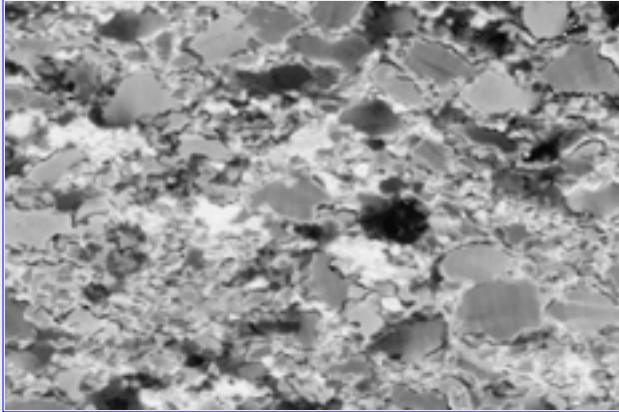
For the same reasons as before, the chipmunk is a little spotty,...

Left, from top to bottom:

- inclination image (incp) of Black Hills quartzite
- stereographic projection (note orientation !) and orthogonal representation of look-up table for inclination image
- the spotty chipmunk...

2.8 CALCULATING THE PRIMARY IMAGES

[top](#) / [contents](#) / [section 2](#) / [2.1](#) -- [2.2](#) -- [2.3](#) -- [2.4](#) -- [2.5](#) -- [2.6](#) -- [2.7](#) -- [2.8](#) -- [2.9](#) -- [2.10](#) -- [2.11](#)



The error image

There are a number of causes that lead to the errors associated with the curve fitting of the brightness function:

- the inclination itself: 0° and 180° inclinations tend to have larger errors than 90° inclinations (compare error image and circular polarization image, left)
- the superposition of two differently oriented grains along oblique grain boundaries
- the presence of biaxial minerals such as feldspar...etc.

Taking the inverse of the error image allows one to discuss the so-called quality image...

Left, from top to bottom:

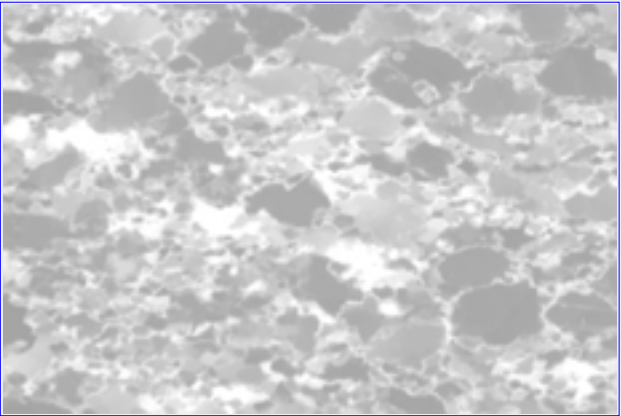
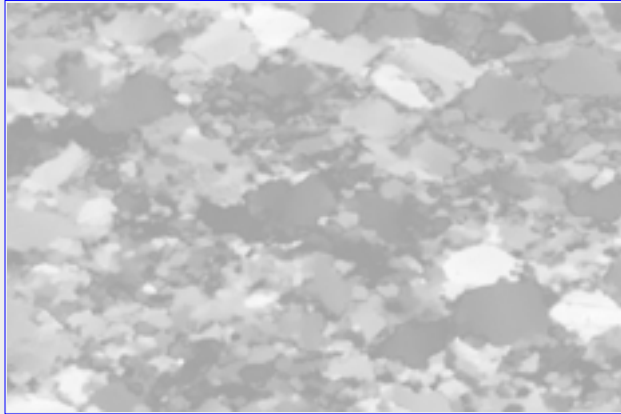
- error image of Black Hills quartzite (black = large error, white = small error)

- circular polarization image of Black Hills quartzite

- the faulty chipmunk... (black = large error, white = small error)

2.9 CALCULATING THE PRIMARY IMAGES

[top](#) / [contents](#) / [section 2](#) / [2.1](#) -- [2.2](#) -- [2.3](#) -- [2.4](#) -- [2.5](#) -- [2.6](#) -- [2.7](#) -- [2.8](#) -- [2.9](#) -- [2.10](#) -- [2.11](#)



The misorientation images

In the two-dimensional case of optical c-axes, the misorientations are defined by the angular difference, either between a given axis and a constant reference direction ("global" misorientation) or between a given axis and its neighbours ("local" misorientation or orientation gradient).

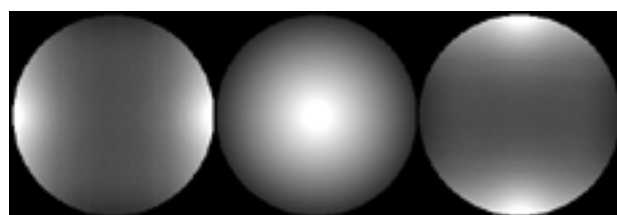
Here, "global" misorientation images are shown. They are referred to as principal orientation images because they show misorientations with respect to three principal directions: North, East, Heaven. It is possible to calculate other misorientation images with respect to any other reference directions (for example, see section 3.8).

Left, from top to bottom:

- Misorientation with respect to East
- Misorientation with respect to Heaven
- Misorientation with respect to North

Below:

- stereographic projection of look-up table for misorientation images



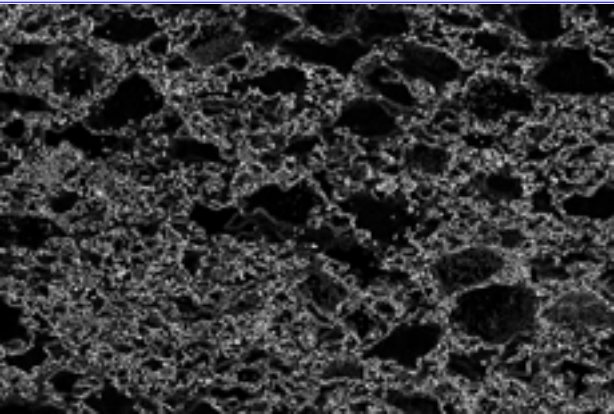
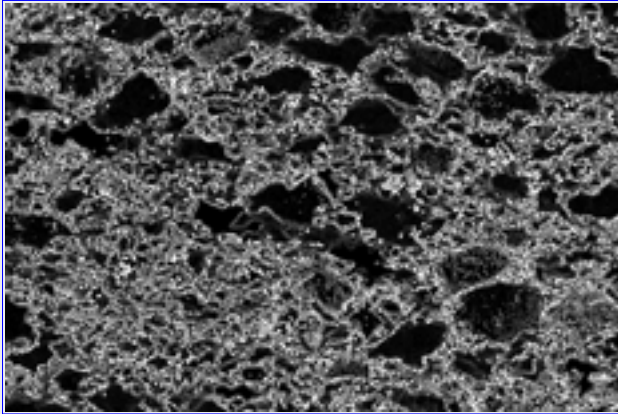
misE

misH

misN

2.10 CALCULATING THE PRIMARY IMAGES

[top](#) / [contents](#) / [section 2](#) / [2.1](#) -- [2.2](#) -- [2.3](#) -- [2.4](#) -- [2.5](#) -- [2.6](#) -- [2.7](#) -- [2.8](#) -- [2.9](#) -- [2.10](#) -- [2.11](#)



The orientation gradient images

In the two-dimensional case of optical c-axes, the misorientations are defined by the angular difference, either between a given axis and a constant reference direction ("global" misorientation) or between a given axis and its neighbours ("local" misorientation or orientation gradient).

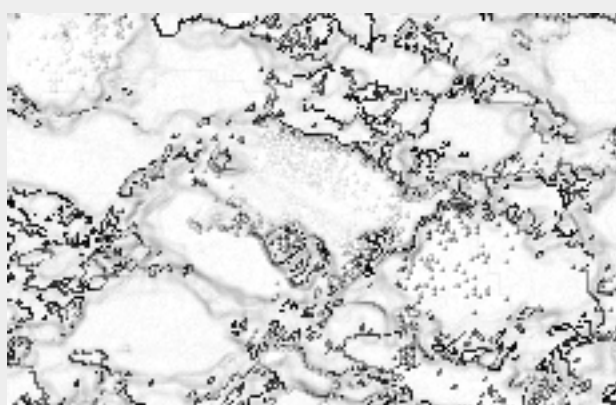
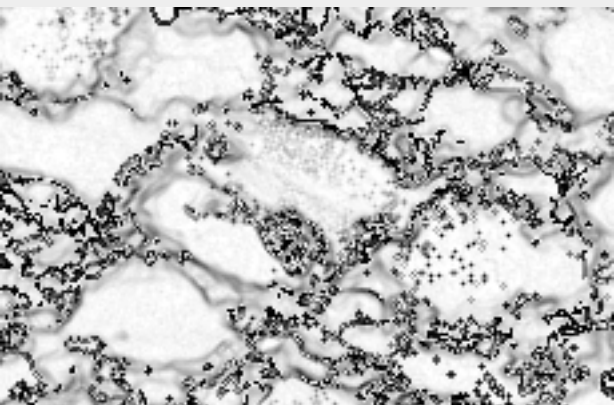
Here the orientation gradient images are shown, they were calculated taking either 4 or 2 neighbours into consideration. Because of its spotty inclinations, the chipmunk also appears quite mottled on the orientation gradient image.

Left, from top to bottom:

- Orientation gradient, 4 neighbours
- Orientation gradient, 2 neighbours
- Orientation gradient around chipmunk, 4 neighbours

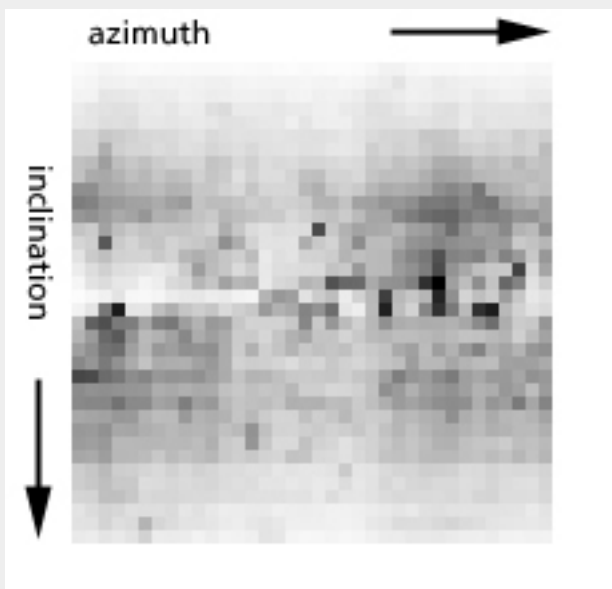
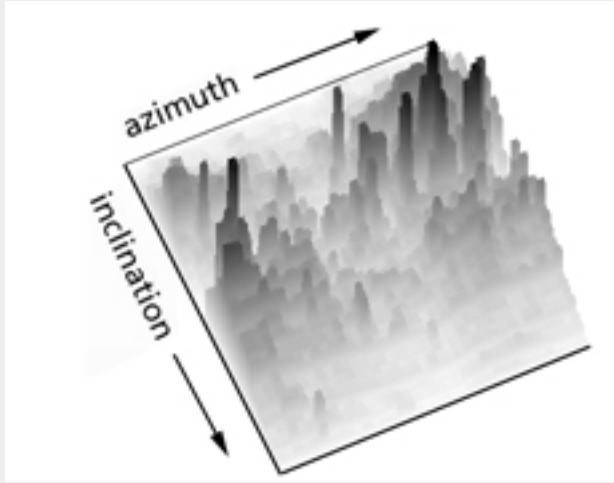
Below:

- Orientation gradient around chipmunk, 2 neighbours



2.11 CALCULATING THE PRIMARY IMAGES

[top](#) / [contents](#) / [section 2](#) / [2.1](#) -- [2.2](#) -- [2.3](#) -- [2.4](#) -- [2.5](#) -- [2.6](#) -- [2.7](#) -- [2.8](#) -- [2.9](#) -- [2.10](#) -- [2.11](#)



The c-axis polefigure

One of the beauties of CIP orientation imaging is that one can easily obtain c-axis pole figures from the azimuth and inclination files. The grey values of those two files are collected into a 2-D histogram, using a class width (or bin size) of 5° by 5° and projected onto a stereoplot. Such a pole figure is area weighted, i.e., volume weighted, and is thus directly comparable to x-ray texture goniometry data.

The statistics are the same as in texture goniometry: if only a few grains are present in a given image, the texture index (i.e., the c-axis maximum) will go up, irrespective of the image size.

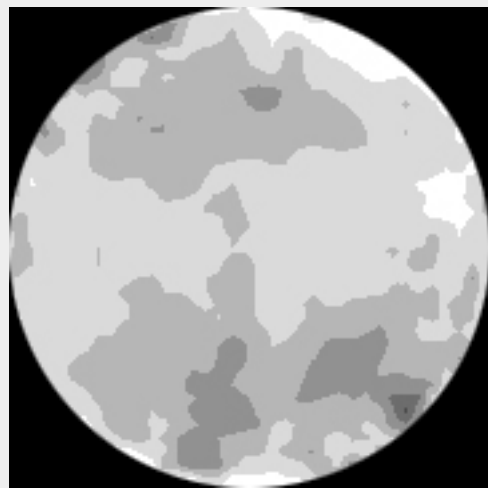
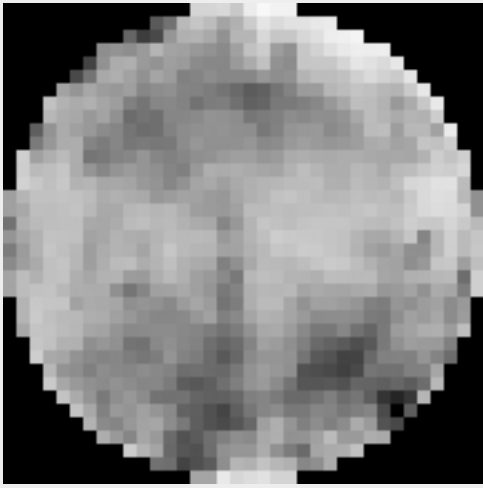
By selecting certain regions of interest (according to grain size or given crystallographic directions) one can also obtain partial pole figures.

Left, from top to bottom:

- oblique view of 2-D histogram of azimuth and inclinations
- grey value representation of 2-D histogram of azimuth and inclinations
- stereographic projection of 2-D histogram

Below:

- smoothed and contoured stereoplot of c-axis orientations.



3 VISUALIZING ORIENTATIONS

[top](#) / [contents](#) / [section3/](#) pages -- [3.1](#) -- [3.2](#) -- [3.3](#) -- [3.4](#) -- [3.5](#) -- [3.6](#) -- [3.7](#) -- [3.8](#) -- [3.9](#)

[3.1](#) Colour-coding the azimuth image

[3.2](#) Colour-coding the inclination image

[3.3](#) Checking the inclination image (cirpol)

[3.4](#) The c-axis orientation image (COI)

[3.5](#) Various colour look-up tables (CLUTs) for the c-axis orientation image

[3.6](#) Making masks from the error and background images

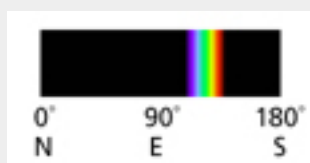
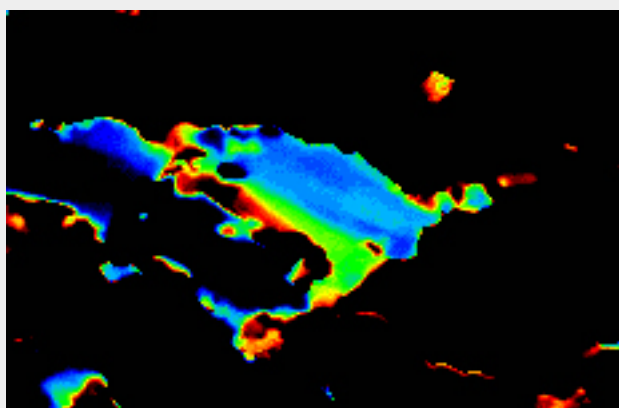
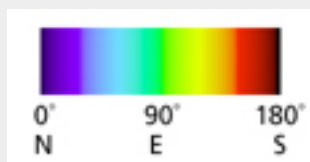
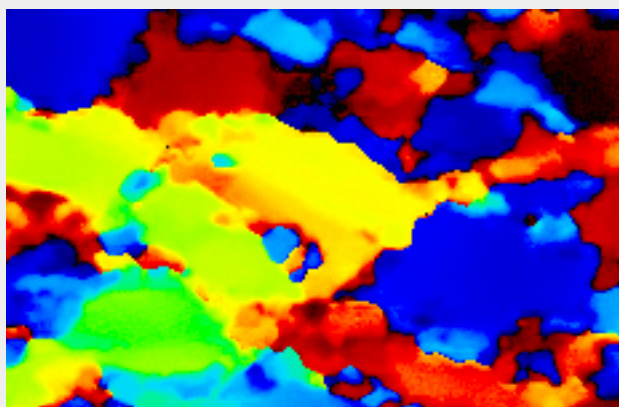
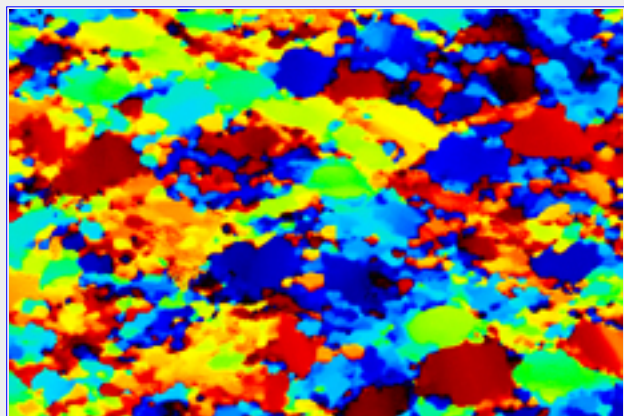
[3.7](#) Principal misorientation images

[3.8](#) Misorientation with respect to reference direction

[3.9](#) Analysis of orientation gradient images

3.1 VISUALIZING ORIENTATIONS

[top](#) / [contents](#) / [section3/](#) pages -- [3.1](#) -- [3.2](#) -- [3.3](#) -- [3.4](#) -- [3.5](#) -- [3.6](#) -- [3.7](#) -- [3.8](#) -- [3.9](#)



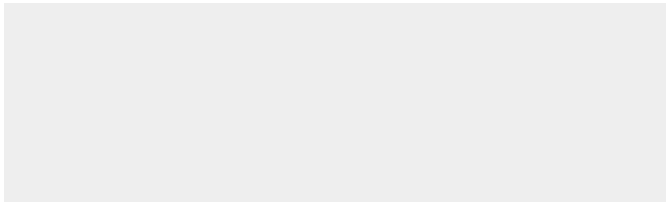
Colour-coding the azimuth image

The [azimuth image](#) (see section 2.5) is a monochrome image whose grey values correspond to the azimuths of the c-axes at each pixel (see sign convention, section 1). Using NIH Image (or Scion Image) and the Lazy LUT macro ("spectrum black-blue-red-black", see appendix 2), the azimuth image can be colour-coded in terms of the visible spectrum of light: blue (short wavelengths) for low, red (long wavelengths) for high values.

Using a 1-D Look-up table (LUT), the grey values can be colour-coded. To achieve an interpretable colour-coding, one may want to design LUTs that are not provided by NIH Image. Here we use a 1-D spectrum LUT which grades into black at the lower and upper end. If the LUT covers the entire range between 0° and 180° , the azimuths in the N-S direction (0° or 180°) are rendered black, in NE-SW direction (45°) blue, in E-W direction (90°) green, and in NW-SE direction (135°) red. In order to highlight small, local azimuthal differences, the LUT can be compressed, in the example shown, the spectrum is compressed between 120° and 150° , green indicating the central value (135°).

The 1-D LUT can be represented as stereographic colour look-up table (CLUT). Note that this CLUT is not the same as the 2-D spectrum CLUT for c-axis orientation images (see CLUT library), since there is no variation of colour saturation as a function of inclination (i.e. from the center of the stereographic projection of the CLUT to the periphery).

Left, from top to bottom:



- Colour-coded azimuth image of experimentally deformed Black Hills quartzite

- Detail of above using same LUT

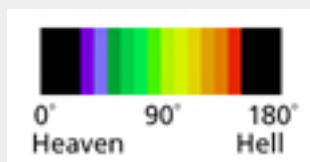
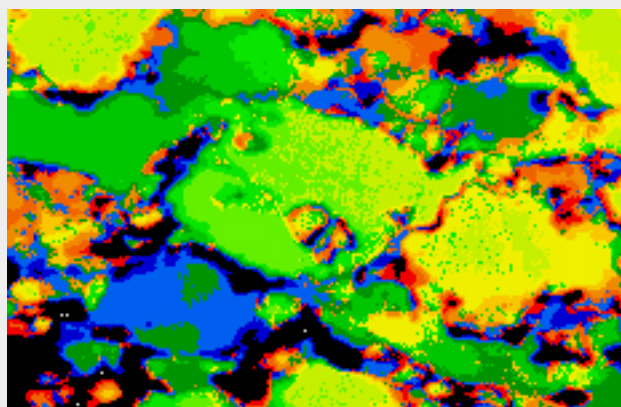
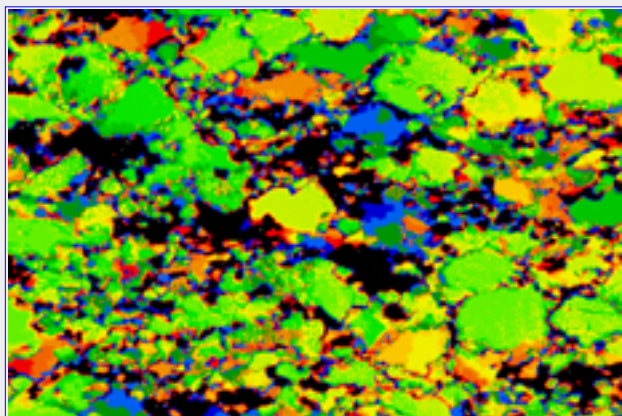
- Same detail using compressed LUT

3.2 VISUALIZING ORIENTATIONS

[top](#) / [contents](#) / [section3/](#) pages -- [3.1](#) -- [3.2](#) -- [3.3](#) -- [3.4](#) -- [3.5](#) -- [3.6](#) -- [3.7](#) -- [3.8](#) -- [3.9](#)

Colour-coding the inclination image

Like the azimuth image, the [inclination image](#) (see section 2.6 or 2.7) is monochrome, the grey values denoting inclinations from 0° to 180° with respect to the image plane (see sign convention, section 1). Using NIH Image (or Scion Image) and the Lazy LUT macro (key B: "INC strips black 30", see appendix 2), the inclination image can be colour-coded in terms of the visible spectrum of light: blue (short wavelengths) for low, red (long wavelengths) for high values, with 10° colour intervals. Using "INC strips black 30" rather than "INC strips" causes inclination in a cone of 30° about the image normal to be rendered black.

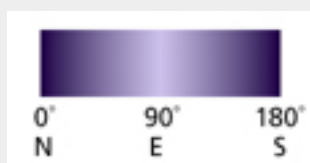
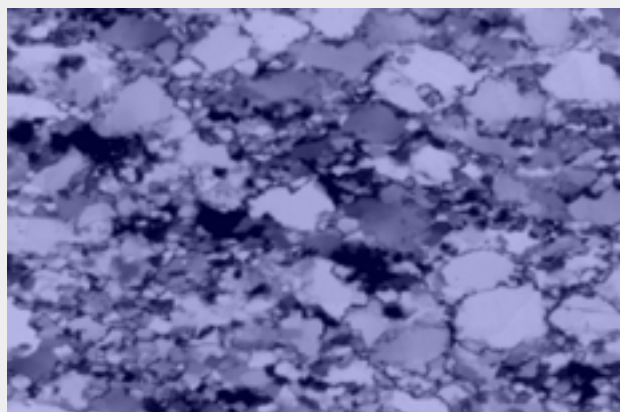
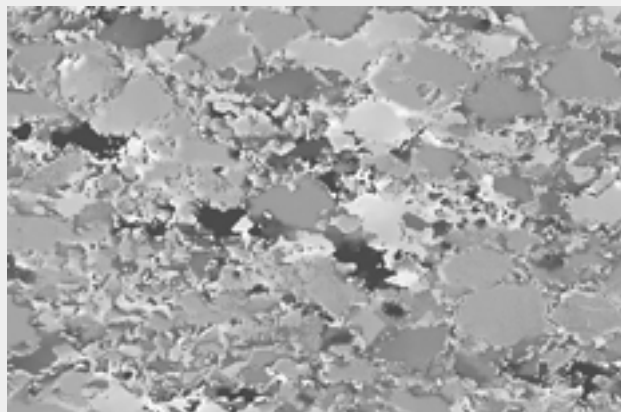


Left, from top to bottom:

- Colour-coded inclination image of experimentally deformed Black Hills quartzite
- Detail of above using same LUT

3.3 VISUALIZING ORIENTATIONS

[top](#) / [contents](#) / [section3/](#) pages -- [3.1](#) -- [3.2](#) -- [3.3](#) -- [3.4](#) -- [3.5](#) -- [3.6](#) -- [3.7](#) -- [3.8](#) -- [3.9](#)



Checking the inclination image (cirpol)

In order to check the calculated inclination image against the circular polarization image, the Lazy LUT macro (key C: "INC to CirPol", see appendix 2) is used. The histogram of the converted inclination image reveal an approximate sine relation between inclination and grey-value (Since NIH Image is based on optical density rather than brightness, the sine relation is inverted). The histogram is indicative of a texture which is random or nearly random with respect to inclination (not necessarily with respect to azimuth).

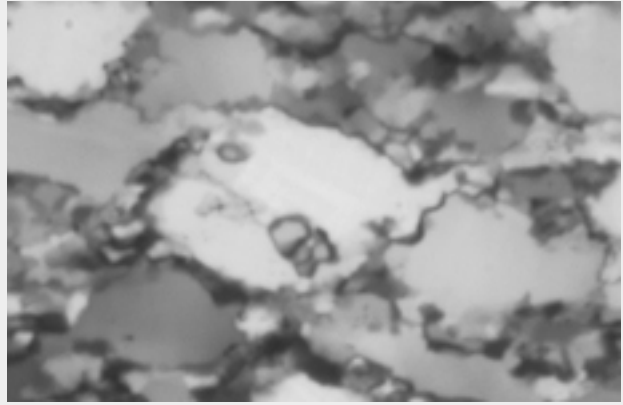
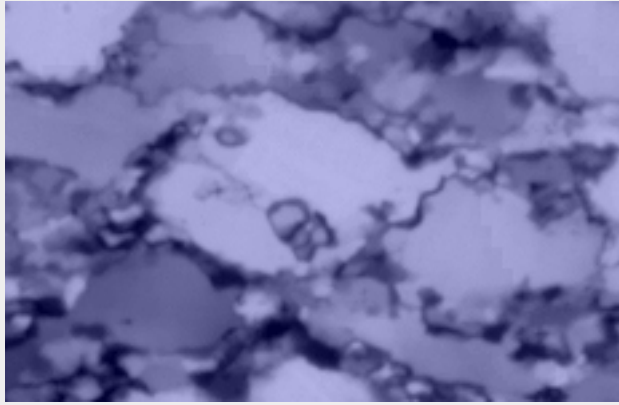


Left, from top to bottom:

- Inclination image (incp) exp. def. Black Hills quartzite
- Inclination image (incp), after applying "INC to CirPol" macro

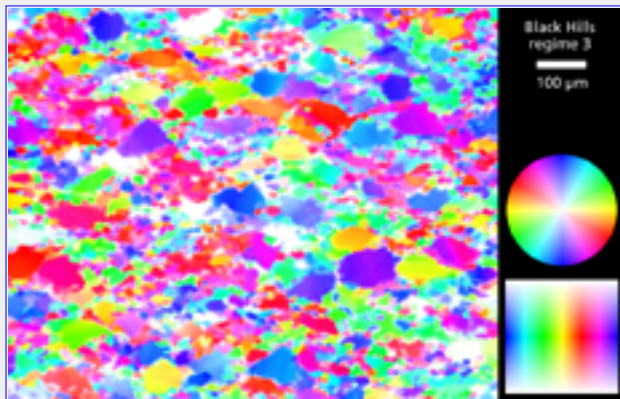
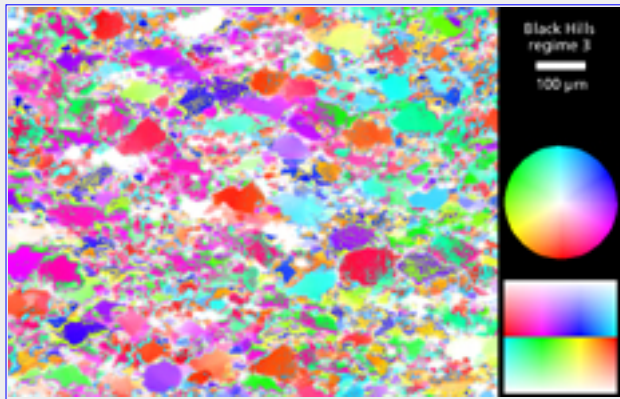
Below, left to right:

- Detail of converted inclination image
- Detail of circular polarization image, for comparison



3.4 VISUALIZING ORIENTATIONS

[top](#) / [contents](#) / [section3/](#) pages -- [3.1](#) -- [3.2](#) -- [3.3](#) -- [3.4](#) -- [3.5](#) -- [3.6](#) -- [3.7](#) -- [3.8](#) -- [3.9](#)



The c-axis orientation image (COI)

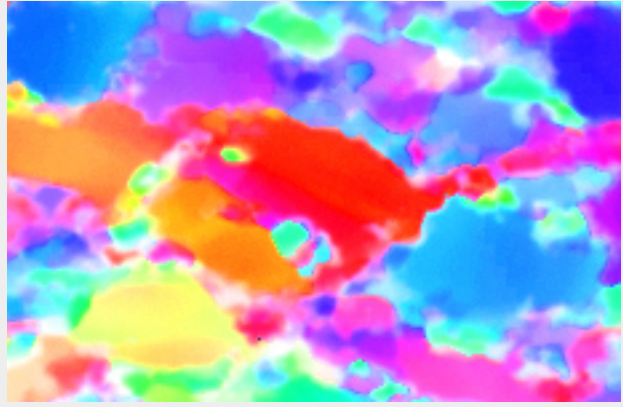
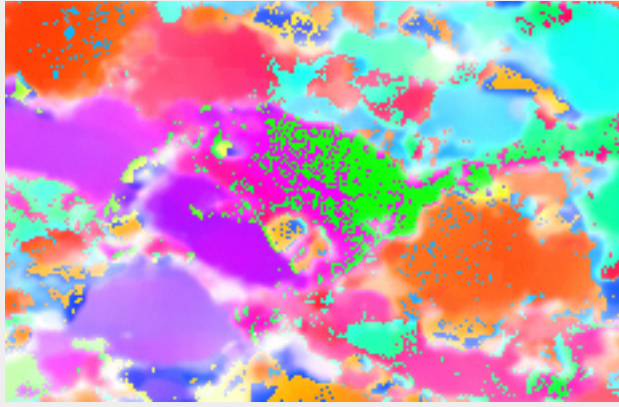
To create a c-axis orientation image (COI), two channels (azimuth and inclination image), and a 2-D colour look-up table (CLUT) are necessary. The CIP-Standard CLUT assigns one unique colour to each of the 180×180 possible orientations. Two problems arise: 1. the CIP-Standard CLUT has a colour discontinuity between $\text{incl}=90^\circ$ and $\text{incl} = 91^\circ$. Thus, axes dipping slightly above and slightly below the image plane appear with a maximum colour contrast (e.g. red-cyan) while in reality the orientational difference is very small. 2. The most critical part in the CIP calculation is the derivation of the correct inclination, i.e., the decision if axes dip above or below the image plane. This step often introduces some noise in the inclination image, causing the corresponding COIs to be spotted. Both of these problems are overcome if the symmetric CIP-Spectrum CLUT is used.

Left:

Two c-axis orientation images (COIs) of experimentally deformed Black Hills quartzite, using the CIP-Standard and the CIP-Spectrum CLUT

Below:

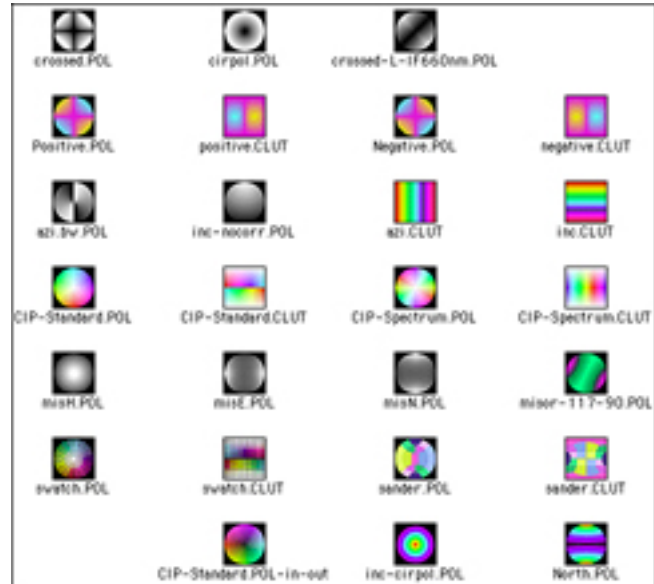
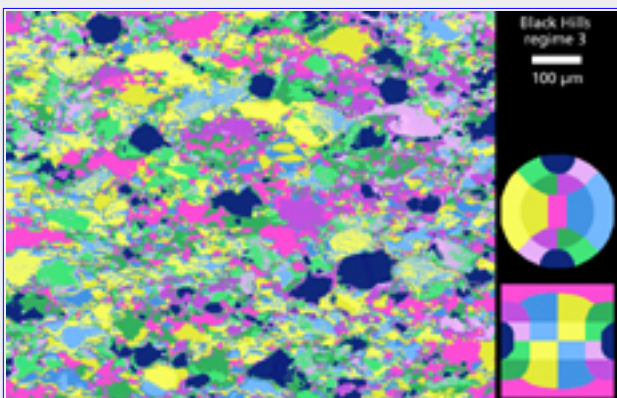
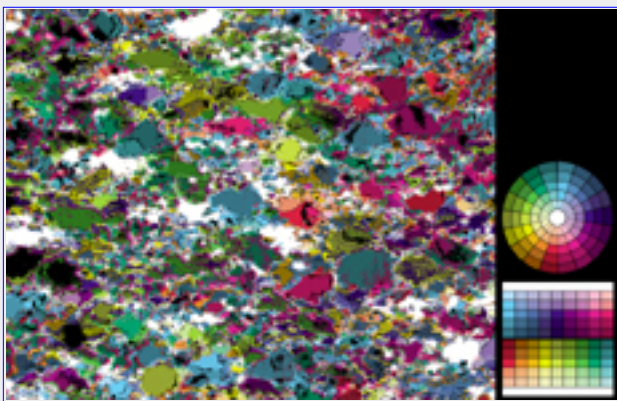
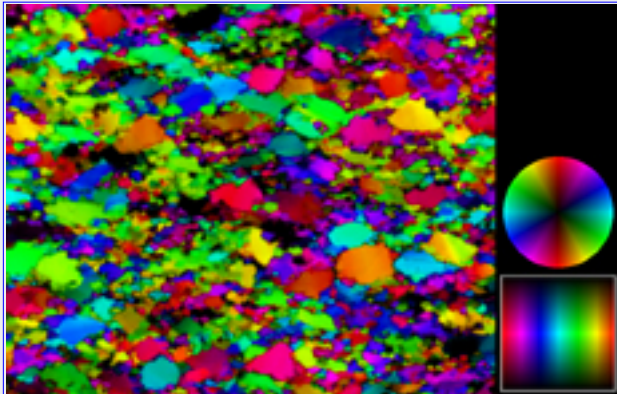
- Detail of COIs



3.5 VISUALIZING ORIENTATIONS

[top](#) / [contents](#) / [section3/](#) pages -- [3.1](#) -- [3.2](#) -- [3.3](#) -- [3.4](#) -- [3.5](#) -- [3.6](#) -- [3.7](#) -- [3.8](#) -- [3.9](#)

Various colour look-up tables (CLUTs) for the c-axis orientation image

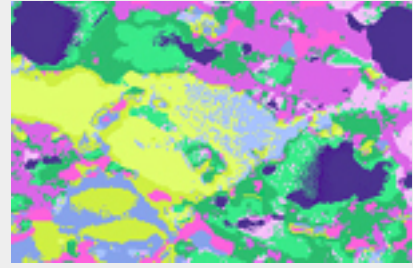
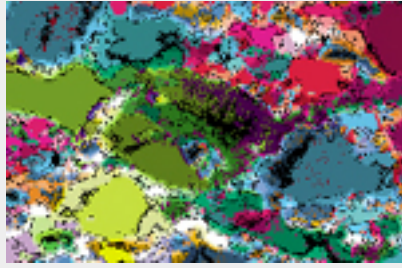
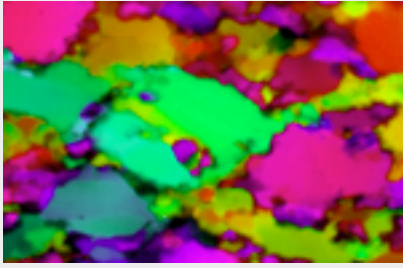


In order to highlight the characteristics of a given microstructure, new CLUTs have to be designed. Here a three examples are shown:

1. inverted CIP-Spectrum.CLUT: a colour-coding which assigns black (rather than white) to inclinations $0^{\circ}/180^{\circ}$.
Suggestion: Use Photoshop and montages of COIs with the appropriate CLUT or POL representations and manipulate the colour-coding by applying the "Adjust...Hue/Saturation" function.
2. swatch.CLUT: the message here: one shouldn't leave black lines in the CLUT
3. sander.CLUT: classification of c-axis orientations into orientation domains that would be preferred for different glide systems in quartz

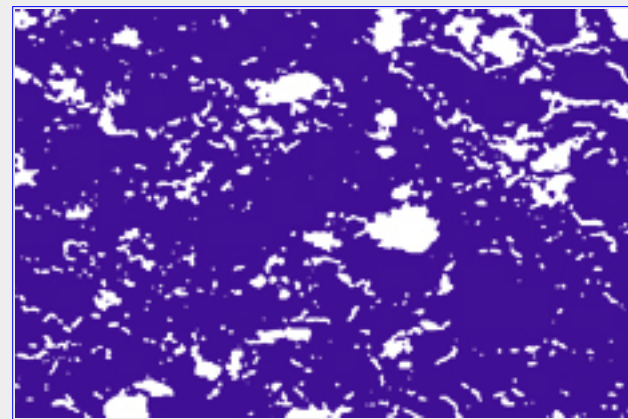
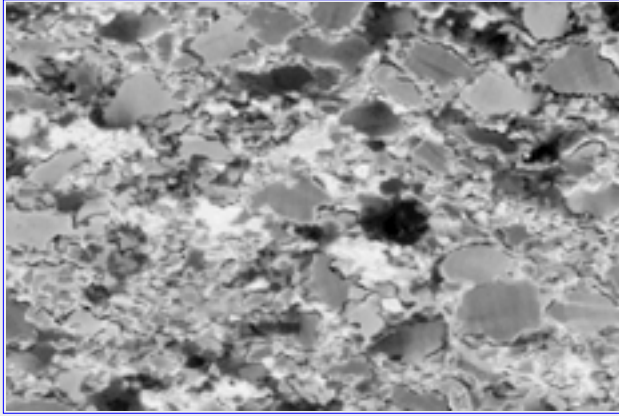
Left: colourcoding with different CLUTs

Below: how to turn chipmunks into frogs, toads and spotty twits



3.6 VISUALIZING ORIENTATIONS

[top](#) / [contents](#) / [section3/](#) pages -- [3.1](#) -- [3.2](#) -- [3.3](#) -- [3.4](#) -- [3.5](#) -- [3.6](#) -- [3.7](#) -- [3.8](#) -- [3.9](#)



Making masks from the error and background images

In order to select certain data from a given c-axis orientation image, it may be necessary to mask the COIs. Masks may be derived in a number of way, here the design of an error and scratch mask is shown. On the basis that non-uniaxial minerals yield high errors, an error mask may help to eliminate feldspar grains form the analysis. For CIP, the masking part has to be non-zero (here=black).

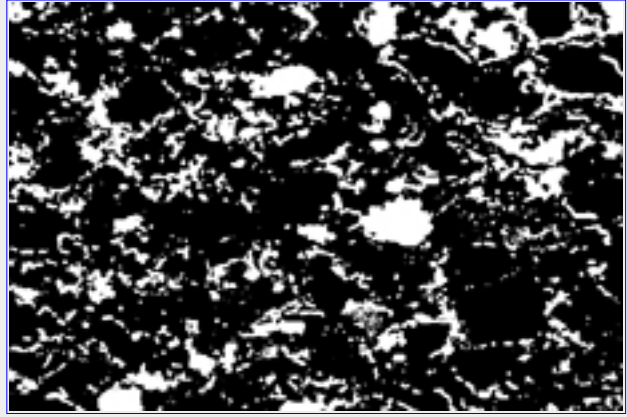
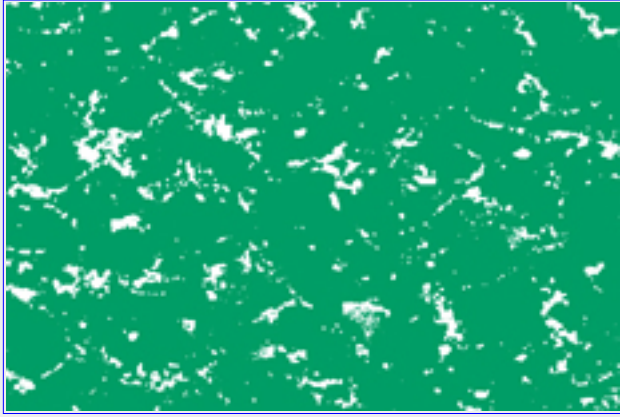
A mask blocking out sites with high CIP errors is obtained by thresholding the calculated error image. For a dust&scratch mask, a plane polarized image of the thin section is recorded. Scratches, holes, glue drops, dust particles, grinding powder, general dirt, etc. appear black and can be thresholded. (A further use fo this this type of background image is to correct for uneven lighting.)

Left, from top to bottom:

- error image
- thresholded error image
- thresholded dust&scartch mask

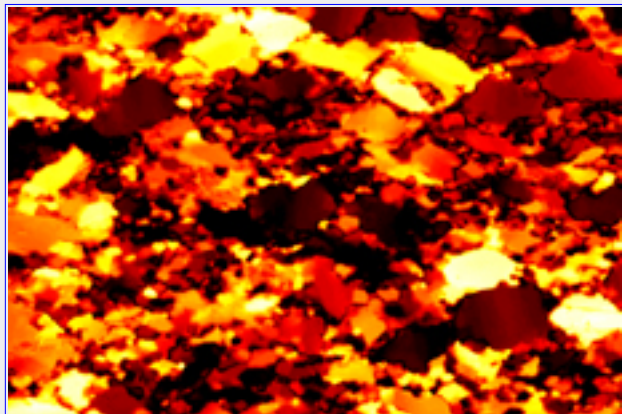
Below:

- combined error and dirt mask



3.7 VISUALIZING ORIENTATIONS

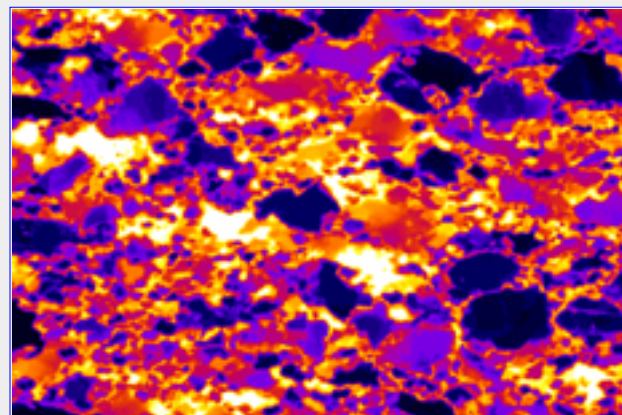
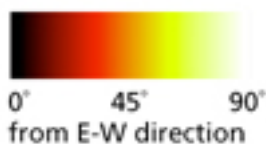
[top](#) / [contents](#) / [section3/](#) pages -- [3.1](#) -- [3.2](#) -- [3.3](#) -- [3.4](#) -- [3.5](#) -- [3.6](#) -- [3.7](#) -- [3.8](#) -- [3.9](#)



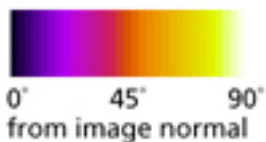
Principal misorientation images

The principal misorientation images with respect to North ([misN](#)), East ([misE](#)), Heaven ([misH](#)) (see section 2.9) are monochrome images; here they have been colour-coded, using three different (1-D) look-up tables (LUTs) provided by NIH Image.

Fire 1 for misN



Fire 2 for misE



Ice for misH

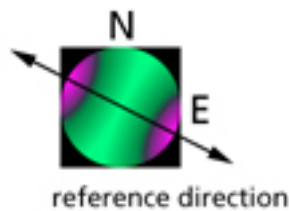
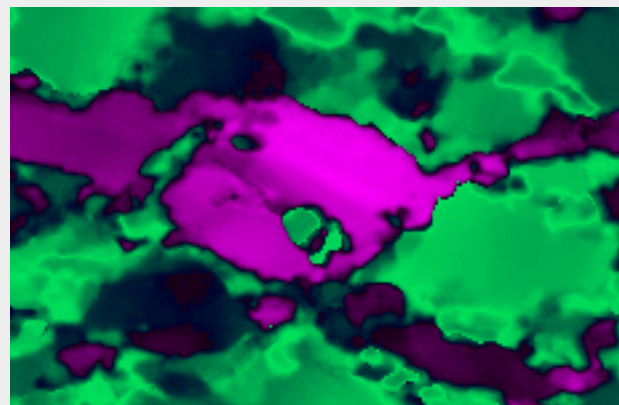
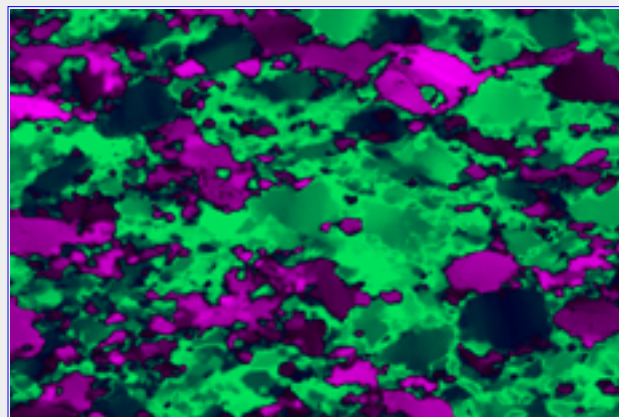


3.8 VISUALIZING ORIENTATIONS

[top](#) / [contents](#) / [section3/](#) pages -- [3.1](#) -- [3.2](#) -- [3.3](#) -- [3.4](#) -- [3.5](#) -- [3.6](#) -- [3.7](#) -- [3.8](#) -- [3.9](#)

Misorientation with respect to reference direction

Misorientation images can be calculated with respect to any direction; here, for example, the average c-axis orientation of the chipmunk is taken as the reference direction ($azi=117$, $inc=90$). Using NIH Image (or Scion Image) and the Lazy LUT macro (key M: "Misor LUT 45° =black", see appendix 2), the image is colour-coded. In this manner the misorientation of the grains surrounding the chipmunk can be observed: orientations within a 45° cone appear purple, outside the cone green.

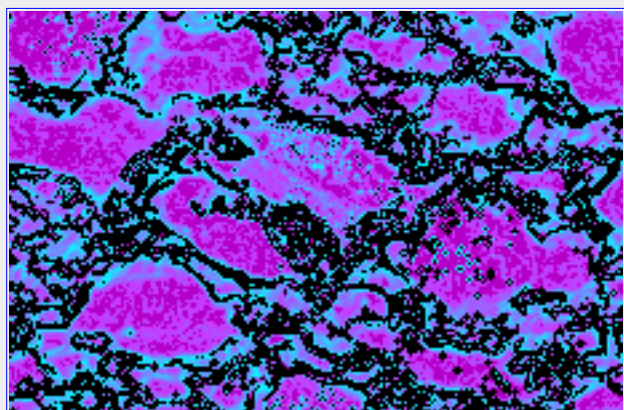
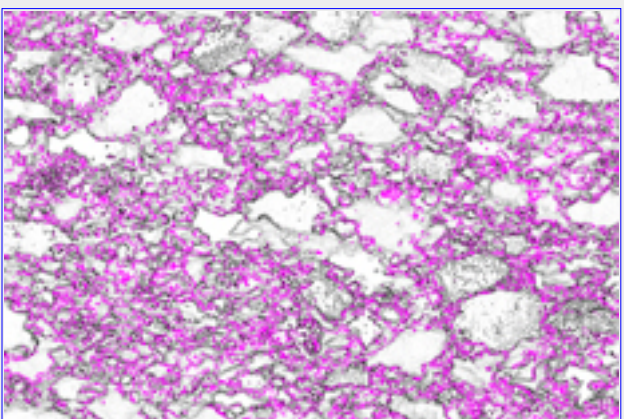
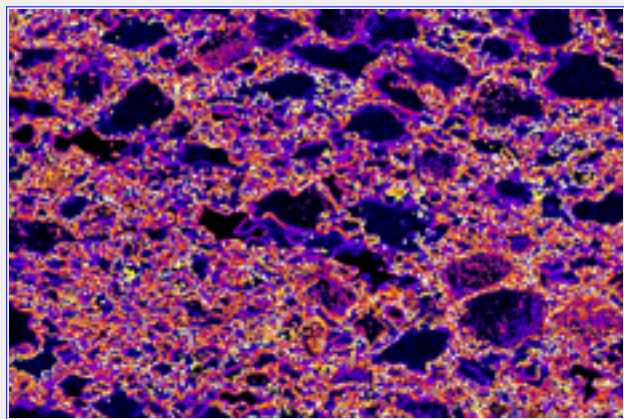


Left, from top to bottom:

- misorientation image with respect to reference direction 117/90
- colour-coded misorientation image
- Detail of colour-coded misorientation image

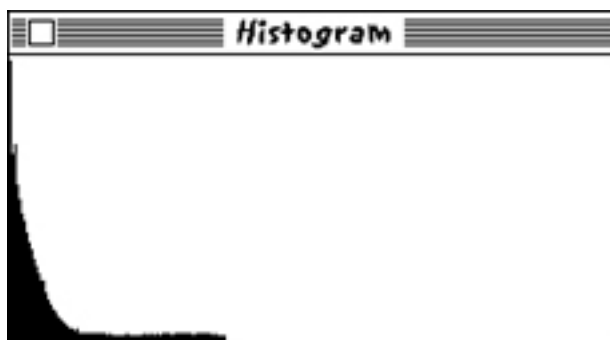
3.9 VISUALIZING ORIENTATIONS

[top](#) / [contents](#) / [section3/](#) pages -- [3.1](#) -- [3.2](#) -- [3.3](#) -- [3.4](#) -- [3.5](#) -- [3.6](#) -- [3.7](#) -- [3.8](#) -- [3.9](#)



Analysis of orientation gradient images

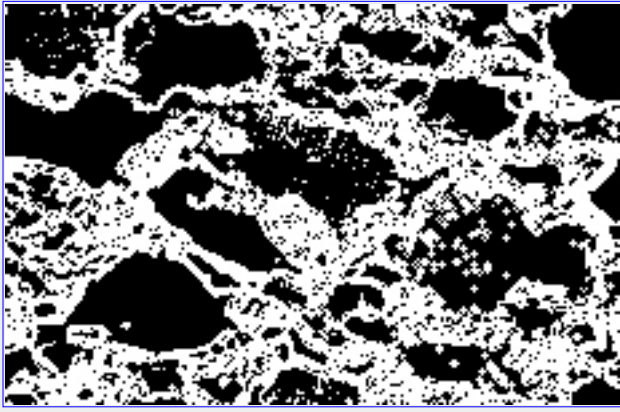
The orientation gradient image (see section 2.10) is a monochrome image and can be colour-coded by any suitable 1-D LUTs (as for example Fire 2 of NIH Image). Using NIH Image (or Scion Image) and the Lazy LUT macro (key E: "EDG2 & EDG4 -> histo", see appendix 2) twice, the orientation gradient image is pre-processed (angles $> 90^\circ$ converted to $< 90^\circ$)



Applying key K: "Contrast low edges", and choosing 45° , edges $> 45^\circ$ are rendered a tasteful lilac, angles between 0° and 45° are contrast-enhanced.

Using key U: "Colour edges", and a suitable range of angles (here 2° - 12°), that interval is colour-coded, grading from purple (min.angle) to cyan (max.angle).

Thresholding the orientation gradient image at a low value such as would be considered compatible with orientation variation within one grain, contiguous regions of constant c-axis orientation, i.e., orientationally coherent grains are detected.



Left, from top to bottom:

- colour-coded orientation gradient image (LUT=Fire2)
- orientation gradient image, angles $<45^\circ$ enhanced, angles $>45^\circ$ lilac
- orientation gradient image, range 2° - 10° enhanced
- orientation gradient image, values $< 12^\circ$ black

4 ORIENTATION IMAGES OF EXPERIMENTALLY DEFORMED ROCKS

[top](#) / [contents](#) / [section 4](#) / pages -- [4.1](#) -- [4.2](#) -- [4.3](#) -- [4.4](#) -- [4.5](#) -- [4.6](#) -- [4.7](#)

[4.1](#) Starting material: Black Hills quartzite and Heavitree quartzite

[4.2](#) Regime 1, 2 and 3 of dynamic recrystallization

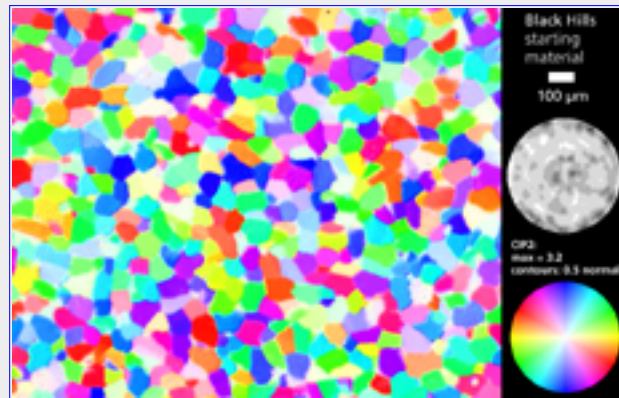
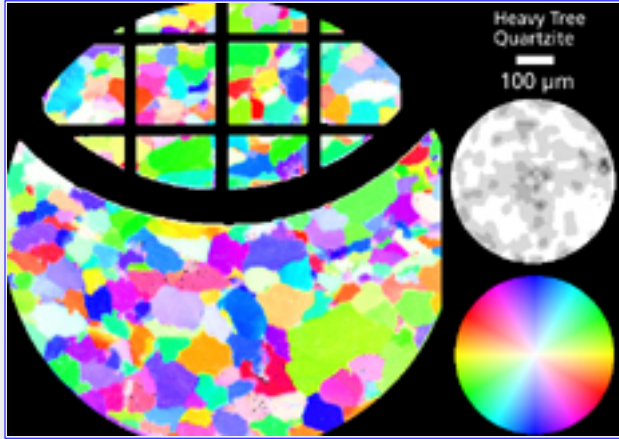
[4.3](#) Partial textures of regime 1, 2 and 3 of dynamic recrystallization

[4.4](#) Annealed microstructures of regime 1, 2 and 3 of dynamic recrystallization

[4.5](#) More detail on regime 3 of dynamic recrystallization

[4.6](#) Making use of sample heterogeneity

[4.7](#) Dynamic recrystallization of quartzite along deformation gradient



Starting material: Black Hills quartzite and Heavitree quartzite

Heavitree quartzite: Non-porous quartzite, with ~1% impurities, and equant grains with average diameter ~200 μm . Diagenetic overgrowths visible.

Black Hills quartzite: Quartzite with up to 1% porosity and very few impurities. Equant grains have an average diameter of ~100 μm .

Here, the input images were taken with a rotating microscope stage and fixed polarizers and lambda plate (rather than fixed stage and rotating polarizers and lambda plate). This is why only a central portion of the image can be used. The Heavitree quartzite was one of the first c-axis orientation images (COIs) calculated for this type of input. For rematching purposes, a TEM holder was placed on the thin section. This, however proved to be unnecessary. Using NIH Image (or Scion Image) and the Lazy stack macro (see appendix 2), the input can be rematched easily.

Left, from top to bottom:

- Heavitree quartzite, undeformed, average grain diameter approx. 300 μm

- Black Hills quartzite, undeformed, average grain diameter approx. 100 μm

4.2 ORIENTATION IMAGES OF EXPERIMENTALLY DEFORMED ROCKS

[top](#) / [contents](#) / [section 4](#) / pages -- [4.1](#) -- [4.2](#) -- [4.3](#) -- [4.4](#) -- [4.5](#) -- [4.6](#) -- [4.7](#)

Regime 1, 2 and 3 of dynamic recrystallization

Quartz aggregates (Black Hills quartite), experimentally deformed by dislocation creep, exhibit three distinct microstructural and mechanical regimes, dependent on temperature and strain rate, characterized by different mechanisms of dynamic recrystallization: regime 1 at low T is characterized by little or no dislocation climb and recrystallization involves grain boundary migration; regime 2 at intermediate T involves easy dislocation climb and recrystallization by progressive subgrain rotation; and regime 3 at high T is also characterized by easy climb but recrystallization occurs mostly by grain boundary migration (Tullis & Heilbronner, 1999).

Experimental conditions:

regime 1:

- $p_c = 1.5$ GPa
- $T = 850^\circ\text{C}$
- strain rate = 10^{-5} s $^{-1}$
- as-is

regime 2:

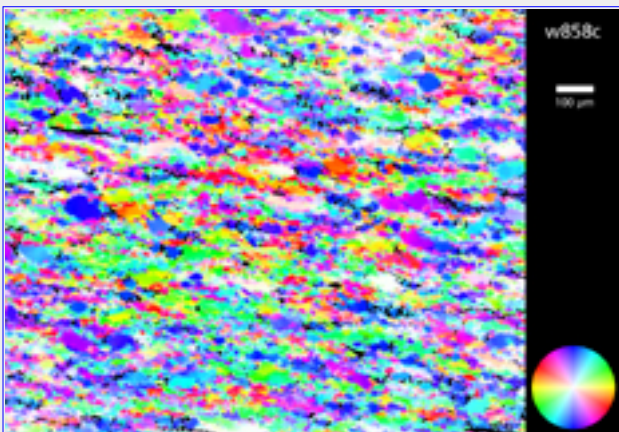
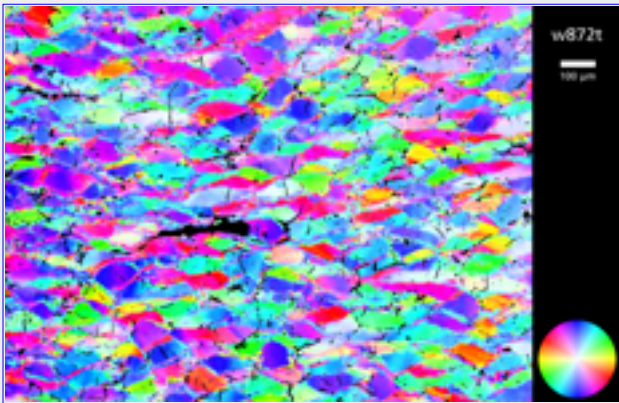
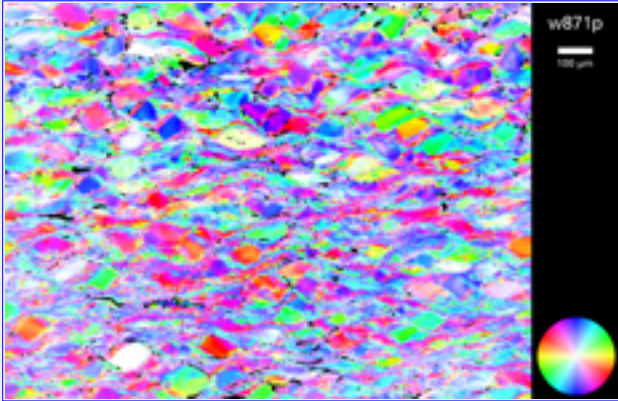
- $p_c = 1.5$ GPa
- $T = 900^\circ\text{C}$
- strain rate = 10^{-5} s $^{-1}$
- 0.17 wt% water added

regime 3:

- $p_c = 1.5$ GPa
- $T = 900^\circ\text{C}$
- strain rate = 10^{-6} s $^{-1}$
- 0.17 wt% water added

Left, from top to bottom:

- Regime 1 (w875)



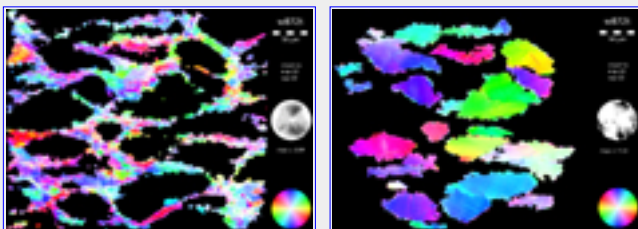
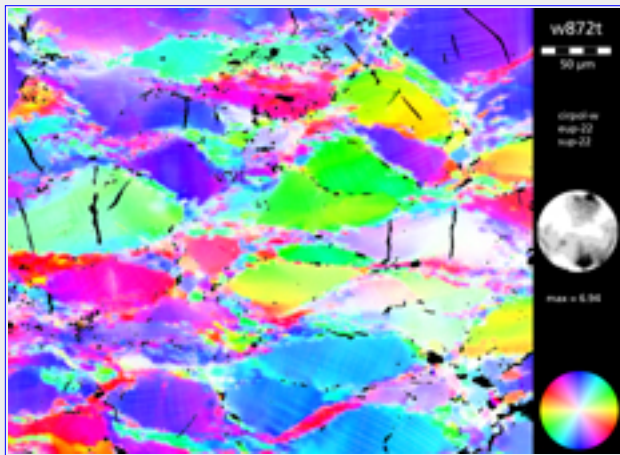
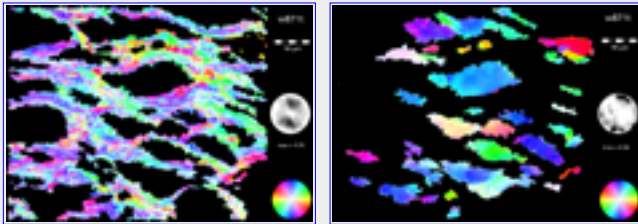
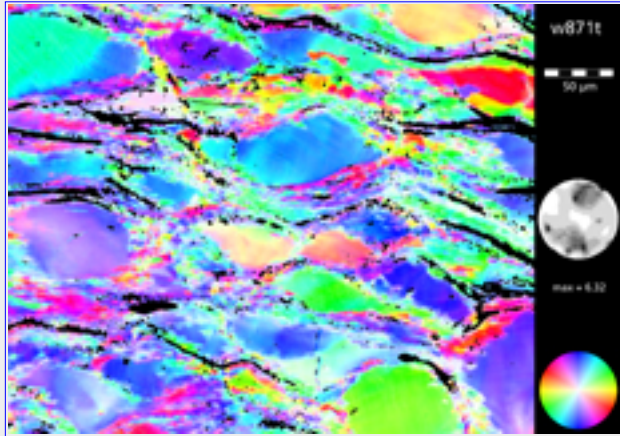


- Regime 2 (w874)

- Regime 3 (w860)

4.3 ORIENTATION IMAGES OF EXPERIMENTALLY DEFORMED ROCKS

[top](#) / [contents](#) / [section 4](#) / pages -- [4.1](#) -- [4.2](#) -- [4.3](#) -- [4.4](#) -- [4.5](#) -- [4.6](#) -- [4.7](#)



Partial textures of regime 1, 2 and 3 of dynamic recrystallization

Higher magnification of experimentally deformed Black Hills quartzite (compare 4.5) and selective texture analysis of old grains and recrystallized grains (Tullis & Heilbronner, 1999).

Experimental conditions:

regime 1 (W871):

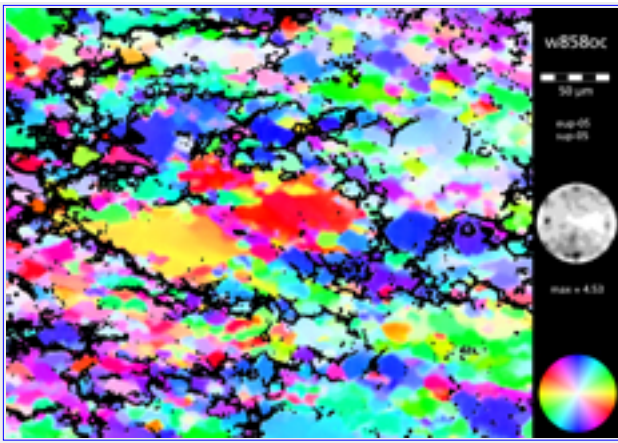
- pc = 1.5 GPa
- T = 850°C
- strain rate = 10^{-5} s $^{-1}$
- as-is

regime 2 (W872):

- pc = 1.5 GPa
- T = 900°C
- strain rate = 10^{-5} s $^{-1}$
- 0.17 wt% water added

regime 3 (W858):

- pc = 1.5 GPa
- T = 900°C
- strain rate = 10^{-6} s $^{-1}$
- 0.17 wt% water added



Left, from top to bottom:

- Regime 1 (w871)
- Regime 1 (w871): recrystallized grains only (left), old grains only (right)
- Regime 2 (w872)
- Regime 2 (w872): recrystallized grains only (left), old grains only (right)
- Regime 3 (w858)

4.4 ORIENTATION IMAGES OF EXPERIMENTALLY DEFORMED ROCKS

[top](#) / [contents](#) / [section 4](#) / pages -- [4.1](#) -- [4.2](#) -- [4.3](#) -- [4.4](#) -- [4.5](#) -- [4.6](#) -- [4.7](#)

Annealed microstructures of regime 1, 2 and 3 of dynamic recrystallization

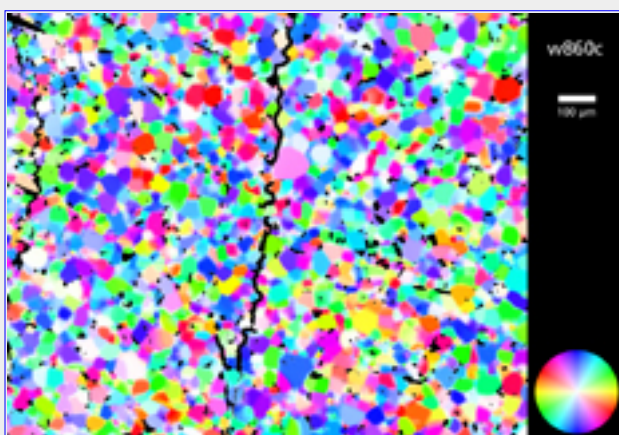
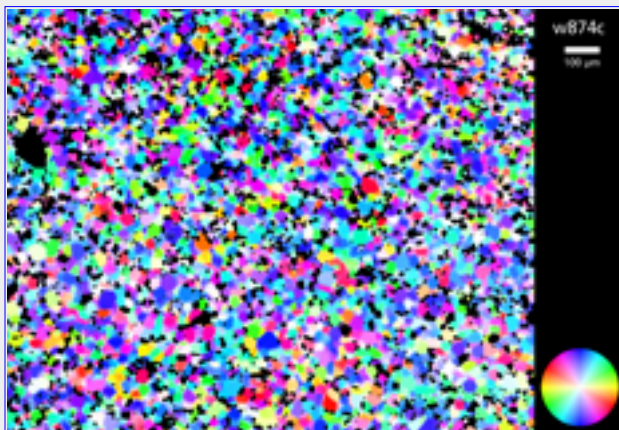
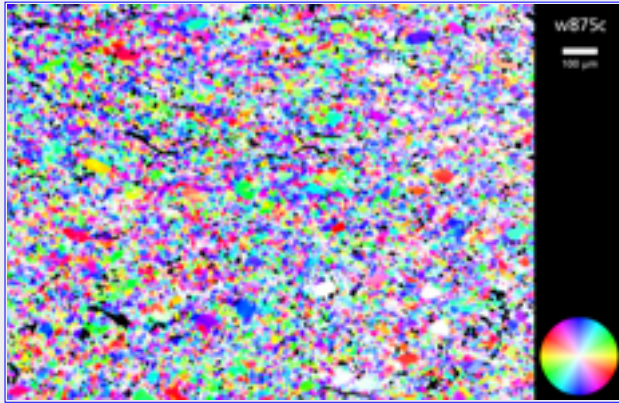
Samples of Black Hills quartzite have been deformed in three regimes of dislocation creep (see 4.5 and 4.6), quenched, removed, carefully cut in half longitudinally, and a portion of the central section from one half was weld-sealed in Pt and annealed at the same P and T as the prior deformation, for about 5 days. These experiments allow us to correlate more exactly between the deformed material and the annealed equivalent.

Preliminary results:

Regime 1: Deformed original grains develop a broad maximum of c axes parallel to compression; annealing replaces the work-hardened original grains with polygonal strain-free grains with a weaker LPO.

Regime 2: Deformed original grains as well as new grains dynamically recrystallized by subgrain rotation develop a small circle girdle of c-axes about compression; annealing produces a change in the microstructure, to polygonal strain-free grains, but no change in the LPO.

Regime 3: Original grains are replaced by dynamically recrystallized grains after low strain, so their LPO depends on selective survival; dynamically recrystallized grains develop a weak small circle girdle of c-axes about compression. Annealing does not substantially change the microstructure or the LPO (Tullis & Heilbronner, 1999).



Left, from top to bottom:

- Annealed regime 1 (w875)
- Annealed regime 2 (w874)
- Annealed regime 3 (w860)

4.5 ORIENTATION IMAGES OF EXPERIMENTALLY DEFORMED ROCKS

[top](#) / [contents](#) / [section 4](#) / pages -- [4.1](#) -- [4.2](#) -- [4.3](#) -- [4.4](#) -- [4.5](#) -- [4.6](#) -- [4.7](#)

More detail on regime 3 of the dynamic recrystallization

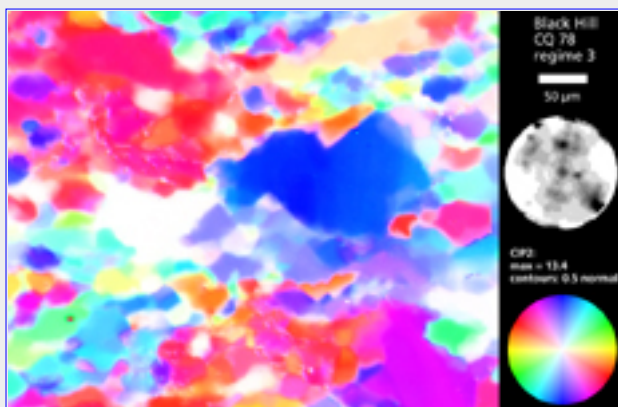
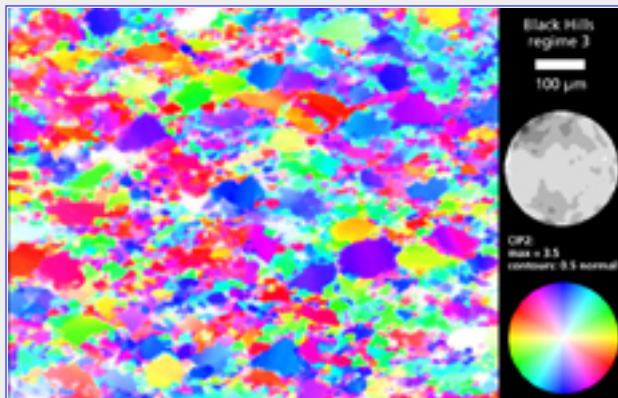
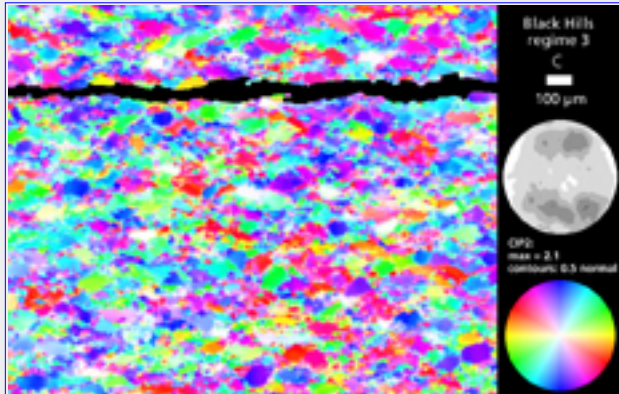
Experimentally deformed Black Hills quartzite, sample CQ78, site C (see previous page 4.2). Deformation occurred in the transition region between regime 2 and regime 3 dislocation creep (Hirth & Tullis, 1992).

Experimental conditions:

- $p_c = 1.5$ GPa,
- $T = 900^\circ\text{C}$,
- strain rate = 10^{-6}s^{-1} ,
- total shortening: 36%.

The input images have been captured using three Zeiss Epiplan Pole microscope objectives of increasing magnifying power and numerical aperture: 2.5x/0.075, 5x/0.15 and 10x/0.30. The spatial resolution of optical orientation imaging and the depth of the analyzed volume depends on the numerical aperture, and is as good as the optical resolution of the microscope.

As the image area gets smaller, the statistics of the pole figure deteriorates; the texture index increases as single crystal measurements are approximated.



Left, from top to bottom:

- CQ78, site C, using 2.5x objective
- CQ78, site C, using 5x objective
- CQ78, site C, using 10x objective

4.6 ORIENTATION IMAGES OF EXPERIMENTALLY DEFORMED ROCKS

[top](#) / [contents](#) / [section 4](#) / pages -- [4.1](#) -- [4.2](#) -- [4.3](#) -- [4.4](#) -- [4.5](#) -- [4.6](#) -- [4.7](#)

Making use of sample heterogeneity

Axial thin sections of experimentally deformed rock samples (typically cylinders of 6 mm diameter) constitute planar volumes of approximately orthorhombic or even lower symmetry. In the center of a homogeneously shortened cylinder, the predominant mass flux is in a radial direction, near the periphery, it is tangential; accordingly, on the thin section, the strain ellipse is elongated radially near the center and isotropic or elongated axially near the periphery. The strain history of each subvolume depends on its distance from the central axis, the amount of axial compression, and the type and concentration of deformation at that point. High concentrations of pure shear occur in the central part of the rock cylinder, away from the pistons. Near the piston-specimen interfaces, conical zones of high intensity shearing may occur

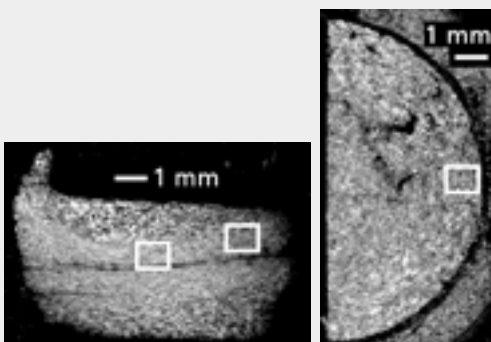
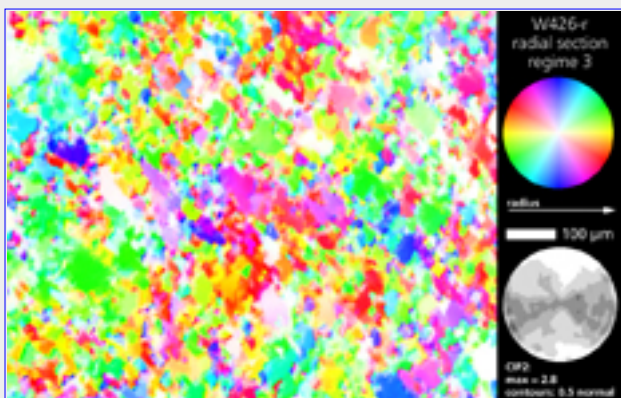
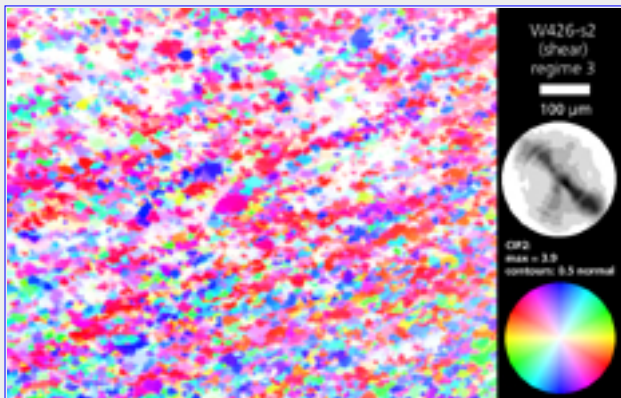
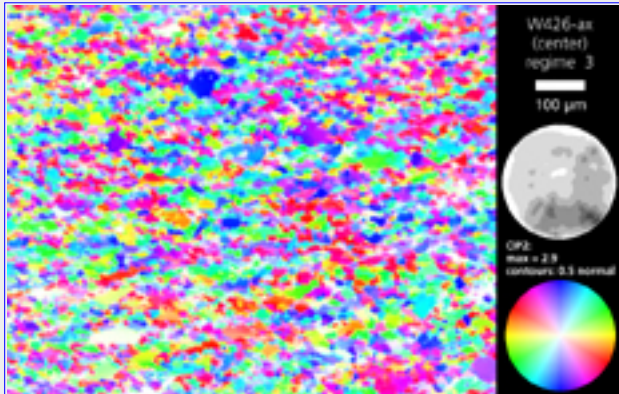
On axial and radial sections, a number of different and interesting textures and microstructures can be observed. It is argued that the comparison between the textures of naturally and experimentally deformed rocks has to rely on the analysis of local textures and microstructures: significant information is lost if bulk textures or profiles are used (Heilbronner & Tullis, 1999).

Experimental conditions:

Material: Black Hills quartzite

(regime 3 of dislocation creep)

- $p_c = 1.5 \text{ GPa}$
- $T = 1200^\circ\text{C}$
- strain rate = 10^{-5} s^{-1}
- dry



Left, from top to bottom:

- W426C, site 1, predominantly pure shear
- W426S, site 2, predominantly simple shear
- W426R, site 3, radial section
- view of thin sections, frames from left to right denote sites 1, 2, 3 of thin sections

4.7 ORIENTATION IMAGES OF EXPERIMENTALLY DEFORMED ROCKS

[top](#) / [contents](#) / [section 4](#) / pages -- [4.1](#) -- [4.2](#) -- [4.3](#) -- [4.4](#) -- [4.5](#) -- [4.6](#) -- [4.7](#)

Dynamic recrystallization of quartzite along deformation gradient

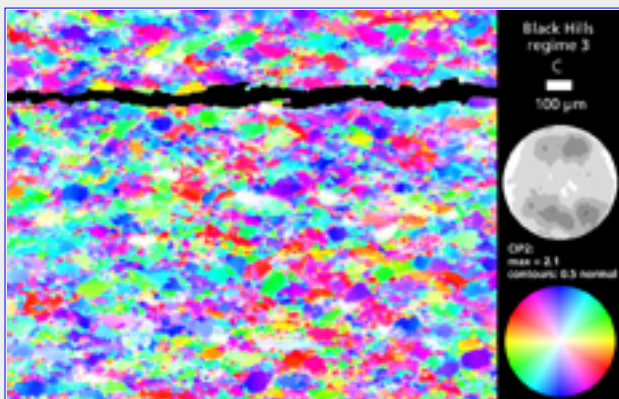
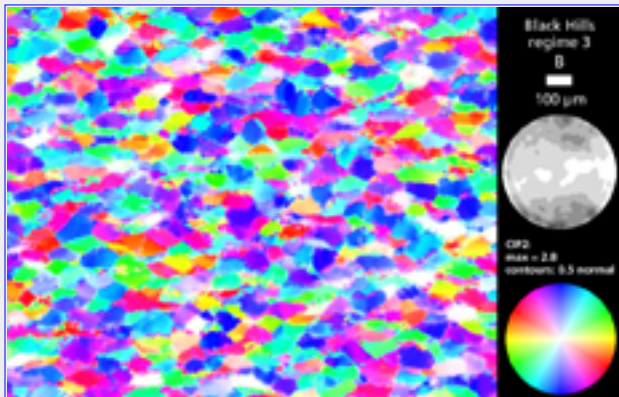
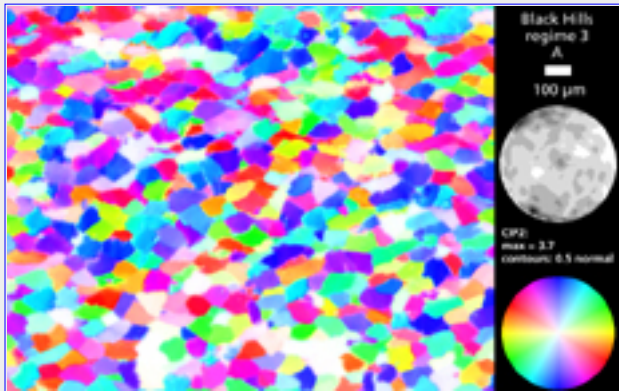
Experimentally deformed Black Hills quartzite. Deformation occurred in the transition region between regime 2 and regime 3 dislocation creep (Hirth & Tullis, 1992).

Experimental conditions:

- $p_c = 1.5$ GPa
- $T = 900^\circ\text{C}$
- strain rate = 10^{-6} s $^{-1}$
- 0.16wt% water added

The total shortening of sample CQ78 (A,B,C) and sample CQ82(D) is 36% and 57% respectively. However, the deformation intensity increases from sample site A to C.

Note also, how the bulk c-axis pole figure changes, from near random (starting material) in A to a small circle distribution with discrete maxima in C and D (80-90% recrystallized).

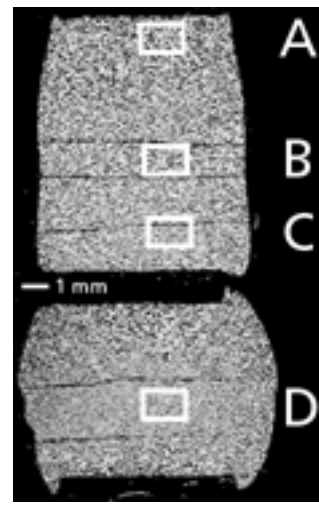
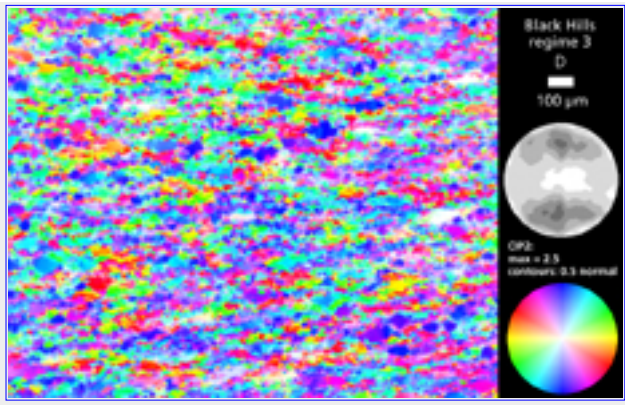


Left, from top to bottom:

- CQ78, site A, B, C
- CQ82, site D

Below:

axial sections of sample CQ78 and CQ82, image sites indicated



5 ORIENTATION IMAGES OF NATURALLY DEFORMED ROCKS

[top](#) / [contents](#) / [section 5](#) / pages -- [5.1](#) -- [5.2](#) -- [5.3](#) -- [5.4](#) -- [5.5](#) -- [5.6](#)

[5.1](#) Quartz mylonite from the Simplon fault zone

[5.2](#) Quartz mylonite from the Corvatsch

[5.3](#) Quartz veins from the Glarus thrust

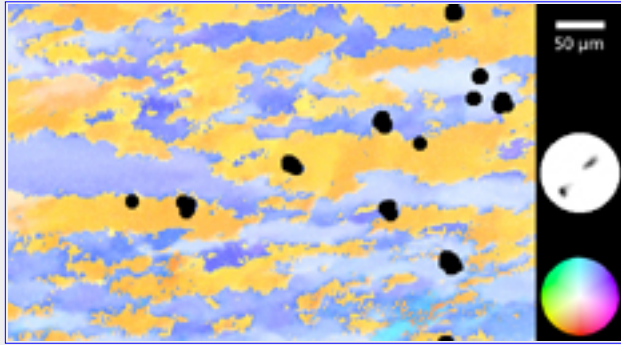
[5.4](#) Quartz veins from the Tonale fault

[5.5](#) ...more on the quartz veins from the Tonale fault

[5.6](#) Carrara Marble

5.1 ORIENTATION IMAGES OF NATURALLY DEFORMED ROCKS

[top](#) / [contents](#) / [section 5](#) / pages -- [5.1](#) -- [5.2](#) -- [5.3](#) -- [5.4](#) -- [5.5](#) -- [5.6](#)



Quartz mylonite from the Simplon fault zone

(Christian Pauli)

This particular c-axis orientation image is the first one we ever produced.

The thin section is from a quartz mylonites of the Simplon fault zone (SFZ). The regional geology of the SFZ, the c-axis pole figures and X-ray textures of many deformed quartz veins have been described and determined in detail by Mancktelow (1985, 1987, 1990). Specimen SP 178 is from the Simplon Pass area, where the deformation occurred under conditions of greenschist-facies metamorphism overprinting earlier amphibolite facies assemblages.

SP178 was collected from a strongly deformed quartz vein near the Simplon Line itself. Its c-axes (determined with the U-stage) lie on a slightly kinked single girdle. The microstructure consists of elongate to ribbon shaped 'old grains', with a dispersed development of elongate subgrains and new grains of an average grain size of approximately 80 μm . A shape fabric due to elongate subgrains, new grains and asymmetric grain boundary bulges is developed.

Reference:

Panozzo Heilbronner, R. and C. Pauli (1993). "Integrated spatial and orientation analysis of quartz c-axes by computer-aided microscopy." *J. Struct. Geol.* 15(3-5): 369-382.

Pauli, C., PhD thesis, Dept. of Geosciences, Basel University (<http://www.unibas.ch/earth/>)

5.2 ORIENTATION IMAGES OF NATURALLY DEFORMED ROCKS

[top](#) / [contents](#) / [section 5](#) / pages -- [5.1](#) -- [5.2](#) -- [5.3](#) -- [5.4](#) -- [5.5](#) -- [5.6](#)

Quartz mylonite from the Corvatsch

(Christian Pauli)

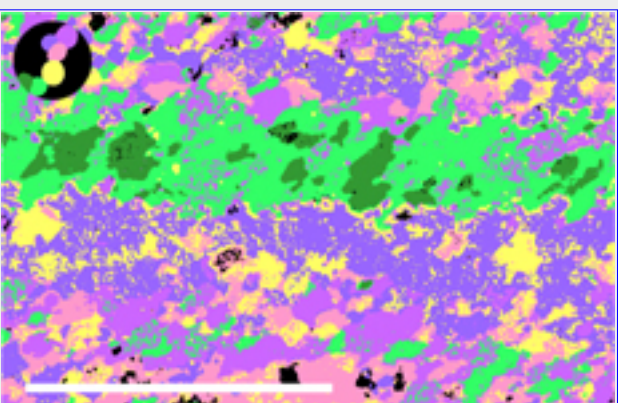
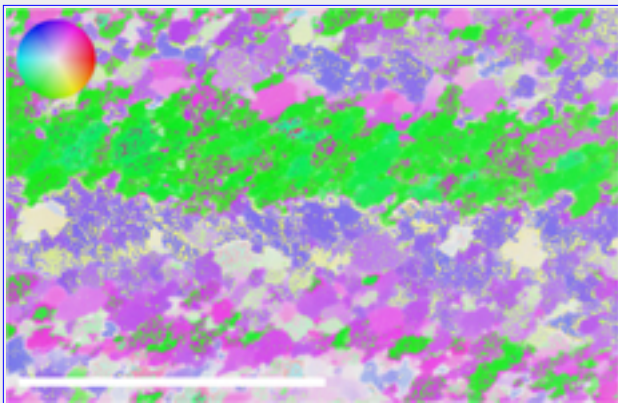
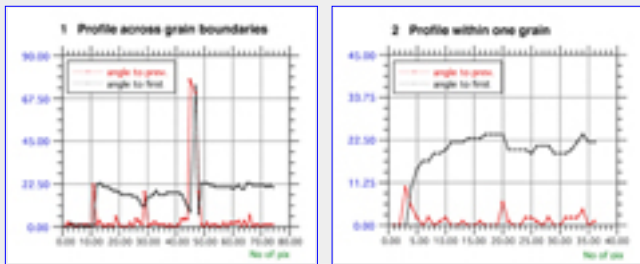
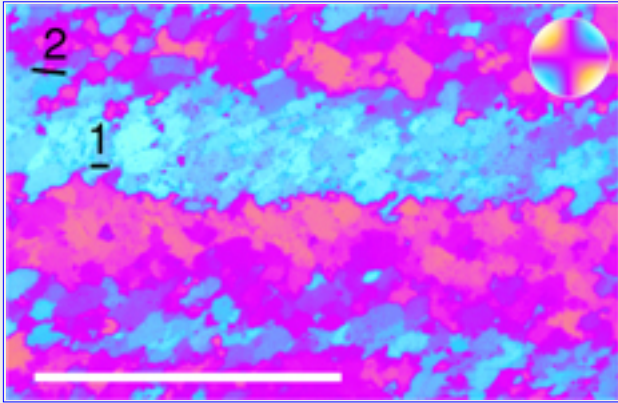
The quartz sample discussed here is taken from a quartz vein of the Corvatsch mylonite. The Corvatsch mylonite zone is located in SE Switzerland and represents an extensional fault zone that formed during the collapse of the Austroalpine nappes stack, built up in Early Alpine times [19]. The quartz vein is parallel to the fault zone, lineated and about 5 cm thick. It has formed in pre-fault zone times. The mylonitization is contemporaneous with a marked pressure decrease (8- \rightarrow 6 kbar) and occurs under temperatures between 350° and 400°C. The strongly domainal nature of the sample, in particular, the herring bone microstructure, could be attributed to a flattening component of the displacement along the fault zone. In this case, the shape of the domains may be taken as finite strain markers. On the other hand the domainal microstructure could be interpreted as a steady state structure, where deformation and recrystallization are partitioned into a heterogeneous pattern.

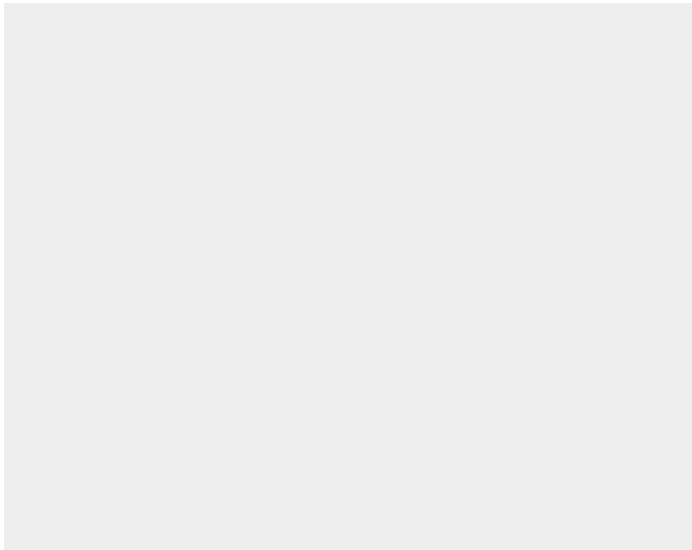
Reference:

Panozzo Heilbronner, R. and C. Pauli (1994). Orientation and misorientation imaging: integration of microstructural and textural analysis. Textures of geological materials. H. J. Bunge, S. Siegesmund, W. Skrotzki and K. Weber. Oberursel, DGM Informationsgesellschaft Verlag: 147-164.

Pauli, C., PhD thesis, Dept. of Geosciences, Basel University (<http://www.unibas.ch/earth/>)

Left, from top to bottom:





(a) image of thin section as it appears under crossed polarizers and lambda plate. Inset shows conoscopic image of quartz. Scale bar is 1mm. 1,2 = traverses of misorientation profiles (not shown here).

(b) Profile 1 crossing grain boundaries at pixel No. 10, 30 and around 47. Profile 2 lies within one grain.

(c) CIP calculated orientation image using standard CLUT.

(d) CIP calculated orientation image using problem oriented, blobby CLUT that enhances the domainal nature of this mylonite.

5.3 ORIENTATION IMAGES OF NATURALLY DEFORMED ROCKS

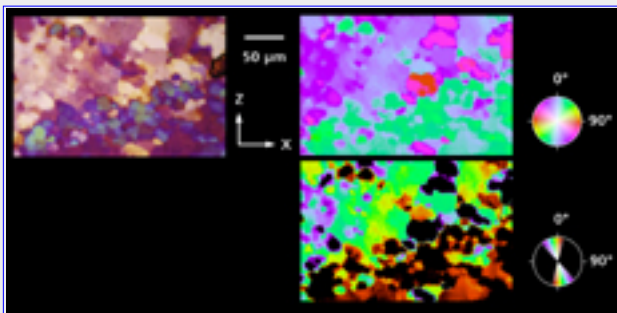
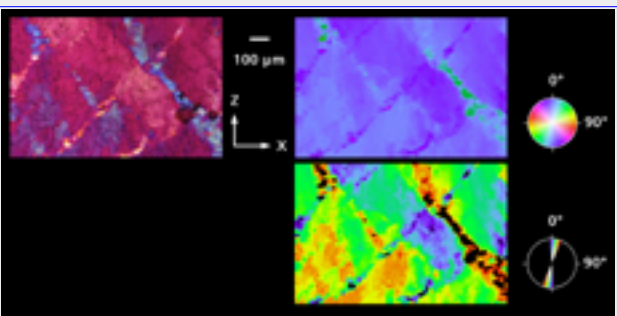
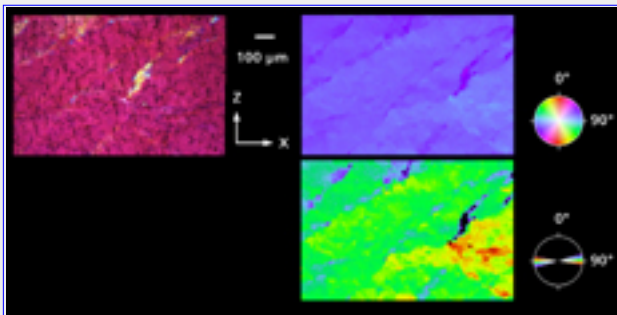
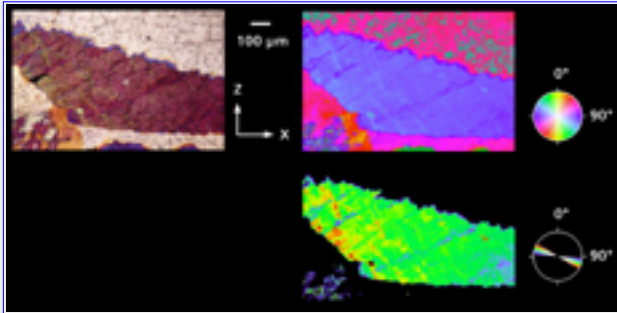
[top](#) / [contents](#) / [section 5](#) / pages -- [5.1](#) -- [5.2](#) -- [5.3](#) -- [5.4](#) -- [5.5](#) -- [5.6](#)

Quartz veins from the Glarus thrust

(Mirjam van Daalen)

Four samples of syntectonic quartz veins were collected in the Verrucano in close proximity to the Glarus thrust. The veins are embedded in a metapelitic host rock. The sampling locations of sample A, B, C, and D correspond to temperatures of 270, 300, 350, and 370°C, respectively. Peak temperatures are constrained by careful illite crystallinity measurements.

Typically, the quartz veins are oriented parallel or subparallel to the foliation. They consist of fibres which are less than one millimeter wide and a few millimeters long. Fibre long axes are oriented approximately parallel to the lineation direction. (more on page [6.4](#))



Orientation images of samples A, B, C, D:

Each plate consist of the following parts:

Left: Optical micrograph: Crossed polarizers and lambda plate; foliation normal is vertical, lineation is horizontal; shear sense is top to the left, which is (geographic) North in each case. White cross is marker point which corresponds to red cross on orientation contrast image (4).

Top right: CIP derived C-axis orientation image (COI): Spectral CLUT is oriented such that the orientation of the c-axis of the host grain is represented by blue.

Bottom right: CIP derived C-axis orientation image (COI): Condensed CLUT is oriented such that the orientation of the c-axis of the host grain is represented by green.

Reference:

van Daalen, M., R. Heilbronner, et al. (1999). "Orientation analysis of localized shear deformation in quartz fibres at the brittle-ductile transition."

Tectonophysics 303: 83-108.

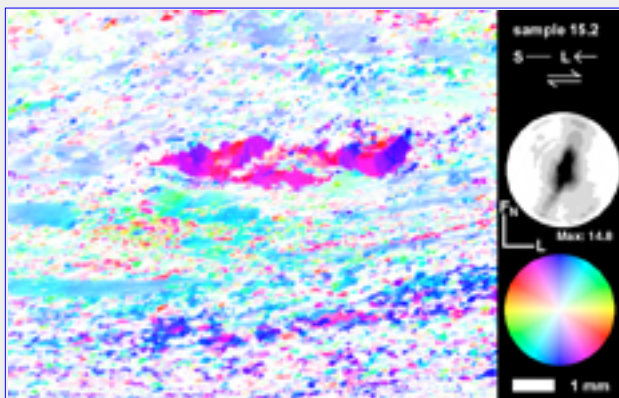
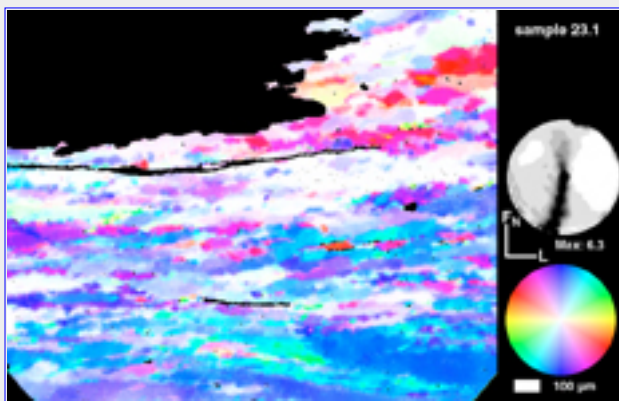
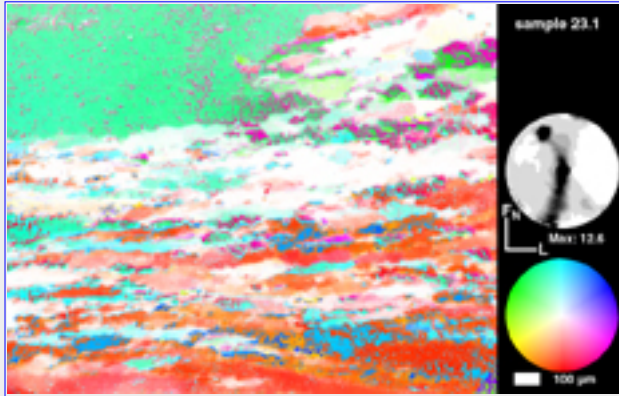
van Daalen, M., PhD thesis, Dept. of Geosciences, Basel University (<http://www.unibas.ch/earth/>)

5.4 ORIENTATION IMAGES OF NATURALLY DEFORMED ROCKS

[top](#) / [contents](#) / [section 5](#) / pages -- [5.1](#) -- [5.2](#) -- [5.3](#) -- [5.4](#) -- [5.5](#) -- [5.6](#)

Quartz veins from the Tonale fault

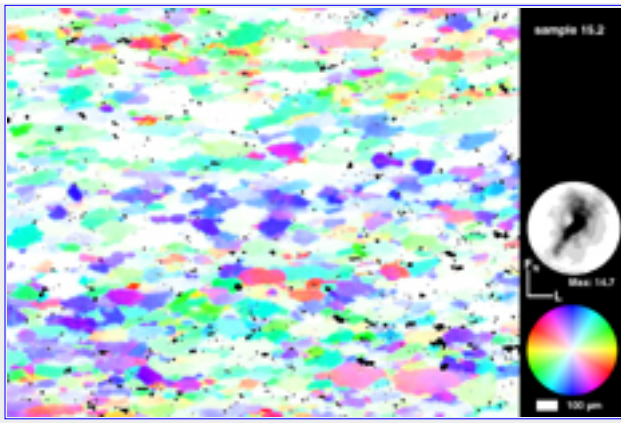
(Michael Stipp)



The c-axis-orientation images are sheared quartz veins from the Tonale fault, a major segment of the Periadriatic fault system. The Tonale fault cuts the contact aureole of the Adamello pluton, i. e. it is contemporaneous with the thermal event, resulting in a temperature gradient from about 700 °C to 280 °C in the syndeformational mylonites. The deformed lithologies, which contain the quartz veins used for microstructural analysis, consist of a series of metasediments yielding critical mineral assemblages for p,T-estimates. For quartz, the complete range of dynamic recrystallization (bulging, subgrain rotation and grain boundary migration recrystallization) from the brittle-ductile transition up to nearly melting conditions is developed. With increasing metamorphic temperature, the samples display a strong increase in the recrystallized grain size from 5 µm up to more than 5 mm. Three samples from the subgrain rotation and grain boundary migration recrystallization regimes are shown.

MS23-1 (about 450°C): Subgrain rotation recrystallization: large ribbon grains (masked in the CIP-image) surrounded by recrystallized grains which can be described as core and mantle structures (visible only at lower magnifications); the recrystallized grains form an oblique fabric with respect to the main foliation and have a prolate shape anisotropy. The c-axis pattern shows an oblique single girdle for the recrystallized grains and a single crystal maximum for the unmasked ribbon grain.

MS15-2 (about 500°C): Subgrain rotation recrystallization: ribbon grains are almost totally consumed by progressive subgrain rotation, and to a small extent by grain boundary migration;



the recrystallized grains form an oblique fabric with respect to the main foliation and the prolate shape anisotropy is increased in comparison to sample MS23-1. The c-axis pattern shows a strong maximum in the Y-direction of the pole figure indicating dominant prism $\langle a \rangle$ slip; a weak crossed girdle (relict of lower temperature deformation?) can also be observed.

MS66-3 (about 650°C): Grain boundary migration recrystallization: completely dynamically recrystallized sample with "island grains" and a "dissection" microstructure (masked zones contain cordierite, sillimanite, plagioclase, biotite); chess-board extinction indicating high temperature deformation at the transition from a- to b-quartz is also visible. The c-axis pattern shows a first maximum parallel to Y, comparable to that one of sample MS15-2, and a second maximum close to the stretching lineation (X) which can probably be interpreted as combined prism $\langle a \rangle$ and prism $\langle c \rangle$ slip.

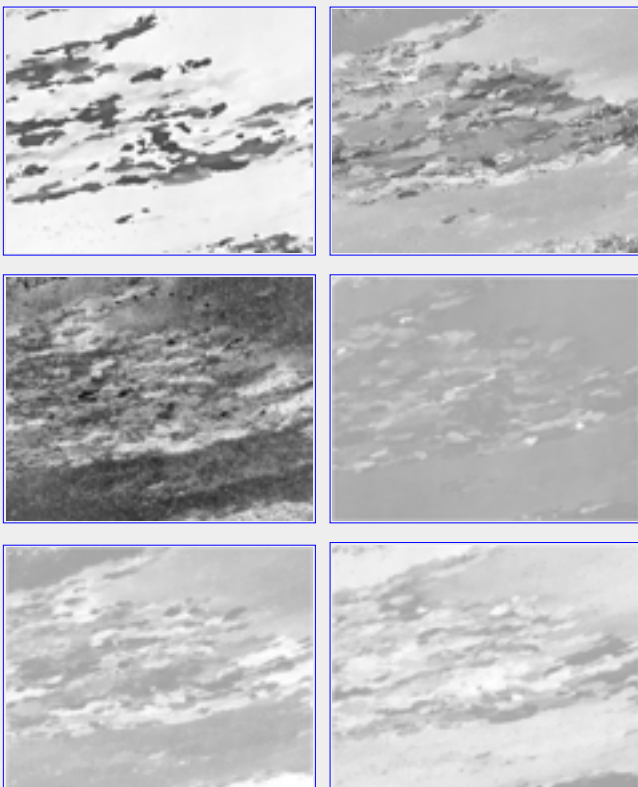
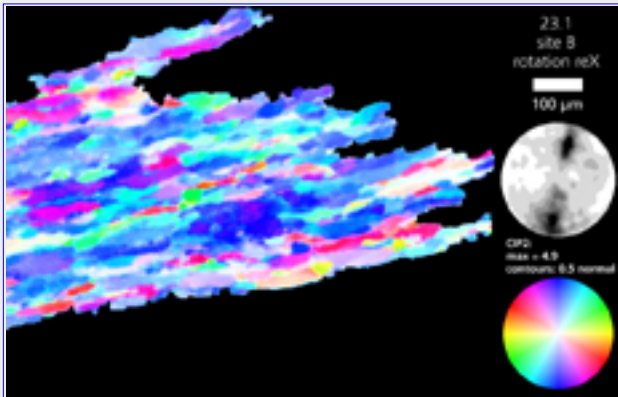
Stipp, M., PhD thesis, Dept. of Geosciences, Basel University (<http://www.unibas.ch/earth/>)

5.5 ORIENTATION IMAGES OF NATURALLY DEFORMED ROCKS

[top](#) / [contents](#) / [section 5](#) / pages -- [5.1](#) -- [5.2](#) -- [5.3](#) -- [5.4](#) -- [5.5](#) -- [5.6](#)

...more on the quartz veins from the Tonale fault

Here, the complete output of another site of sample MS23-1 (see [page 5.4](#)) is shown.



From top to bottom, left to right:

Full c-axis orientation image, Standard CLUT

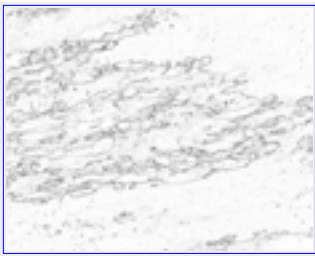
Masked c-axis orientation image, Spectrum CLUT

Azimuth image - inclination image

Error image - Misorientation image (East)

Misorientation image (Heaven) - Misorientation image (North)

Orientation gradient image (4 neighbours) - Orientation gradient image (2 neighbours)



5.6 ORIENTATION IMAGES OF NATURALLY DEFORMED ROCKS

[top](#) / [contents](#) / [section 5](#) / pages -- [5.1](#) -- [5.2](#) -- [5.3](#) -- [5.4](#) -- [5.5](#) -- [5.6](#)

Carrara Marble

(Nils Oesterling)

Carrara Marble is cropping out in the Western part of the Alpi Apuane tectonic window. In this region two deformation phases are distinguishable (Carminigiani & Kligfield, 1990).

The main deformation phase (D1, Oligocene-Miocene) is characterized by greenschist facies conditions associated with isoclinally folding and the initiation of West dipping thrust faults producing an antiformal stack at the crustal scale. After D1 the region was heated statically, i.e. annealing occurred while, obliterated most of the D1-deformation structures. The peak metamorphic temperatures during annealing vary between 380°C in the East and 430°C in the West.

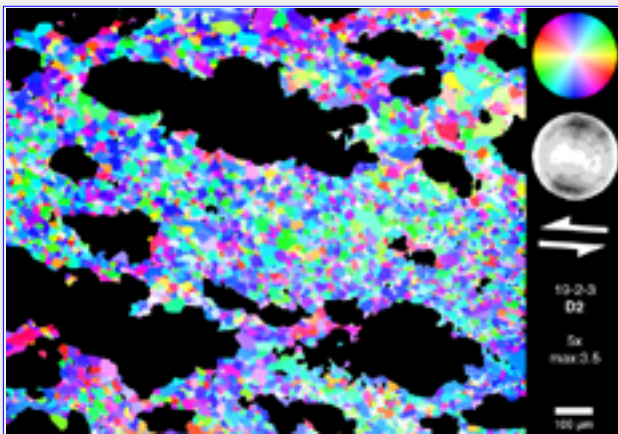
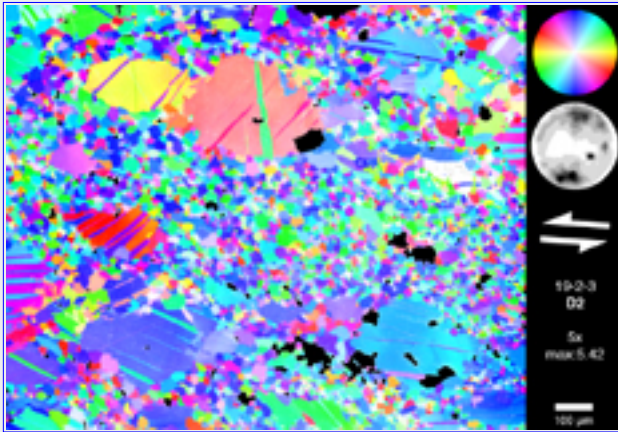
During the second deformation phase (D2, Miocene) the whole complex was refolded under retrograde conditions in an extensional region. As a result of this deformation millimeter- to centimeter-scale shear zones were formed.

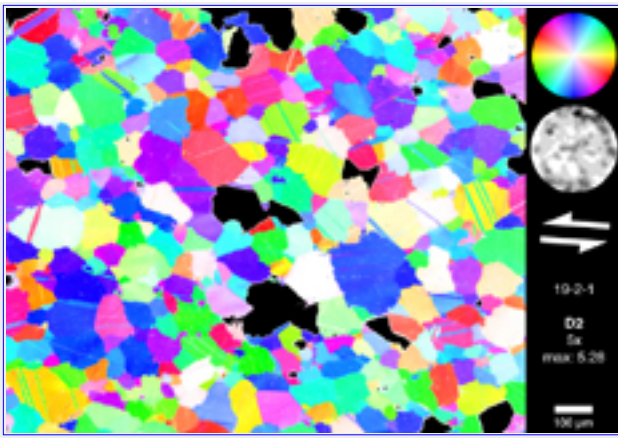
Left, from top to bottom:

Fig. 1: CIP-c-axis-orientation-image of the center of the D2 shear zone. The core-mantle-structure are typical for subgrain rotation recrystallization. The calculated pole figure shows two discrete maxima which are slightly inclined towards the compression direction. This feature is indicative of twin gliding.

Fig. 2: CIP-c-axis-orientation-image of the center of the D2 shear zone. Relict grains are masked. The calculated polefigure shows two diffuse maxima indicating subgrain rotation recrystallization. The influence of the relict grains on the bulk texture can be seen by comparison with Fig. 1.

Fig. 3: CIP-c-axis-orientation-image of the





boundary region of the D2-shear zone. The calculated pole figure shows two maxima slightly inclined toward the compression direction (indicative of twin gliding), two maxima subparallel to the shear zone boundary, and a single maximum subperpendicular to the shear zone boundary.

Fig. 4: CIP-c-axis-orientation-image of the annealed pre-D2 marble. The calculated pole figure is isotropic showing maybe a very weak maximum subperpendicular to the shear zone boundary. In addition to this feature, the equiaxial grainsize is an evidence of annealing.

Oesterling, N., PhD thesis, Dept. of Geosciences, Basel University (<http://www.unibas.ch/earth/>)

6 WHERE CAN WE GO FROM HERE ?

[top](#) / [contents](#) / [section 6](#) / pages -- [6.1](#) -- [6.2](#) -- [6.3](#) -- [6.4](#) -- [6.5](#) -- [6.6](#) -- [6.7](#) -- [6.8](#)

[6.1](#) Grain boundary detection based on misorientations

[6.2](#) Grain size sensitive texture analysis

[6.3](#) Grain size analysis

[6.4](#) Comparing CIP and EBSD

[6.5](#) Shape - texture relations

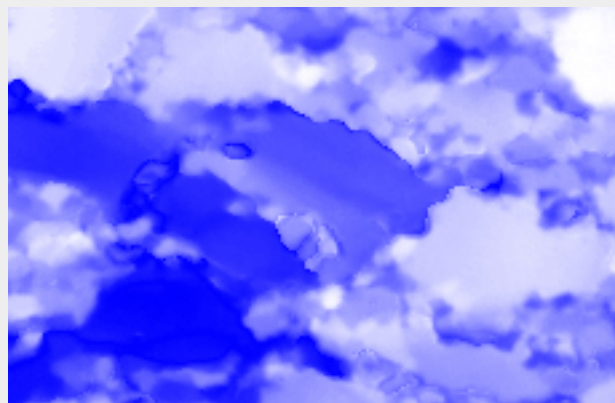
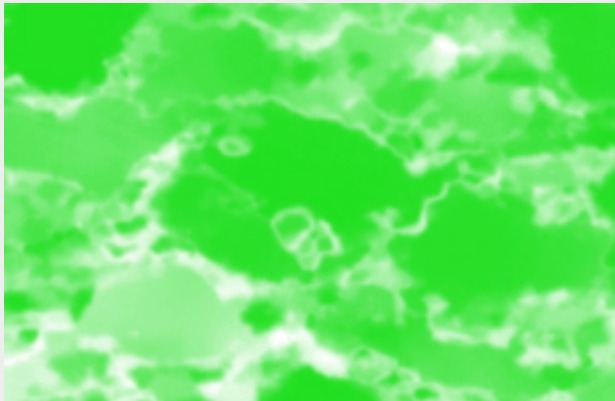
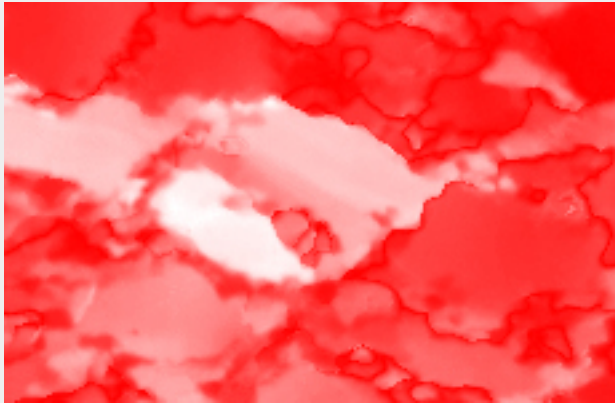
[6.6](#) Misorientation analysis of grains undergoing dynamic recrystallization

[6.7](#) Misorientation analysis of host grain - recrystallized grain relation

[6.8](#) Misorientations at grain boundaries of "flat" orientation images

6.1 WHERE CAN WE GO FROM HERE ?

[top](#) / [contents](#) / [section 6](#) / pages -- [6.1](#) -- [6.2](#) -- [6.3](#) -- [6.4](#) -- [6.5](#) -- [6.6](#) -- [6.7](#) -- [6.8](#)



Grain boundary detection based on misorientations

Using "Lazy grain boundaries" (= macro for NIH Image) and three misorientation images (with respect to three orthogonal directions), a grain boundary map can be derived (Heilbronner, in press).

([on-line manual](#))

Left from top to bottom:

Misorientation image with respect to East

Misorientation image with respect to Heaven

Misorientation image with respect to North

Below:

Derived grain boundary map

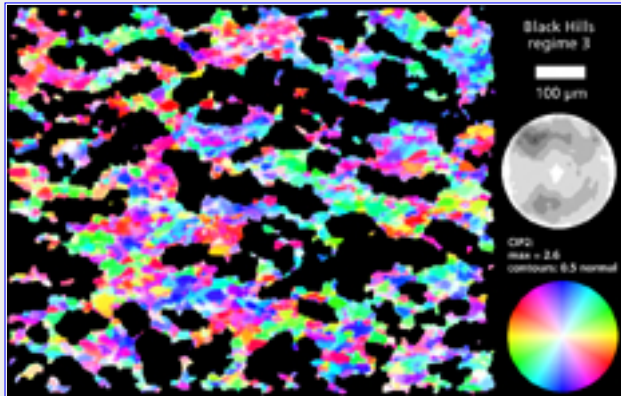
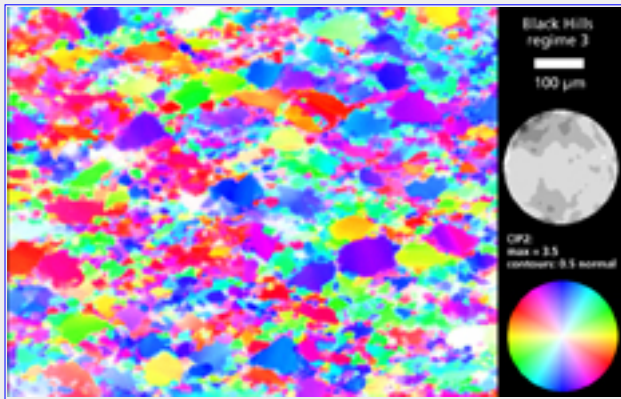


6.2 WHERE CAN WE GO FROM HERE ?

[top](#) / [contents](#) / [section 6](#) / [pages -- 6.1 -- 6.2 -- 6.3 -- 6.4 -- 6.5 -- 6.6 -- 6.7 -- 6.8](#)

Grain size sensitive texture analysis

Using "Lazy grain boundaries" (= macro for NIH Image) (see previous page 6.1), grain boundary maps may be derived and used for creating masks for large and small grain size, maskL and maskS, respectively. Using these masks, separate c-axis orientation images (COIs) and pole figures can be derived for old grains (large grain size) and recrystallized grains (small grain size).

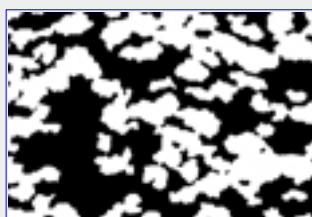
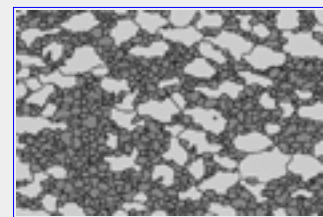
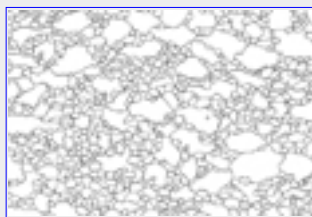
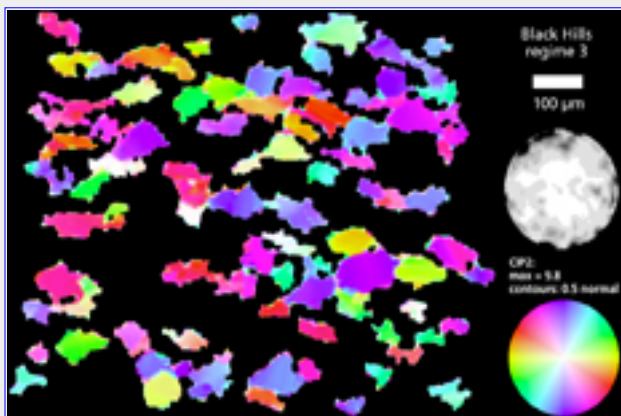


Left from top to bottom:

- bulk COI and pole figure
- COI and pole figure for old grains
- COI and pole figure for recrystallized grains.

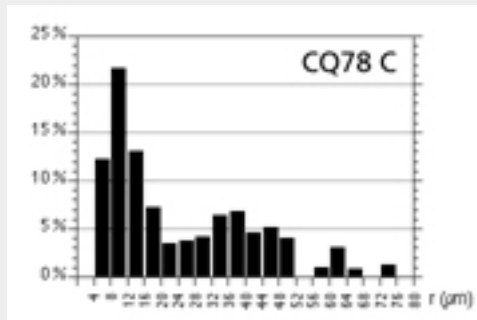
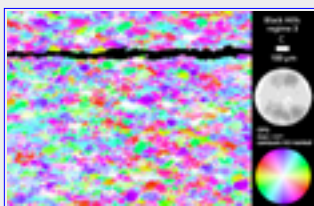
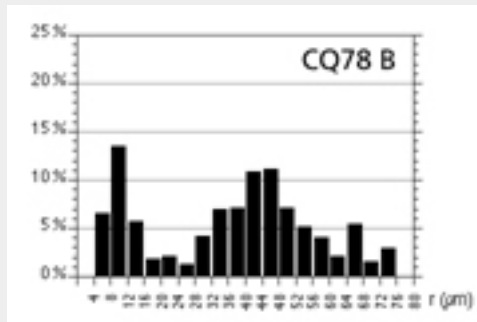
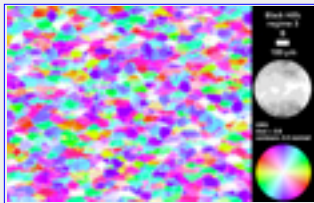
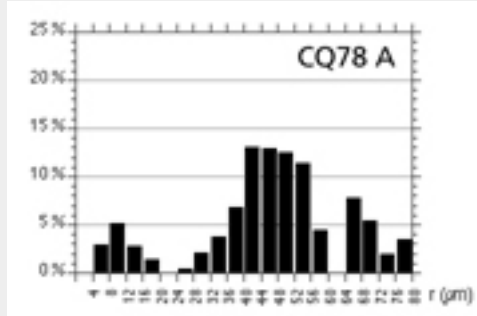
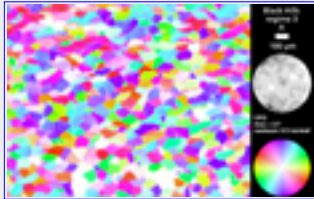
Below:

1. grain boundary map, 2. two different grey values for large and small grains, 3. maskL (for masking large grain sizes), 4. maskS (for masking small grain sizes)



6.3 WHERE CAN WE GO FROM HERE ?

[top](#) / [contents](#) / [section 6](#) / pages -- [6.1](#) -- [6.2](#) -- [6.3](#) -- [6.4](#) -- [6.5](#) -- [6.6](#) -- [6.7](#) -- [6.8](#)



Grain size analysis

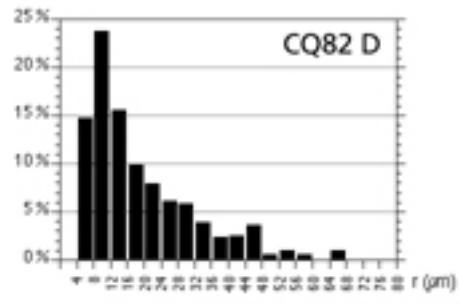
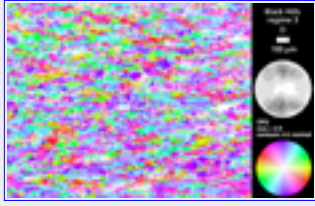
Using grain boundary maps, a grain size analysis can be carried out ([see manual](#)). The results of StripStar (for software, see appendix) are histograms of volume densities of 3-D grain size (radii of spheres).

Grain size analysis of experimentally deformed Black Hills quartzite (see 4.2) shows that the recrystallized grain size is constant, i.e., the volume of recrystallized grains increases as recrystallization progresses but not the grain size itself. In contrast, both the volume fraction and the grain size of the old grains decrease with increasing recrystallization (Heilbronner & Tullis, 1999a)

Left from top to bottom:

c-axis orientation image and volume density histogram of 3-D grain size of

- CQ78, site A, B, C
- CQ82, site D

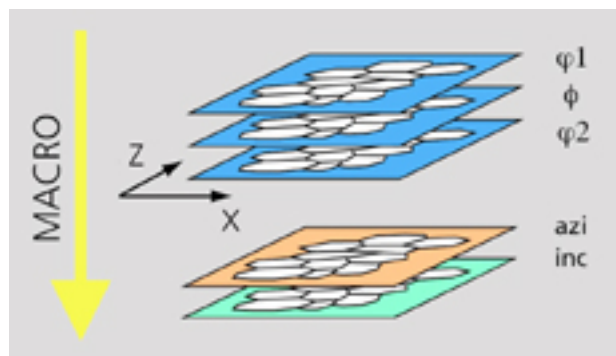


6.4 WHERE CAN WE GO FROM HERE ?

[top](#) / [contents](#) / [section 6](#) / pages -- [6.1](#) -- [6.2](#) -- [6.3](#) -- [6.4](#) -- [6.5](#) -- [6.6](#) -- [6.7](#) -- [6.8](#)

Comparing CIP and EBSD

In order to compare the crystallographically complete but discrete information of the EBSD analysis with the spatially continuous but crystallographically incomplete information provided by the CIP analysis, the following procedure can be adopted:

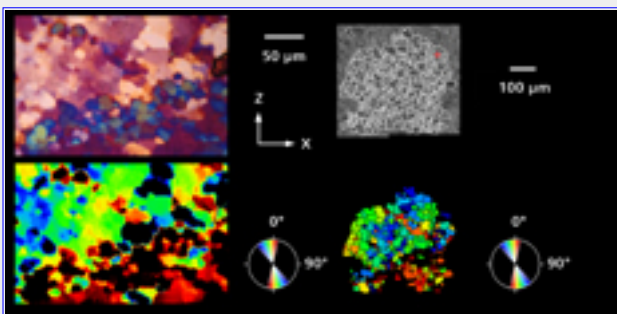
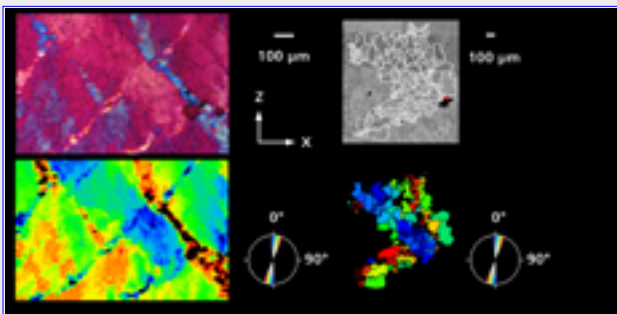
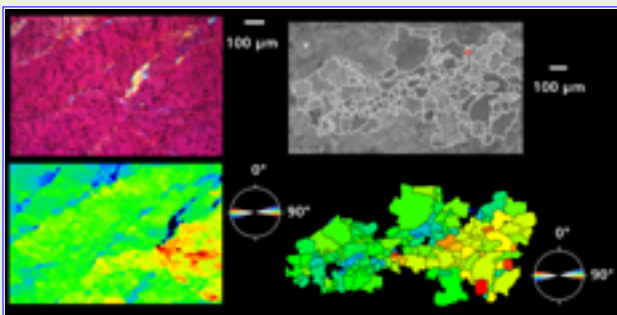
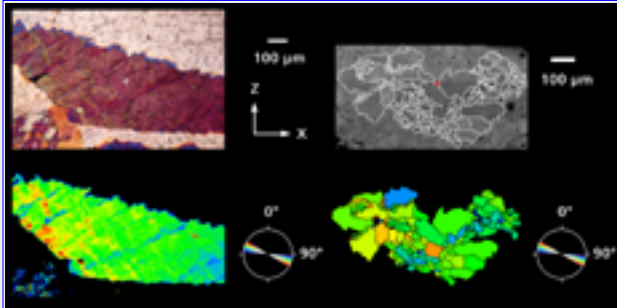


Using NIH Image and the "Lazy Euler" macro, the azimuths and inclinations of the c-axis orientations are calculated from the three Euler angles. The macro fills the outlines of the first, the second and the third slice with the grey levels that correspond to the phi1-, psi- and phi2-values obtained from EBSD measurements. From these, the azimuths and inclinations of the c-axes (azi, inc) are calculated the corresponding grey values are filled into the outlines of the fourth and fifth slice.

Left, from top to bottom (clockwise from upper left):

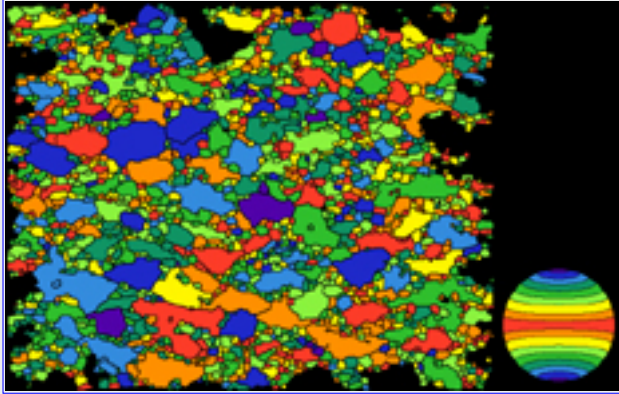
Photomicrograph, OC contrast image, orientation image from EBSD measurements, and optical orientation image (COI)

- for samples A, B, C, D (same samples as on page [5.3](#))



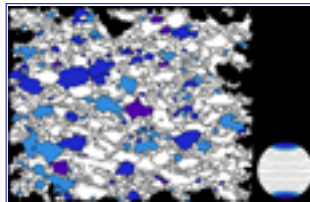
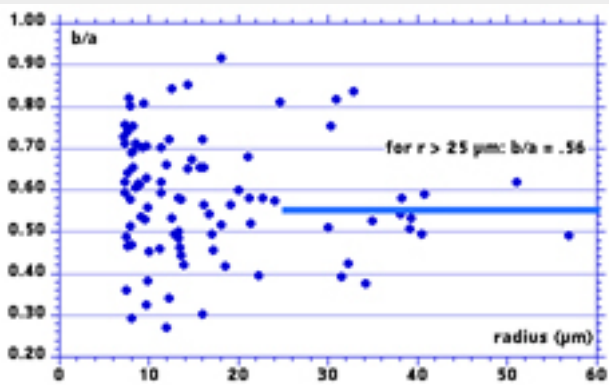
6.5 WHERE CAN WE GO FROM HERE ?

[top](#) / [contents](#) / [section 6](#) / [pages](#) -- [6.1](#) -- [6.2](#) -- [6.3](#) -- [6.4](#) -- [6.5](#) -- [6.6](#) -- [6.7](#) -- [6.8](#)

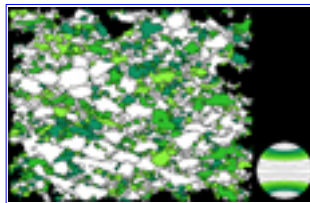
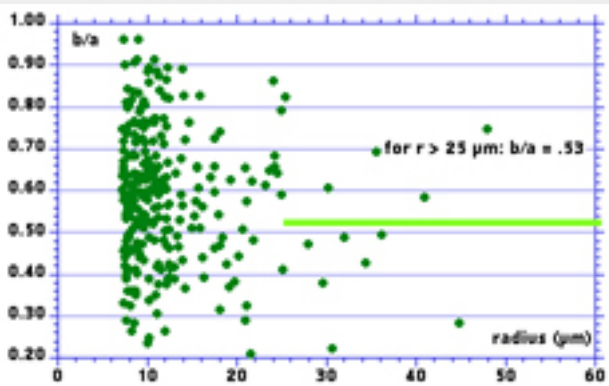


Shape - texture relations

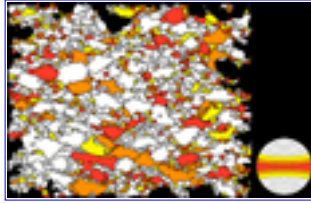
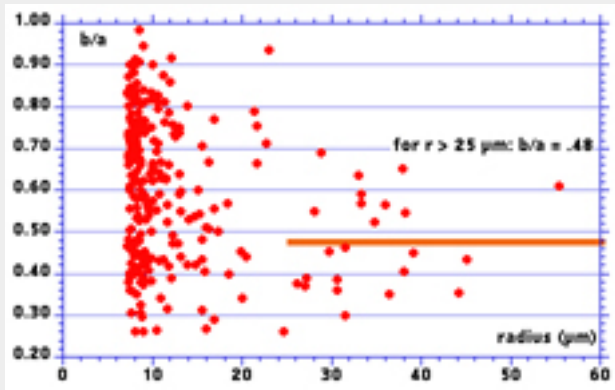
In order to derive the relation between grain shape and c-axis orientation) of the old grains of experimentally deformed Black Hills quartzite (sample CQ78C, page 4.3), the microstructure is subdivided into three orientation domains: c-axes with misorientation 0° - 30° , 30° - 60° , and 60° - 90° about the compression direction. For each partial microstructure the axial ratio of, b/a (short/long), has been evaluated (using NIH Image) and plotted as a function of size (radius r of equivalent circle). The average b/a value for all grains with a diameter of $> 50 \mu\text{m}$ ($r > 25 \mu\text{m}$), is determined. b/a decreases with increasing misorientation of the c-axis from the compression direction, indicating that grains with c-axis orientations subparallel to the compression direction are least flattened.



c-axis misorientation 0° - 30°



c-axis misorientation 30° - 60°

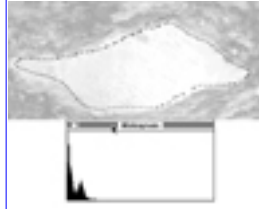
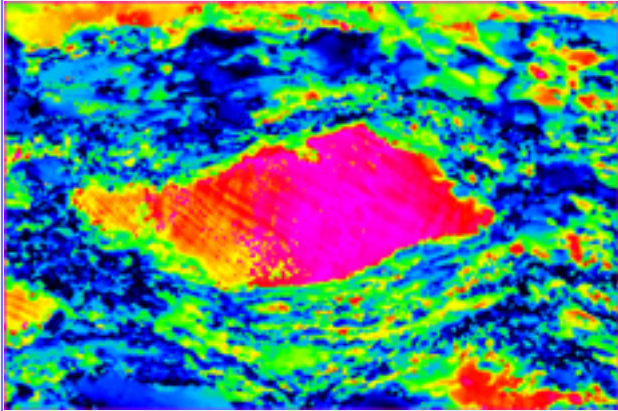


c-axis misorientation 60° - 90°

6.6 WHERE CAN WE GO FROM HERE ?

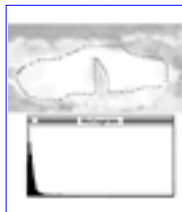
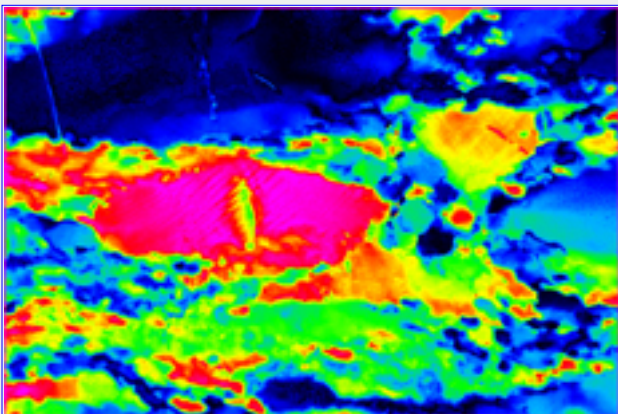
[top](#) / [contents](#) / [section 6](#) / pages -- [6.1](#) -- [6.2](#) -- [6.3](#) -- [6.4](#) -- [6.5](#) -- [6.6](#) -- [6.7](#) -- [6.8](#)

Misorientation analysis of grains undergoing dynamic recrystallization



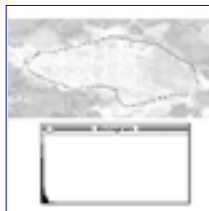
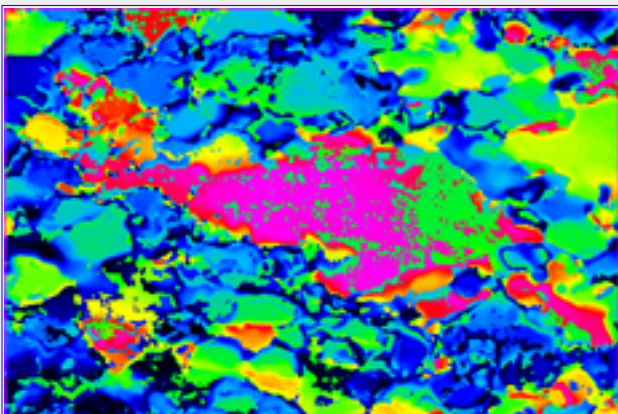
Above: histogram of misorientation angles in old grain
Left: misorientation image:
purple-red = 0-30°; yellow-green= 30-60°; blue = 60-90°

Old grain shows strong lattice distortions:
misorientation within grain up to 36°.



Above: histogram of misorientation angles in old grain
Left: misorientation image:
purple-red = 0-30°; yellow-green= 30-60°; blue = 60-90°

Old grain shows medium lattice distortions:
misorientation within grain up to 20°.



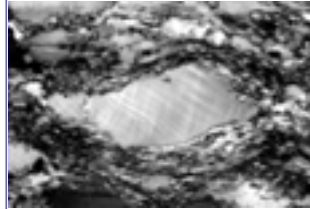
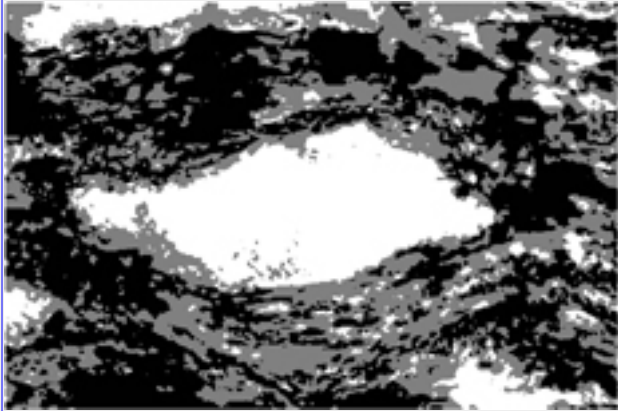
Above: histogram of misorientation angles in old grain
Left: misorientation image:
purple-red = 0-30°; yellow-green= 30-60°; blue = 60-90°

Old grain shows little lattice distortions (green spots are artefacts, compare cirpol image):
misorientation within grain (width of peaks) up to 10°.

6.7 WHERE CAN WE GO FROM HERE ?

[top](#) / [contents](#) / [section 6](#) / pages -- [6.1](#) -- [6.2](#) -- [6.3](#) -- [6.4](#) -- [6.5](#) -- [6.6](#) -- [6.7](#) -- [6.8](#)

Misorientation analysis of old grain - recrystallized grain relation

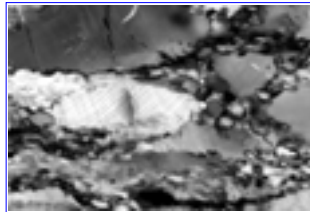
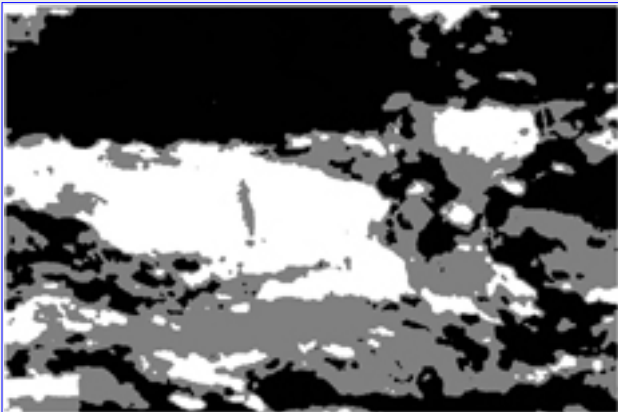


Above: hcirpol image

Left: misorientation image:

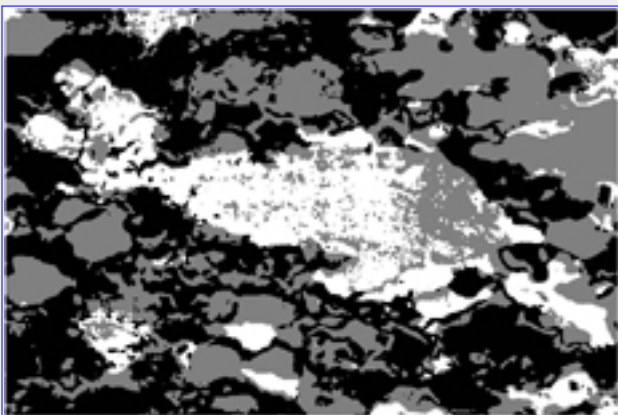
white = 0-30°; grey = 30-60°; black = 60-90°

Recrystallizing layer (where misor < 30° (!)) is very narrow: < 5 μm wide.



cirpol image

Recrystallizing layer (where misor < 30°) is very irregular, on average > 10 μm wide, with long tails of > 60 μm.

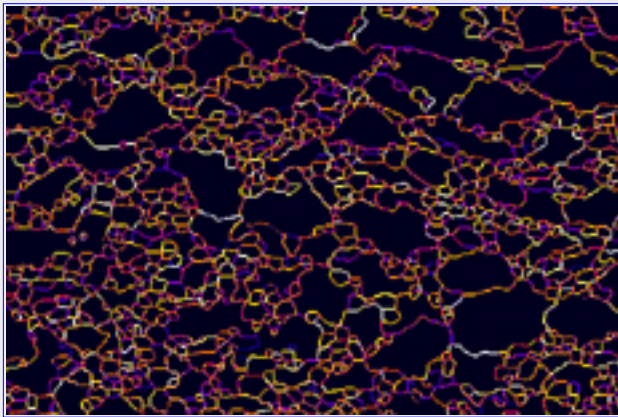
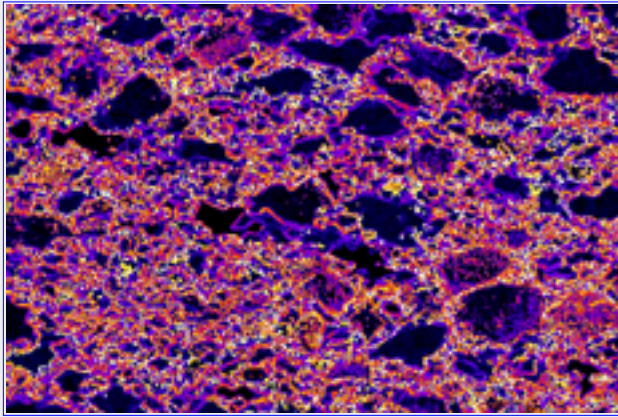
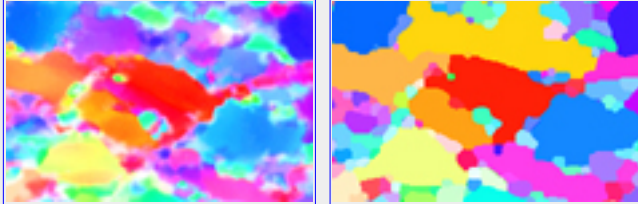


cirpol image

Recrystallizing layer cannot be defined.

6.8 WHERE CAN WE GO FROM HERE ?

[top](#) / [contents](#) / [section 6](#) / pages -- [6.1](#) -- [6.2](#) -- [6.3](#) -- [6.4](#) -- [6.5](#) -- [6.6](#) -- [6.7](#) -- [6.8](#)



Misorientations at grain boundaries of "flat" orientation images

Using NIH Image and the "Lazy azi inc & flat" macro, the azi and inc images, and the grain boundary map are used to create azi and inc images where each grain on the grain boundary map is assigned the average azimuth or average inclination of that grain. From these "flat" azi and inc images "flat"COIs and orientation gradient images can be calculated. The orientation gradient images show sharp grain boundaries of one pixel width., the slope of the gradient is really the angular difference between the grains.

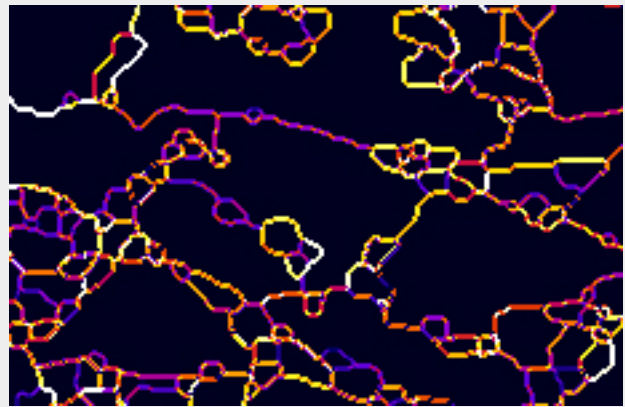
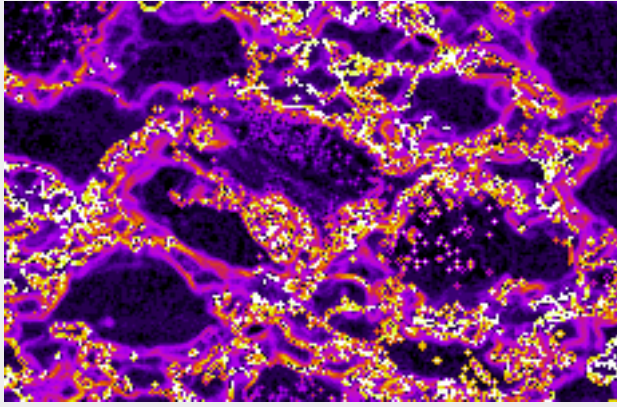
Left, from top to bottom:

- Illustration of conversion from c-axis orientation image with continuously variable orientations to one where each grain has only one constant orientation
- Orientation gradient image of regular input images
- Orientation gradient image of flat input images

Detail of orientation gradient image (regular input)

Below:

detail of orientation gradient image (regular input)



A1 LIBRARY OF ORIENTATION AND MISORIENTATION IMAGES

[top](#) / [contents](#) / [appendix 1](#) / pages -- [A1.1](#) -- [A1.2](#) -- [A1.3](#) -- [A1.4](#) -- [A1.5](#)

[A1.1](#) Micrographs, circular polarization

[A1.2](#) Orientation images

[A1.3](#) Input images

[A1.4](#) List of image sets

[A1.5](#) List of topics

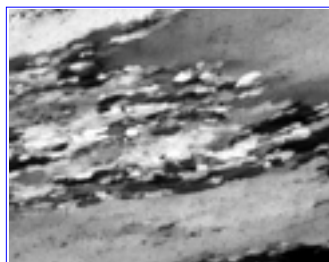
A1.1 LIBRARY OF ORIENTATION AND MISORIENTATION IMAGES

[top](#) / [contents](#) / [appendix 1](#) / pages -- [A1.1](#) -- [A1.2](#) -- [A1.3](#) -- [A1.4](#) -- [A1.5](#)

Micrographs, circular polarization

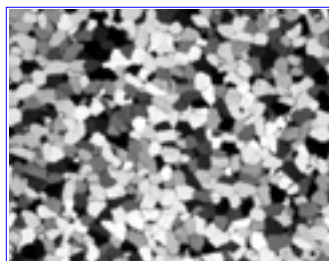
(all micrographs are in folder Cirpol, the folder names above the images indicate where the corresponding orientation images can be found)

Stipp-RH



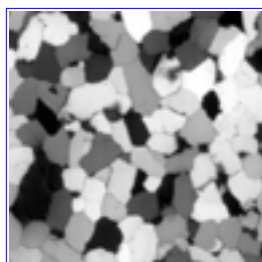
23-1-b.cirpol

bhq starting



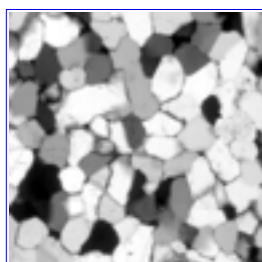
bh.cirpol

BHQ-03



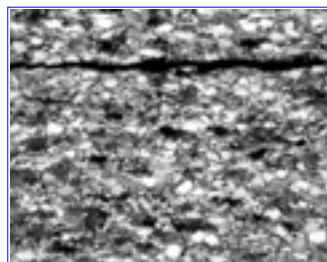
bhq-03.cirpol

BHQ-20



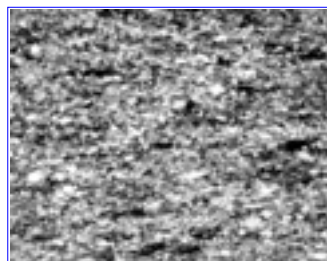
bhq-20.cirpol

cqC



CQ78-C.cirpol

cqD



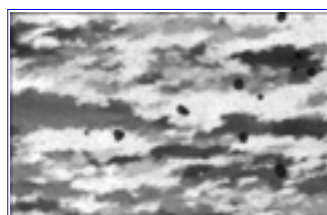
cq82-d.cirpol

HT



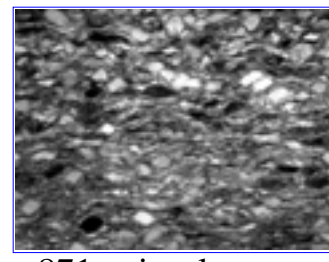
HT.CIRPOL

Pauli



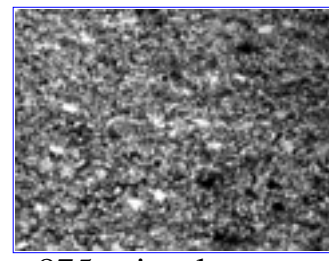
s178.cirpol

W05-1



w871p.cirpol

W05-1A



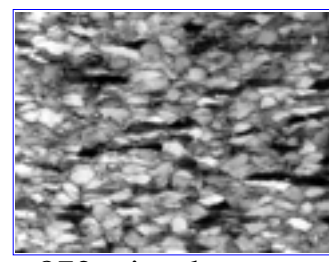
w875c.cirpol

W20-2



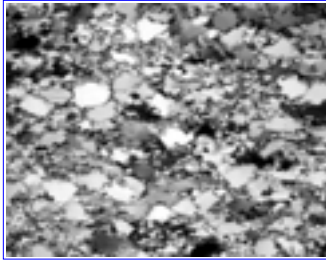
w872t20.cirpol

W05-2



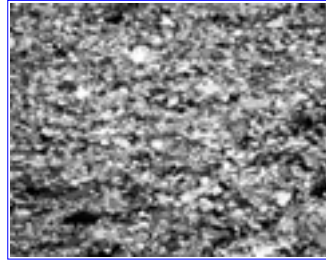
w872t.cirpol

cq05



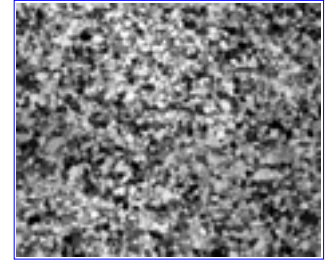
cq78-05x.cirpol

W426C



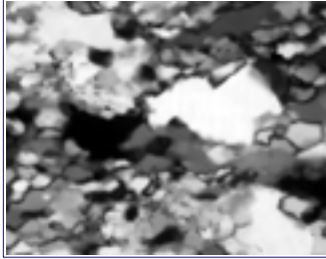
w426ax.cirpol

W05-2A



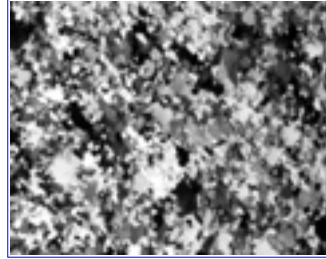
w874c.cirpol

cq10



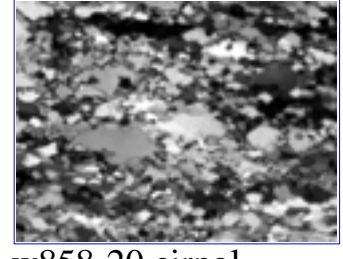
cq78-10x.cirpol

W426R



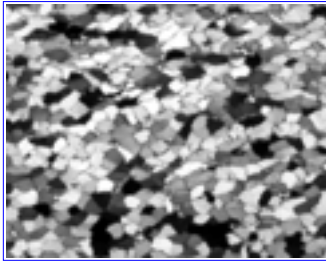
w426r.cirpol

W20-3



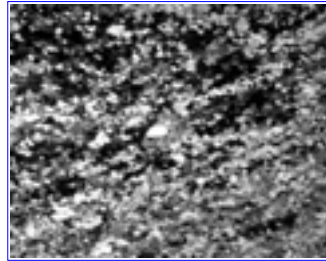
w858-20.cirpol

cqA



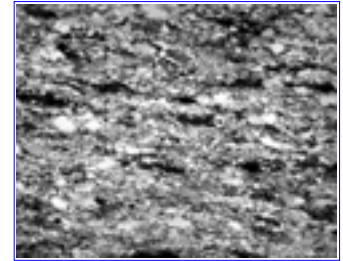
CQ78-A.cirpol

W426S



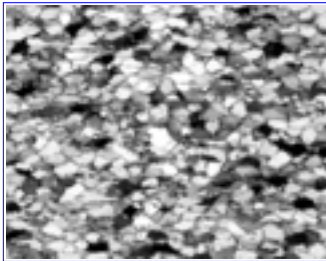
w426s2.cirpol

W05-3



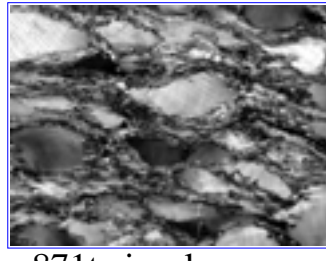
w858c.cirpol

cqB



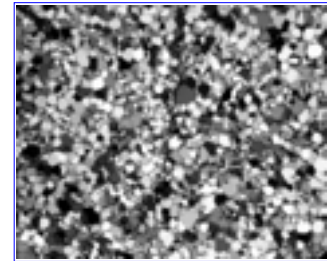
CQ78-B.cirpol

W20-1



w871t.cirpol

W05-3A



w860c.cirpol

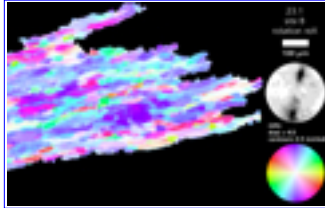
A1.2 LIBRARY OF ORIENTATION AND MISORIENTATION IMAGES

[top](#) / [contents](#) / [appendix 1](#) / pages -- [A1.1](#) -- [A1.2](#) -- [A1.3](#) -- [A1.4](#) -- [A1.5](#)

Orientation images

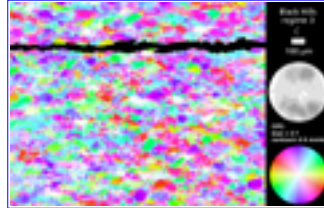
(the folder names above the images indicate where the orientation images can be found)

Stipp-RH



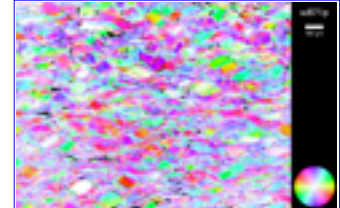
23-1b.coi2

cqC



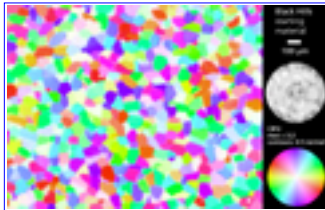
cq78-c.coi2

W05-1



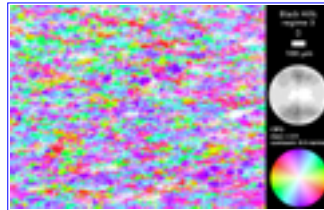
w871p.coi2

bhq starting



bh.coi2

cqD



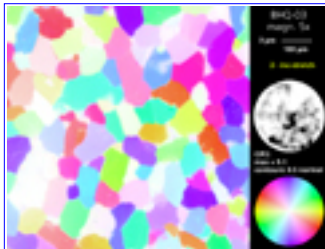
cq82-d.coi2

W05-1A



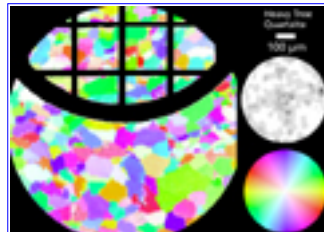
w875c.cirpol

BHQ-03



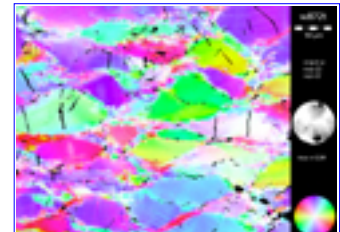
bhq-03.coi-cip2

HT



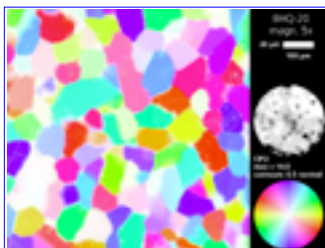
ht.coi-2

W20-2



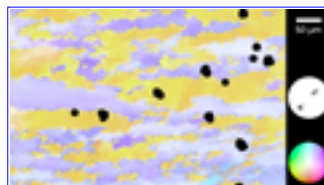
w872t20.cirpol

BHQ-20



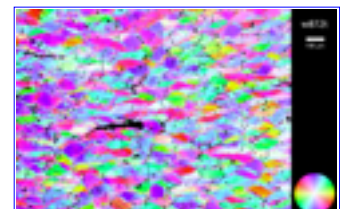
bhq-20.coi2

Pauli



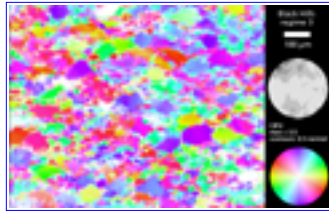
s178.coi2

W05-2



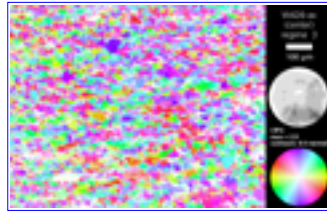
w872t.cirpol

cq05



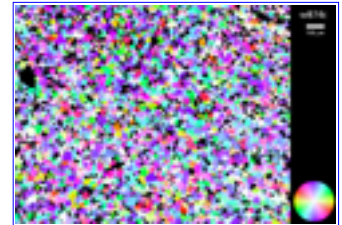
cq78-5x.coi2

W426C



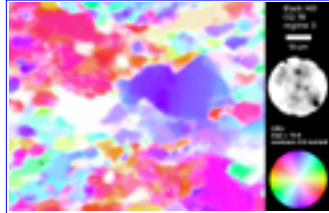
w426ax.coi2

W05-2A



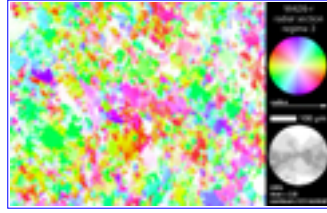
w874c.cirpol

cq10



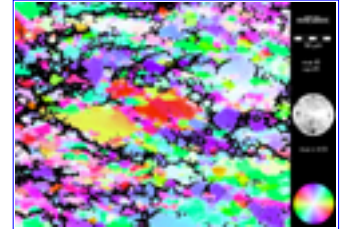
cq78.coi2

W426R



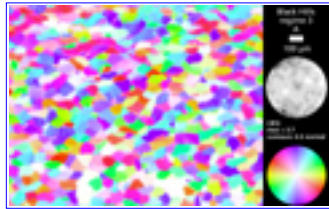
w426r.coi2

W20-3



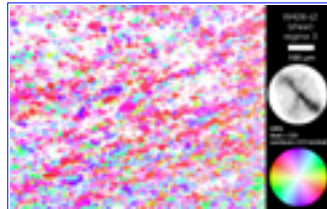
w858-20.cirpol

cqA



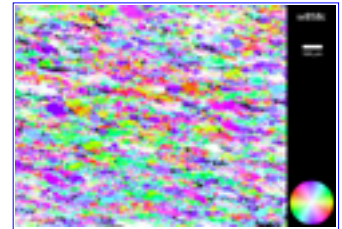
cq78-a.coi2

W426S



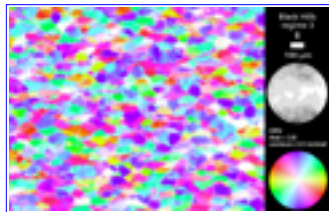
w426s2.coi2

W05-3



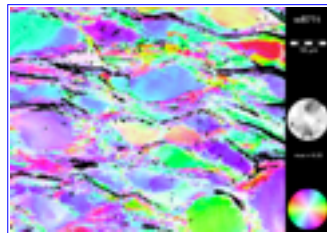
w858c.cirpol

cqB



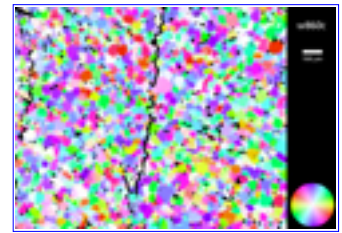
cq78-b.coi2

W20-1



w871t.coi2

W05-3A



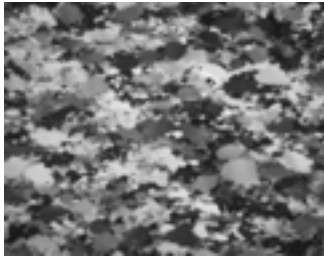
w860c.cirpol

A1.3 LIBRARY OF ORIENTATION AND MISORIENTATION IMAGES

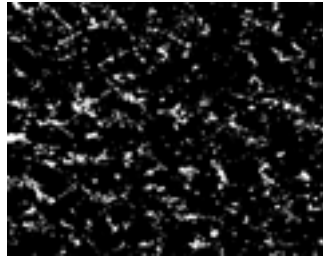
[top](#) / [contents](#) / [appendix 1](#) / pages -- [A1.1](#) -- [A1.2](#) -- [A1.3](#) -- [A1.4](#) -- [A1.5](#)

Input images

(folder cqx input, image size 780*620)



18 rotation images



1 dust & scratch mask



1 circular polarization image



1 mask to block large grains



2 tilt images



1 mask to block small grains

A1.4 LIBRARY OF ORIENTATION AND MISORIENTATION IMAGES

[top](#) / [contents](#) / [appendix 1](#) / pages -- [A1.1](#) -- [A1.2](#) -- [A1.3](#) -- [A1.4](#) -- [A1.5](#)

List of image sets

micrograph (folder Cirpol)	scale	folder name
1. 23-1-b.cirpol	100 μm = 78 pixel	Stipp-RH
2. bh.cirpol	100 μm = 41 pixel	bhq starting
3. bhq-03.cirpol	100 μm = 78 pixel	BHQ-03
4. bhq-20.cirpol	100 μm = 78 pixel	BHQ-20
5. cq78-05x.cirpol	100 μm = 78 pixel	cq05, cqx, cqx flat, cqx input
6. cq78-10x.cirpol	100 μm = 156 pixel	cq10
7. CQ78-A.cirpol	100 μm = 41 pixel	cqA
8. CQ78-B.cirpol	100 μm = 41 pixel	cqB
9. CQ78-C.cirpol	100 μm = 41 pixel	cqC
10. CQ78-D.cirpol	100 μm = 56 pixel	cqD
11. HT.CIRPOL	100 μm = 41 pixel	HT
12. s178.cirpol	100 μm = 78 pixel	Pauli
13. w426ax.cirpol	100 μm = 78 pixel	w426C
14. w426r.cirpol	100 μm = 78 pixel	w426R
15. w426s2.cirpol	100 μm = 78 pixel	w426S
16. w871t.cirpol	100 μm = 312 pixel	w20-1
17. w871p.cirpol	100 μm = 78 pixel	w05-1
18. w875c.cirpol	100 μm = 78 pixel	w05-1A
19. w872t20.cirpol	100 μm = 312 pixel	w02-2
20. w872t.cirpol	100 μm = 78 pixel	w05-2
21. w874c.cirpol	100 μm = 78 pixel	w05-2A
22. w858-20.cirpol	100 μm = 312 pixel	w20-3
23. w858c.cirpol	100 μm = 78 pixel	w05-3
24. w860c.cirpol	100 μm = 78 pixel	w05-3A

List of topics

folder	type of deformation
Stipp-RH	Natural deformation, Tonale Line
bhq starting	Experimental deformation, starting material
BHQ-03	Experimental deformation, starting material, ultrathin
BHQ-20	section
Pauli	Undeformed Black Hills quartzite
cq05, cqx, cqx flat, cqx	Natural deformation, Simplon
input	Experimental deformation, regime 3, higher magn.
cq10	Experimental deformation, regime 3, higher magn.
cqA	Experimental deformation, regime 3
cqB	Experimental deformation, regime 3
cqC	Experimental deformation, regime 3
cqD	Experimental deformation, regime 3
HT	Undeformed Heavy Tree quartzite
w426C	Experimental deformation, regime 3, axial section
w426R	Experimental deformation, regime 3, radial section
w426S	Experimental deformation, regime 3, shear deformation
w20-1	Experimental deformation, regime 1, high magn.
w05-1	Experimental deformation, regime 1
w05-1A	Experimental deformation, regime 1, annealed
w02-2	Experimental deformation, regime 2, high magn.
w05-2	Experimental deformation, regime 2
w05-2A	Experimental deformation, regime 2, annealed
w20-3	Experimental deformation, regime 3, high magn.
w05-3	Experimental deformation, regime 3
w05-3A	Experimental deformation, regime 3, annealed

[top](#) / [contents](#) / [appendix 2](#) / pages -- [A2.1](#) -- [A2.2](#) -- [A2.3](#) -- [A2.4](#) -- [A2.5](#) -- [A2.6](#)

[A2.1](#) Lazy stack

[A2.2](#) Lazy LUT

[A2.3](#) Lazy grain boundaries

[A2.4](#) StripStar

[A2.5](#) Colour look-up tables

[A2.6](#) References

A2.1 SOFTWARE, LOOK-UP TABLES AND REFERENCES

[top](#) / [contents](#) / [appendix 2](#) / pages -- [A2.1](#) -- [A2.2](#) -- [A2.3](#) -- [A2.4](#) -- [A2.5](#) -- [A2.6](#)

Detail of pile [D]

Enlarged detail of pile [E]

make ROI [S]

make ROI to low-right corner [5]

make ROI there [X]

make ROI top half [F]

make ROI left half [G]

move ROI right [5]

move ROI down [6]

move ROI left [7]

move ROI up [8]

make center ROI [C]

Crop and Scale-Fast [1]

Crop and Scale-Smooth [2]

Average stack [A]

rotate to 0° EOS stack for cirpol=2.0 [R]

rotate to 0° EOS stack for cirpol=1 [P]

rotate entire EOS stack 180° [Q]

Crop center of EOS [3]

post stack crop [-]

Pict to raw and close [S]

Move dx dy [M]

Rotate [N]

Rotate 180 [T]

median filter stack [U]

sobel stack [O]

sharpen stack [H]

threshold stack [B]

density slice stack [D]

set 0-32 to 0 [0]

skeletonize stack [K]

max of stacked windows [Z]

max of stacked windows [W]

Lazy stack

Lazy stack is an NIH Image macro for pre-processing the input stack ([-> source](#)), (for procedure, see section 4 of [CIP manual](#))

A2.2 SOFTWARE, LOOK-UP TABLES AND REFERENCES

[top](#) / [contents](#) / [appendix 2](#) / pages -- [A2.1](#) -- [A2.2](#) -- [A2.3](#) -- [A2.4](#) -- [A2.5](#) -- [A2.6](#)

<i>ROT to opt.+ LUT [T]</i> <i>ROT to opt.- LUT [-]</i> <i>ROT to +Pol LUT [L]</i>
<i>INC to CirPol [C]</i> <i>INC strips [Q]</i> <i>INC strips black [A]</i> <i>INC strips black 30 [B]</i>
<i>Correct INC [Z]</i> <i>Inflect LUT [G]</i>
<i>Spectrum red-blue-red [1]</i> <i>Spectrum dark-blue-red-dark [2]</i> <i>Spectrum black-blue-purple [3]</i> <i>Spectrum black-black [4]</i> <i>Spectrum black-black all > 0 [5]</i>
<i>Misor LUT 45°=black [M]</i> <i>Misor 0-30 [I]</i> <i>Misor 30-60 [J]</i> <i>Misor 60-90 [N]</i> <i>Misor inv.spectrum 0°=red 90°=dark [O]</i>
<i>Sawtooth 90 [S]</i> <i>EDG2 & EDG4 → histo [E]</i> <i>Contrast low edges [K]</i> <i>Colour edges [U]</i>
<i>Enhance & Apply [Q]</i> <i>Plot LUT [T]</i> <i>Export LUT [E]</i> <i>Reset [R]</i>

Lazy LUT

Lazy LUT is an NIH Image macro for post-processing the output images. ([-> source](#))

A2.3 SOFTWARE, LOOK-UP TABLES AND REFERENCES

[top](#) / [contents](#) / [appendix 2](#) / pages -- [A2.1](#) -- [A2.2](#) -- [A2.3](#) -- [A2.4](#) -- [A2.5](#) -- [A2.6](#)

<i>Crop and Scale-Fast [1]</i> <i>Crop and Scale-Smooth [2]</i>
<i>Average stack [A]</i> <i>Max of stack [Z]</i> <i>Max of windows [W]</i>
<i>Median filter stack [U]</i> <i>Sobel stack [O]</i> <i>Sharpen stack [H]</i> <i>Enhance stack [C]</i> <i>Threshold stack [B]</i> <i>Adaptive -mean- threshold stack [G]</i> <i>Adaptive -mode- threshold stack [V]</i> <i>Adaptive -mixed- threshold stack [N]</i> <i>Density slice stack [D]</i> <i>Skeletonize stack [K]</i> <i>Prune stack [P]</i>
<i>Median filter image [M]</i> <i>Prune image [I]</i> <i>Skeletonize image [J]</i> <i>Density slice image [E]</i> <i>Density slice image about 128 [L]</i> <i>Thicken lines [T]</i>
<i>Info on histo [F]</i> <i>make ROI by width of rim [4]</i> <i>cut away rim [5]</i> <i>Smooth image [6]</i> <i>Smooth image more [7]</i> <i>Smooth enlarge outlines [8]</i> <i>Invert image [Y]</i> <i>Scale to pixel [0]</i>

Lazy grain boundaries

Lazy grain boundaries is an NIH Image macro for the derivation of grain boundary maps from orientation images or polarization micrographs ([-> source](#)) (for procedure and application, see [manual](#)).

Heilbronner, R. (in press). Automatic grain boundary detection and grain size analysis using polarization micrographs or orientation images. *J. Structural Geology*.

A2.4 SOFTWARE, LOOK-UP TABLES AND REFERENCES

[top](#) / [contents](#) / [appendix 2](#) / pages -- [A2.1](#) -- [A2.2](#) -- [A2.3](#) -- [A2.4](#) -- [A2.5](#) -- [A2.6](#)



StripStar

StripStar

Program for the calculation of 3-D grain size distributions from radii of 2-D sections, application for PowerMac ([download](#)). (see [manual](#) for procedure)

A2.5 SOFTWARE, LOOK-UP TABLES AND REFERENCES

[top](#) / [contents](#) / [appendix 2](#) / pages -- [A2.1](#) -- [A2.2](#) -- [A2.3](#) -- [A2.4](#) -- [A2.5](#) -- [A2.6](#)

Colour look-up tables

1-D and 2-D Colour look-up tables (CLUT) are shown as 180*180 image matrices (file name extension CLUT) and/or as stereographic projections (file name extension POL).

(click on icons to get full size 180x180 look-up tables)



crossed.POL



cirpol.POL



crossed-L-IF660nm.POL



Positive.POL



positive.CLUT



Negative.POL



negative.CLUT



azi.bw.POL



inc-nocorr.POL



azi.CLUT



inc.CLUT



CIP-Standard.POL



CIP-Standard.CLUT



CIP-Spectrum.POL



CIP-Spectrum.CLUT



misH.POL



misE.POL



misN.POL



misor-117-90.POL



swatch.POL



swatch.CLUT



sander.POL



sander.CLUT



CIP-Standard.POL-in-out



inc-cirpol.POL



North.POL

A2.6 SOFTWARE, LOOK-UP TABLES AND REFERENCES

[top](#) / [contents](#) / [appendix 2](#) / pages -- [A2.1](#) -- [A2.2](#) -- [A2.3](#) -- [A2.4](#) -- [A2.5](#) -- [A2.6](#)

References

Heilbronner, R. (in press). Automatic grain boundary detection and grain size analysis using polarization micrographs or orientation images. *J. Structural Geology*.

Heilbronner, R. & Tullis, J. (1999). "The parts are more than fractions of the whole": heterogeneous texture evolution in experimentally deformed, dynamically recrystallized quartzite. ICOTOM 12, Augusts 1999, Montreal, Canada.

Heilbronner, R. & Tullis, J. (1999a) Grain Size and Texture Development in Dynamically Recrystallized Quartzite: a new Look at old Deformation Experiments. In: *Deformation Mechanisms, Rheology & Tectonics*. Giessen, Neustadt a.d.W.

Herwegh, M., Handy, M. & Heilbronner, R. 1999. Evolution of mylonitic microfabrics (EMM), a computer application for educational purposes. *Tectonophysics* 303, 141-146.

Hirth, G. & Tullis, J., 1992. Dislocation creep regimes in quartz aggregates. *J. Structural Geology* 14, 145-159.

Oesterling, N., Heilbronner, R. & Molli, G. 1999. Microstructures related to dynamic overprint in statically recrystallized Carrara marble (Alpi Apuane, NW Italy). In: *DRM*, Neustadt.

Panozzo Heilbronner, R. and C. Pauli (1993). "Integrated spatial and orientation analysis of quartz c-axes by computer-aided microscopy." *J. Struct. Geol.* 15(3-5): 369-382.

Panozzo Heilbronner, R. and C. Pauli (1994). Orientation and misorientation imaging: integration of microstructural and textural analysis. *Textures of geological materials*. H. J. Bunge, S. Siegesmund, W. Skrotzki and K. Weber. Oberursel, DGM Informationsgesellschaft Verlag: 147-164.

Pauli, C., Schmid, S. M. & Panozzo Heilbronner, R. 1996. Fabric domains in quartz mylonites: localized three dimensional analysis of microstructure and texture. *J. Structural Geology* 18, 1183-1203.

Sander, B. 1950. *Einführung in die Gefügekunde der geologischen Körper, zweiter Teil: Die Korngefüge*. Springer Verlag, Wien.

Stipp, M., Stünitz, H. & Heilbronner, R. 1999. Temperature dependence of quartz dynamic recrystallization regimes in naturally deformed rocks. In: *Deformation Mechanisms, Rheology & Tectonics*. Giessen, Neustadt a.d.W.

Tullis, J. & Heilbronner, R. (1999). Effect of static annealing on LPOs of

experimentally deformed quartz aggregates. DTR, March 1999, Neustadt, Germany.

van Daalen, M., Heilbronner, R. & Kunze, K. 1999. Orientation analysis of localized shear deformation in quartz fibres at the brittle-ductile transition. *Tectonophysics* 303, 83-108.